ABSTRACT

Title of Document: BIOPHYSICAL STUDIES OF THE MECHANISM OF CERAMIDE CHANNEL DESTABLIZATION BY BCL-XL IN APOPTOSIS AND THE USE OF RECTIFICATION TO PROBE THE STRUCTURE AND DYNAMICS OF A NOVEL ESCHERICHIA COLI CHANNEL

Kai-Ti Chang, Doctor of Philosophy, 2015

Directed By: Professor Marco Colombini
Department of Biology

Ceramide forms a novel type of channel in the mitochondrial outer membrane and these channels are involved the release of intermembrane space proteins from mitochondria, a decision-making step in the apoptotic process. An antiapoptotic protein, Bcl-xL, regulates the apoptotic process and inhibits the formation of ceramide channels. However, there is no precedent to indicate how a protein regulates a lipid channel. We investigated the mechanism of this regulation and identified the hydrophobic groove of the Bcl-xL as the binding site by which Bcl-xL binds to the channel. This was demonstrated by using a combination of experimental and modeling methods, including site-directed mutagenesis, a fluorescence quenching assay, a mitochondrial outer membrane

permeability assay, and molecular dynamic simulations. Interestingly, the hydrophobic groove serves to inhibit another channel former, Bax. We found that the binding sites for Bax and ceramide on Bcl-xL are distinct but overlapping. We used that fact to generate mutants that have differential abilities to inhibit one or the other of these channels. These are useful because although ceramide is important in apoptosis, it is still controversial that whether ceramide channels result in apoptosis *in vivo*. To probe the relative importance of these two channels in apoptosis, Bcl-xL mutant proteins were expressed in Bcl-xL deficient cells. Weakening the inhibitory potency of Bcl-xL on either Bax or ceramide channels resulted in cells being more sensitive to the induction of apoptosis. This is the first evidence for the role of ceramide channels in the apoptotic process *in vivo*.

In a separate investigation, a novel voltage-gated channel unit was found in *E. coli* extracts. The unit is consistent with three channels forming the functional triplet. These channels are highly voltage gated and highly cooperative. Those results indicated that one of the channels is oriented in an antiparallel fashion compared to the rest. This arrangement is very rare in protein channels. Rectification of the current flowing through the channels was used to identify the orientation of the channels to provide evidence for or against the antiparallel hypothesis. The results favor the antiparallel hypothesis but also reveal an unexpected asymmetry in the transmembrane electrostatics.

BIOPHYSICAL STUDIES OF THE MECHANISM OF CERAMIDE CHANNEL DESTABLIZATION BY BCL-XL IN APOPTOSIS AND THE USE OF RECTIFICATION TO PROBE THE STRUCTURE AND DYNAMICS OF A NOVEL ESCHERICHIA COLI CHANNEL

By

Kai-Ti Chang

Dissertation submitted to the Faculty of the Graduate School of the
University of Maryland, College Park, in partial fulfillment
of the requirements for the degree of
Doctor of Philosophy
2015

Advisory Committee:
Professor Marco Colombini, Chair
Professor Jeffery Davis
Professor Douglas Julin
Assistant Professor Paul Paukstelis
Associate Professor Richard Stewart

Acknowledgements

I would like to express my sincere gratitude to my advisor, Dr. Marco Colombini, without whom I would not able to have a fruitful journey in my graduate career. He always clearly explained the concepts and encouraged me to ask questions. Then he showed me how to design and perform experiments by example and inspired me to approach scientific questions with an open mind, curiosity, creativity, critical thinking, and to see the big picture. I would like to thank him for being always available whenever I have questions, for encouraging me to express my ideas, for inspiring me to enjoy the research, and for having confidence in me.

I would like to thank my dissertation committee members, Dr. Jeffery Davis, Dr. Douglas Julin, Dr. Paul Paukstelis, and Dr. Richard Stewart for advice and discussions throughout my graduate career that not only guided my research directions but also revealed the concepts that I did not consider.

I have met intelligent and generous graduate students in Dr. Colombini's lab. We have shared our experiences with each other and enjoyed the time in the lab. I would like to thanks Vidyaramanan Genesan and Meenu Perera for generously sharing all the details of the membrane permeability experiments and giving me invaluable suggestion in my graduate life. In addition, Shang H. Lin and I shared the unique experience of jointly facing the challenge of a scientific question. I enjoyed the time in which we brainstormed and tested our ideas.

I have worked with several undergraduate students (Justin M. Wang, Timothy Walsh, Timothy Troppoli, Benjemin Wu, and Jennifer Kunselman.) who provided assistance to my projects. I was inspired by their motivation, energy and curiosity. It was a wonderful experience to translate my ideas and concepts from head into words. By doing that, I often discovered something I did not understand thoroughly.

I thank my family for giving me the opportunity to pursue graduate studies and for supporting me in every possible way to pursue my academic goals. Those were fundamental to my ability to study abroad.

Table of Contents

List of Figures

List of Tables

List of Abbreviations

AAALAC	Association for Assessment and Accreditation of Laboratory Animal Care
AIF	apoptosis-inducing factor
Apaf-1	apoptotic protease activating factor-1
AVMA	American Veterinary Medical Association
BH	Bcl-2 homology
BSA	bovine serum albumin
bSMase	bacterial sphingomyelinase
Caspases	cysteine-aspartic proteases
DISC	death-inducing signaling complex
DTT	dithiothreitol
ER	endoplasmic reticulum
FBS	fetal bovine serum
GFP	green fluorescent protein
GST	glutathione S-transferase
IMS	intermembrane space
IPTG	isopropyl β-D-1-thiogalactopyranoside
Kir	inwardly rectifying potassium channel
MAC	mitochondrial-induced channel
MEF	mouse embryonic fibroblast
MD	molecular dynamic
MIM	mitochondrial inner membrane
MIS	mitochondrial intermembrane space
MOM	mitochondrial outer membrane
MOMP	mitochondrial outer membrane permeabilization
PBS	phosphate buffered saline
PMSF	phenylmethylsulfonyl fluoride
PVDC	polyvinylidene chloride
S.E.	standard error
t-Bid	truncated Bid
TM	transmembrane domain
VDAC2	Voltage-Dependent Anion Channel isoform 2
VSD	voltage sensor domain

Chapter 1: General Introduction

1.1 Apoptosis

Apoptosis is a type of programmed cell death and occurs during normal development and tissue homeostasis. It is highly regulated to exactly control when and where it will occur. Dysfunction of this process is fundamental to diseases, such as cancer, stroke, and viral infections. It also can result in congenital abnormalities, such as webbed toes. In this process, unwanted cells are removed cleanly. A cell triggers apoptotic process in response to a stress, such as DNA damage, aging, UV light exposure, viral infection and overproduction of reactive oxygen species. Cells dying by apoptosis undergo several morphological changes, including cells shrink and detach from its neighbors, the cytoskeleton collapses, the nuclear envelope disassembles, and chromatin condenses and breaks up into fragments (1). The cell surface becomes irregular and bulges outward to form membrane-enclosed vesicles, also as known as apoptotic bodies. The neighboring cells and macrophage recognize and engulf the apoptotic bodies quickly. In this way, the formation of apoptotic bodies prevents leakage of cellular contents and avoids inflammation or autoimmune reactions, which may damage surrounding tissues. In contrast, when cells undergo necrosis, an uncontrolled and passive cell death, which usually occurs due to trauma, cells swell and the plasma membrane ruptures (2). In this way, dead cells release the cellular contents and induce inflammatory response. Apoptosis is able to remove cells neatly and rapidly. Therefore,

understanding the molecular mechanism of apoptosis is fundamental to the development of diseases and finding and their cure.

1.1.1 Extrinsic and intrinsic apoptotic pathway

Based on the stimuli resources, such as UV light exposure, DNA damage, and aging, apoptosis is divided into two groups: extrinsic pathway and intrinsic pathway, which are triggered by the extracellular and intracellular signals, respectively (Fig. 1.1). In extrinsic pathway, take Fas ligand on the surface of killer lymphocyte for example. When it binds to death receptors in the plasma membrane, this binding activates the intracellular domain of the receptors and recruits proteins (including procaspase-8 or -10) to form death-inducing signaling complex (DISC). Procaspase is an inactive precursor of cysteine-aspartic proteases (caspases). Caspase-8 and -10 then activate caspase-3, -6, and -7, which then activate other caspases and target proteins, and results in the execution of apoptosis and the morphological changes, such as nuclear lamina breakdown, cytoskeleton collapse, and DNA fragments. In contrast, the intrinsic pathway is triggered by intracellular signals, such as DNA damage and lack of nutrients, and release intermembrane space (IMS) proteins, including cytochrome *c*, apoptosis-inducing factor (AIF), heat shock proteins, Smac/Diablo, and endonuclease G, to cytosol (3). It was a surprising discovery that mitochondria are not only as powerhouse, producing ATP via oxidation phosphorylation but also play a role in apoptosis. Cytochrome *c*, a water-soluble protein in electron transport chain and normally resides in IMS, has a different

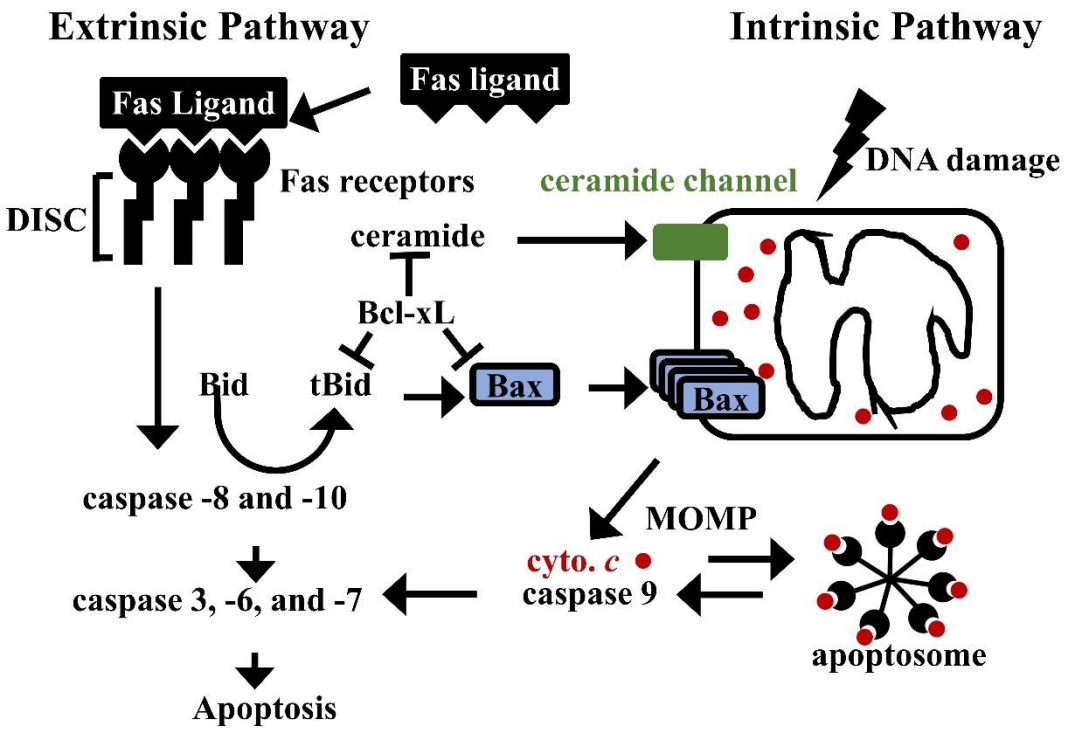

Figure 1.1. Extrinsic and intrinsic pathways of apoptosis. Shown is a simplified schematic view of apoptotic pathways. Apoptosis may be triggered by activation of cell surface receptors (extrinsic pathway) or by intracellular mechanism (intrinsic pathway). Both pathways are able to activate caspase cascade and initiate the execution phase of apoptosis. Both pathways are linked by BH3-only proteins (Bid). Activated Bax and ceramide will cause the mitochondrial outer membrane permeabilization (MOMP) and activate caspase cascade. Bax and ceramide are regulated by antiapoptotic proteins (e.g. Bcl-xL).

function once it is released into cytosol. It recruits apoptotic protease activating factor-1 (Apaf-1) and procaspase-9 to from a complex, apoptosome, and then result in caspase-9 activation. The caspase-9 induces the downstream caspases and the execution of apoptosis. These two pathways are not independent and are linked by a BH3-only protein, Bid. The active caspase-8 in extrinsic pathway cleaves the inactive form of Bid. The truncated and active form of Bid, t-Bid, translocates to mitochondrial outer membrane (MOM), causes the MOM permeabilization (MOMP), and results in the execution of apoptosis.

Normally, the MOM only permeable to molecules less than 5 kD because of porin channel, but the MOM is impermeable to IMS proteins (cytochrome *c* is 12 kD). During the apoptotic process, the IMS proteins are released. This indicates the permeability of the MOM is changed. Several mechanisms may explain the MOMP, including the permeability transition (4), channels formed by Bax oligomers (Bax channel) (5, 6), the mitochondrial-induced channel (MAC) (7), interactions between Bax and ceramide (8, 9), and ceramide channels (10, 11).

1.1.2 Bcl-2 family proteins regulate MOMP

Once MOMP occurs, cells do not recover because of defective function of mitochondria and the irreversible apoptotic process. This process is tightly controlled to ensure the process is triggered in the right time and the right location. Bcl-2 family proteins were discovered to regulate the MOMP. For example, Bcl-2 inhibits the release of cytochrome *c* and Bax and t-Bid cause the membrane permeabilization (12–17).

Bcl-2 family proteins share up to four Bcl-2 homology domains (BH1-4) (Fig. 1.2). In addition, Bcl-2 family proteins can be classified on the basis of the number of Bcl-2 homology domains they process and on their antiapoptotic or proapoptotic function (Fig 1.2). Antiapoptotic proteins are multi-domain proteins, including Bcl-2, Bcl-xL, Bcl-w, Mcl-1, and A1. Proapoptotic proteins include multi-domain proteins (Bax and Bak) and BH3-only proteins. BH3-only proteins contain the conserved BH3 domain and other regions are

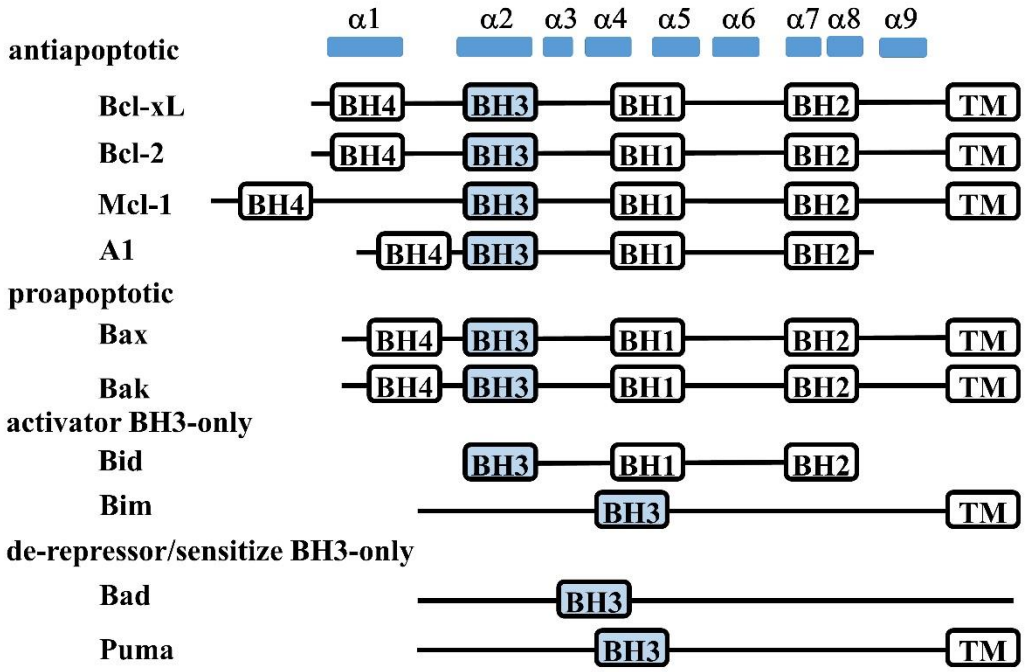

Figure 1.2. The Bcl-2 family proteins. The Bcl-2 family proteins regulates the MOMP. They share up to four Bcl-2 homology (BH) domains. All of them have the critical BH3 domain. They are divided into antiapoptotic, proapoptotic, activator BH3-only, and de-repressor/sensitize BH3-only subgroups. TM stands for transmembrane domain. Helices 1-9 of Bcl-xL are shown on the top. Bid is shown as full-length, an inactive form. Bid is activated following cleavage by caspase-8.

heterogeneous. BH3-only proteins can be subdivided into two groups. One group is activator BH3-only proteins (Bid and Bim), which activate Bax or Bak. The other group is de-repressor/sensitizer BH3-only proteins (Puma, Bad, Bik, Noxa and others), which neutralized the antiapoptotic proteins.

The Bcl-2 family proteins have been found in variety of sub-cellular locations in normal cells. For example, in the mitochondria, Bak resides in the MOM and is inhibited by VDAC2, Voltage-Dependent Anion Channel isoform 2 or antiapoptotic proteins (Bcl-2, Bcl-xL, and Mcl-1) (18–22). In cytosol, the BH3-only proteins form heterodimers with and inactivate Bcl-xL or Mcl-1 (23).

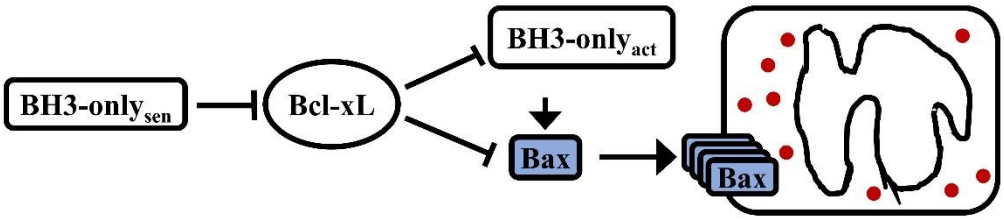

Figure 1.3. Current model for activation of proapoptotic protein. BH3-only proteins are able to activate Bax directly (activator BH3-only proteins) or indirectly (de-repressor/sensitizer BH3-only proteins). Bcl-xL inhibits the activity of Bax either directly (forming heterodimer with Bax) or indirectly (sequester the activity of activator BH3-only proteins.

Bid and most of Bax are cytosolic proteins and some of Bax are loosely attached to the MOM (24, 25).

To occur in the right time and right location, apoptosis is highly regulated by a complicated network. It is general agreed the Bax-induced apoptosis is regulated by the balance of antiapoptotic and proapoptotic proteins. Current model used to explain this balance is illustrated in Fig. 1.3 (14, 26, 27). BH3-only proteins serve as sensors of intrinsic apoptosis, because they respond to DNA damage or ER stress and translocate to MOM. For example, after receiving apoptotic signal, caspase-8 cleavages and activates Bid. Then t-Bid, the active form of Bid, translocates to the MOM. t-Bid recruits and activates Bax and Bax integrates into the MOM (14, 28). After that, the activated Bax in the membrane recruits and activates more Bax and subsequently form Bax channel. While Bax channel forming, IMS proteins are release because of MOMP at the same time. The antiapoptotic proteins are able to inactive Bax or activator BH3-only proteins in the cytosol or the MOM by forming heterodimer (23, 29–33). Moreover, the activity of antiapoptotic proteins is inhibited by the

de-repressor/sensitizer BH3-only proteins. In sum, to occur MOMP, two events are required: all the antiapoptotic proteins are inhibited and Bax is activated. The interactions between Bcl-2 family proteins are primary through their hydrophobic groove and BH3 domain of another proteins.

1.1.2.1 Structures of Bcl-2 family proteins and small molecules interrupt the potency of Bcl-xL

The soluble structures of antiapoptotic and proapoptotic protein are similar. The structure of Bax channel and the apoptotic/antiapoptotic heterodimer in the membrane are not clear. The soluble structures of full-length Bax, Bcl-xLΔC (lacking of transmembrane domain and unstructural loop between α1 and α2), and Bcl-wΔC10 (lacking 10 residues in C-terminal) were solved. The structure shown in Fig. 1.4 are Bcl-xLΔC/Bim (PDB: 1PQ1), Bax (PDB: 1F16), and Bcl-wΔC10 (PDB 1O0L) (34–36). Structure of Bax and Bcl-wΔC10 are composed of nine α-helices (α1 to α9). The α9 (the transmembrane helix) of Bcl-xLΔC is removed. Two hydrophobic helices (α5 and α6) in the center form the core of the protein. Seven amphipathic helices are around these two central helices. Bcl-2 family proteins interact to each other through the hydrophobic groove. BH1, BH2, and BH3 are near to each other and form one end of the hydrophobic groove. α3 and α4 form the other end of the groove.

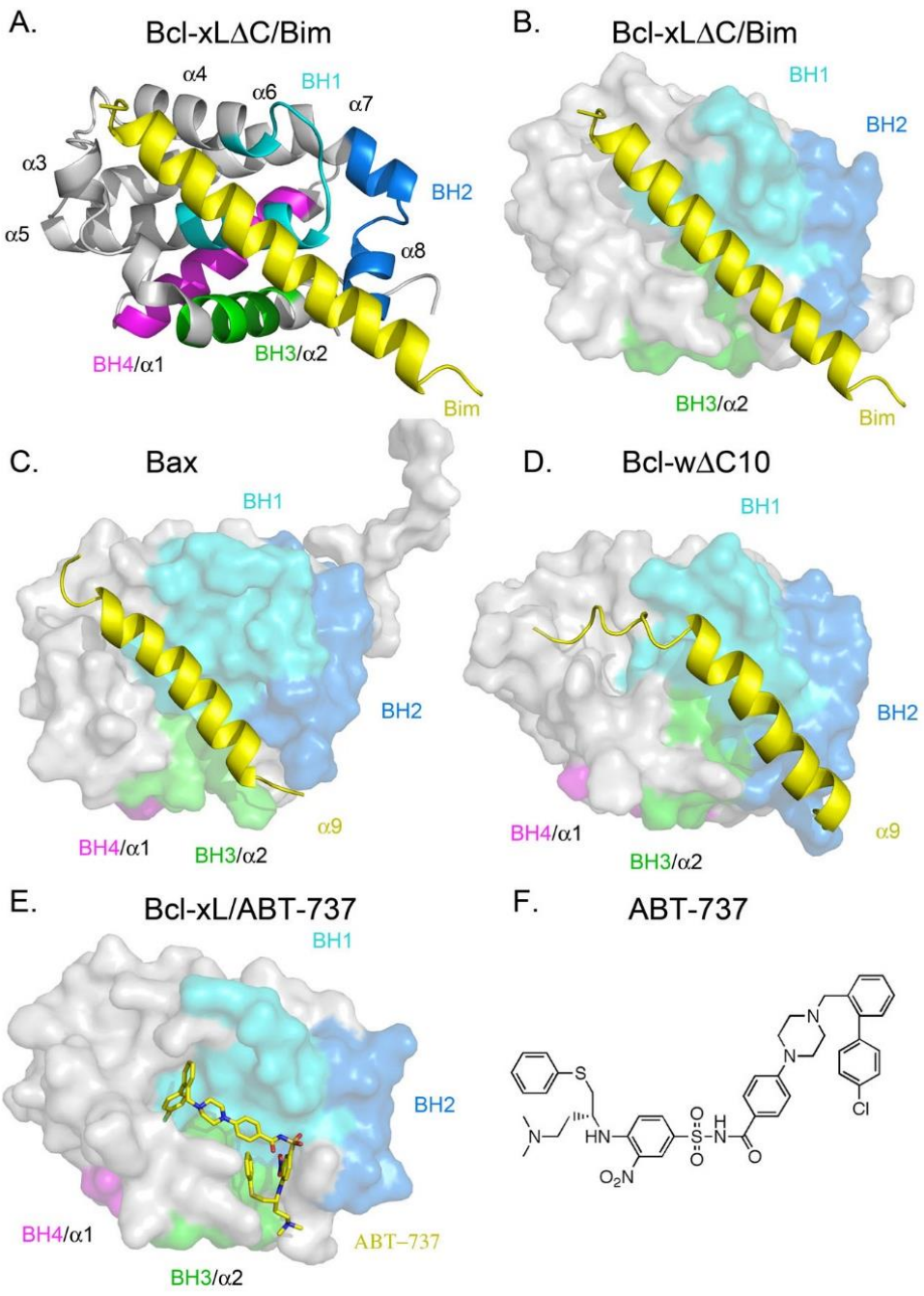

Figure 1.4. Structures of Bcl-2 family proteins. Ribbon representation of (A) Bcl-xLΔC/Bim (PDB: 1PQ1). Connolly surface of (B) Bcl-xLΔC/Bim, (C) Bax (PDB: 1F16), (D) Bcl-wΔC10 (PDB 1O0L), and (E) Bcl-xL/ABT-737(PDB 2YXJ). Substrates bind to the hydrophobic groove are colored in yellow (Bim peptides, the α9 helix of Bax and Bcl-wΔC10 and ABT737). BH1, BH2, BH3, and BH4 region are colored in cyan, blue, green, and magenta, respectively. (F) Structure of ABT-737

The hydrophobic groove is full by the α9 (transmembrane helix) and is capable to bind to the BH3 domain to form heterodimer through hydrophobic interactions. For example, in Bcl-xLΔC/Bak peptide complex (PDB: 1BXL), several hydrophobic residues of Bak peptide (V74, L78, I81, I85) make contact with hydrophobic residues of Bcl-xL (F97, Y101, F105, L108, V126, L130, V141, and F146) (37). The interactions between BH3 domain and the hydrophobic groove are the key aspect of apoptosis regulation. This hydrophobic groove is occupied by transmembrane helix. Therefore, a conformation change of antiapoptotic proteins is required to expose the hydrophobic groove and then form heterodimer with proapoptotic proteins. As would be expected, occupied hydrophobic groove moderate decreases the affinity of BH3 proteins and peptides to antiapoptotic protein (35). In addition, the residues in BH3 domain used to form heterodimer or homo-oligomer point toward the core of the proteins. This indicates another conformational change is required to expose the BH3 domain.

Many cancer cells take an advantage of defects in their apoptotic process. The Bcl-2 antiapoptotic proteins are considered attracted targets of chemotherapy as their overexpress is observed in many cancer cells (38, 39). A small molecule, either nonpeptide or derived from BH3 domains, mimics the BH3-only proteins by occupying the hydrophobic groove of the antiapoptotic proteins, inhibiting their function and then triggering the apoptosis. For example, Antimycin A3, 2-methoxy antimycin A3, ABT-737, and ABT-263 are small molecules and SAHBa is a hydrocarbon-stapled peptide derived from

BID BH3 (40, 41). ABT-737 selective inhibits three antiapoptotic proteins (Bcl-xL, Bcl-2, and Bcl-w) but not Mcl-1 and A1. Its oral derivative, ABT-263, shows promising data of phase I/II clinical trials for various cancer cells (42–46). The crystal structure of Bcl-xL/ABT-737 shows that ABT-737 binds to a part of the hydrophobic groove that is close the BH123 end of the hydrophobic groove.

The membrane structure of Bcl-2 family proteins are still unclear and under investigation. The majority of Bax is in cytosol and small portion of Bax is loosely attached to mitochondria, as it can be extracted by sodium carbonate (47). After apoptotic stimuli, Bax is constitutively inserted into the MOM (48, 49), presumably via its transmembrane helix (α9). When Bax is activated, it undergoes a conformational change, inserts its α5 and α6 into the MOM and then exposes its BH3 domain (48, 50–54). Consequently, Bax channels form and result in the MOMP.

1.1.3 Ceramide role in mitochondrial mediated apoptosis

Ceramide, a sphingolipid, is composed of a sphingoid base (18 carbons) and an acyl chain (14 to 16 carbons) linked via an amide bond at C2 of the sphingoid base (Fig 1.5). The sphingoid base consists of two hydroxyl groups at C1 and C3, a *trans* double bound across C4 and C5, and an amine on C2. Ceramide is involved in several cell processes, such as cell differentiation, cell signaling, growth suppression, and apoptosis. This study focuses on the apoptosis.

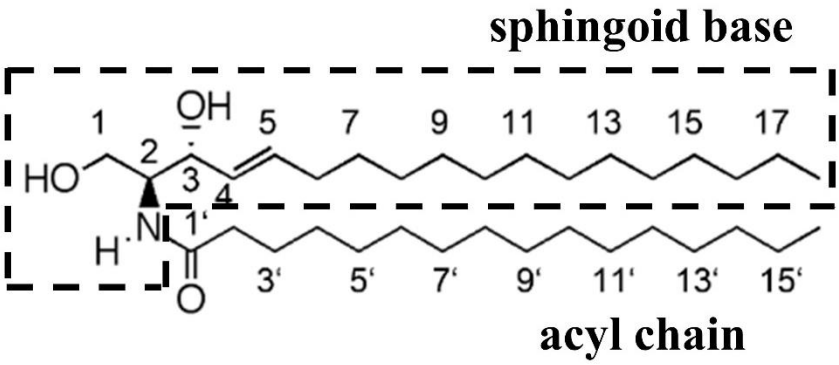

Figure 1.5. Structures of C16 ceramide. Sphingoid base is surrounded by dashed lines.

1.1.3.1 Cellular ceramide is important in apoptosis

Several cellular observations indicate that ceramide plays an important role in apoptosis. First, in various cell types, ceramide generation is a common response to apoptotic reagents, such as TNFα, interleukin-1, or γ–interferon (55–60). Second, the effective dose of these apoptotic reagents required to induce ceramide generation and apoptosis are closely matched (61). Third, apoptotic reagents induce the elevation of cellular ceramide before the execution phase of the apoptotic process (55, 62, 63). Fourth, ceramide-induced apoptosis is specific. For example, dihydroceramide, a ceramide precursor, does not induce apoptosis (60, 64). Fifth, elevation of cellular ceramide induces apoptosis in various cell types. Elevation of ceramide can be done via addition of apoptotic agents, exogenous membrane-permeable ceramide analogues, or inhibitors of ceramide metabolism (55, 60, 65–69). These indicate ceramide is important in apoptotic induction.

1.1.3.2 Mitochondrial ceramide is important in apoptosis

Regulation of ceramide generation in mitochondria is important in apoptosis. Failure in this regulation contributes the immortality of cancer cells. In general, the level of ceramide is kept in low (70). When cells receive proapoptotic signals, the level of ceramide in the mitochondria increases (55, 58, 71). For example, UV irradiation resulted in an increase in mitochondrial ceramide and the release of cytochrome *c* in HeLa cells (71). Inhibition of sphingolipid metabolism prevents ceramide synthesis and also prevents the onset of apoptosis. In addition, Birbes et al. expressed the bacterial sphingomyelinase (bSMase), which converts sphingomyelin to phosphocholine and ceramide, in different organelles in MCF7 breast cancer cells (72). Only when bSMase was targeted to mitochondria and increased the level of mitochondrial ceramide, was cytochrome *c* released from mitochondria and the cells underwent apoptosis. Therefore, the level of mitochondrial ceramide is critical for ceramide-induced apoptosis. Although most sphingolipid metabolism occurs at locations outside of mitochondria, such as the endoplasmic reticulum (ER), the Golgi apparatus, and the plasma membrane, ceramide produced distally can be rapidly transferred to mitochondria. Specialized ER associated with mitochondria, known as mitochondrial associated membranes, can rapidly transfer its ceramide to mitochondria (73). In addition, mitochondria are also able to generate ceramide because they processe ceramide synthase and ceramidase (74–76). This also indicates that the level of mitochondrial ceramide is tightly regulated.

1.1.3.3 The existence of ceramide channels in the MOM

Early studies indicated that elevation of mitochondrial ceramide induces the release of IMS proteins and induces apoptosis (55, 58, 71). The release of IMS proteins indicates that the outer membrane of mitochondria becomes permeable. Whereas the sphingolipid community is focused on ceramide acting on proteins to alter cellular function, ceramide was also shown to form large stable channels in membranes (10, 77–79). The proposal that hundreds of ceramide molecules would self-assemble into a large lipid channel is very novel and not generally accepted. However, the experimental evidence for channel formation is very strong. First, ceramide does not cause the release of the mitochondrial matrix enzyme, fumarase, while it causes the release of IMS proteins such as cytochrome *c* (11). This indicates a specific permeabilization of the MOM. Second, ceramide did not permeabilize the plasma membrane of erythrocytes or destroy the solvent-free planar phospholipid membranes (10, 77), further indicating that the ceramide-induced permeabilization is not merely a non-specific, detergent-like effect. Indeed, this indicates that ceramide selectively permeabilizes the MOM but not the mitochondrial inner membrane (MIM) or the plasma membrane. In addition, bovine serum albumin (BSA) and an antiapoptotic protein, Bcl-xL, are able to reverse the MOMP and restore the permeable barrier of the MOM (17, 77). This indicates that ceramide channels are in dynamic equilibrium with ceramide monomers in the membrane and BSA shifts the equilibrium away from ceramide channels in the MOM to the ceramide monomer bound to BSA in the aqueous solution. Moreover, the size

of the ceramide channel is sensitive to the concentration of ceramide present or added again indicating a dynamic equilibrium. Under certain conditions ceramide allows the release of IMS proteins below 60 kD from mitochondria (10, 11), but larger channels are formed under other conditions (78).

In 2000, Siskind and Colombini reported the formation of ceramide channels in planar phospholipid membranes and later in the MOM (10, 11). Channel formation is not only supported by the observation of discrete increments of conductance in the planar phospholipid membrane, but also the ceramide channels observed in liposomes under the electron microscope (78). They vary in size but have an average size of ten nanometers in diameter (10, 78). Ceramide channels form at physiological mole fractions in the MOM (77). The level of ceramide required for channel formation in the MOM of isolated mammalian mitochondria is a little less than the level of ceramide present in the MOM during the induction phase of the apoptotic process that is before or at the time of cytochrome *c* release (77). This suggests ceramide forms channels in the MOM in the cell at the appropriate time to initiate the execution phase of apoptosis.

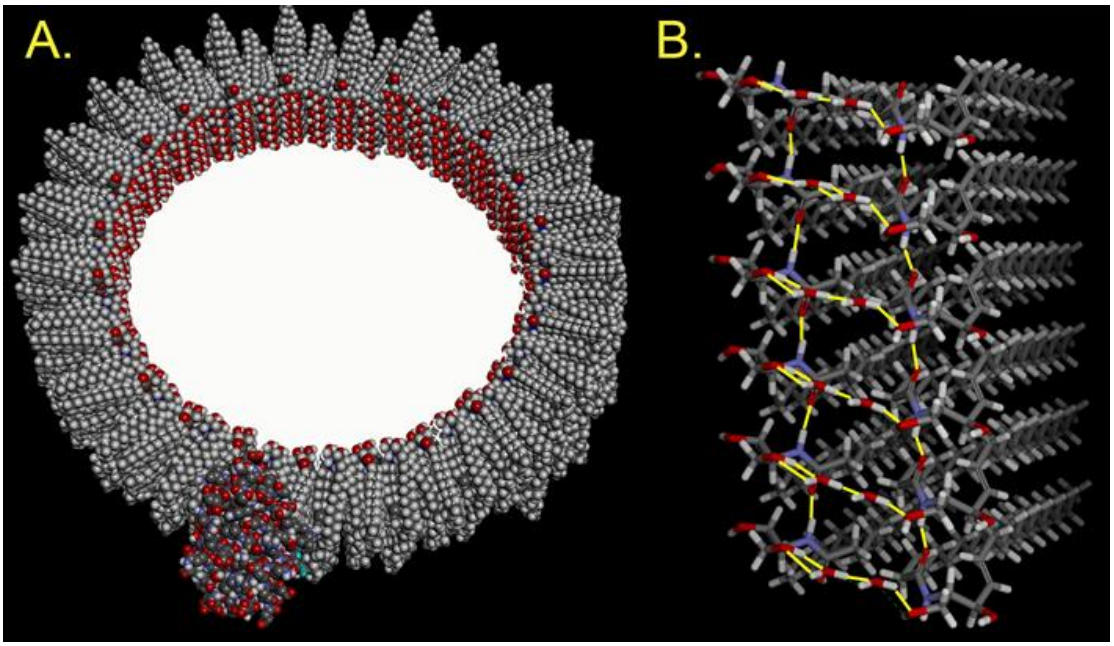

Figure 1.6. Model of the ceramide channel. A. A model of a ceramide channel as it would exist on a membrane. This is composed of 48 ceramide columns arranged in an antiparallel orientation. The red atoms forming the inner lining of the pore are oxygens. The number of columns varies forming channels of different pore diameter. The illustrated structure forms a 10 nm diameter pore and this is the typical size detected by electrophysiological recordings and electron microscopy. The crystal structure of Bcl-xL is superimposed on one portion of the channel, sitting over the apolar tails of the ceramide molecule at the end of one of the columns. B. A pair of ceramide columns in an anti-parallel orientation. Each column consists of 6 ceramide molecules connected by a network of hydrogen bonds (yellow). The amide linkage in the ceramide molecule is believed to be responsible for the major intermolecular hydrogen bond that connects the ceramide molecules. The twin hydroxyls and the bridging water molecules also form part of the hydrogen-bonding network. This image is reproduced from (155).

1.1.3.4 Structure of ceramide channels

A model of the ceramide channel is illustrated in Fig 1.6 (79–81). The channel is doughnut-shaped forming a 10-nanometer diameter pore. This is the typical size determined experimentally. This model consists of 48 ceramide columns. Each ceramide column is composed of six ceramide molecules, the length of which is sufficient to span the hydrophobic part of the membrane. The

inner surface of the channel is composed of the hydrophilic head of the ceramide molecules and the two hydroxyl groups form a hydrogen bonded network with water molecules in the channels. In contrast, the hydrophobic tails embed into the phospholipid bilayer. The six ceramide molecules are held together by intermolecular hydrogen bonding. The carbonyl oxygen of a ceramide molecule forms a hydrogen bond with the amide hydrogen of its adjacent ceramide. This interaction is similar to that of the alpha helix in proteins. This hydrogen bonding between ceramide molecules forms a dipole moment. The alignment of these dipoles parallel to the axis of the column causes a net dipole moment from the free carbonyl at one end of the column to the free amide at the other end. The columns are organized in antiparallel fashion to achieve favorable dipole-dipole interactions between columns. In addition, each ceramide molecule forms C1-C1 and C3-C3 hydroxyl-hydroxyl interactions with adjacent ceramide molecules linking the columns together.

Molecular dynamic (MD) stimulations provide support for the stability of this structure (80). These also reveal how the structural properties of the ceramide molecule affect the channel's shape. In general, the local curvature of a lipid is due to the size ratio of the head group of the lipid to its hydrophobic region. If the ratio is close to one, the curvature will be zero and the lipid will form a planar membrane. If the ratio is bigger than 1, the lipid will generate a positive curvature. If the ratio is smaller than 1, the lipid generates a negative. From the MD simulations, the ceramide molecule in the channel takes the shape of a forceps; the hydrophilic head is the hinge and the two hydrophobic tails are

the two arms. Therefore, the curvature is negative and positive in the plane of the membrane and along the axis of the channel, respectively. This forms a doughnut-shaped channel and an hourglass conductive pathway. As the channel is embedded in the phospholipid membrane, the phospholipids cover the acyl chains of the ceramides at the end of the channel to avoid unfavorable high-energy exposure to the aqueous solution. The interfacial phospholipids curve toward the channel and the ceramides curve toward the phospholipids thus forming a continuous polar surface interfacing with the water phase.

1.1.3.5 Regulation of ceramide channels

Factors involved in the apoptotic process are tightly regulated. Therefore, the formation of ceramide channels in the MOM must be tightly regulated in several ways (82). First, cell regulates the formation of ceramide channels by controlling the ceramide level in the MOM. The formation of ceramide channels is sensitive to the ceramide level in the MOM (77). Cells keep the level of mitochondrial ceramide low. The level only increases in the MOM after the apoptotic signal is delivered (58, 83, 84). The steady level of mitochondrial ceramide would be affected by the activity of mitochondrial enzymes involved in the de novo pathway (ceramide synthase) or hydrolysis pathway (ceramidase) (75, 76). Indeed, cells overexpressing sphingomyelinase targeted to mitochondria undergo apoptosis and release of cytochrome *c* (83). In addition, the cell regulates the formation of ceramide channels through the Bcl-2 family proteins. Antiapoptotic proteins, Bcl-xL, Bcl-2 and CDE-9 (the Bcl-2 homolog of Caenorhabditis elegans), were found to inhibit or reverse the

ceramide-induced MOMP in isolated rat mitochondria (17). In contrast, Bax, a proapoptotic protein, was found to increase MOMP with ceramide synergistically (85).

Although antiapoptotic proteins inhibit ceramide-induced MOMP, it is unclear whether the antiapoptotic proteins interfere with the MOMP directly or indirectly. The antiapoptotic proteins may reduce the MOMP by binding to the endogenous apoptotic proteins, such as BAK, in isolated rat mitochondria. However, the ability of Bcl-xL to reduce MOMP was also observed in mitochondria isolated form yeast, which lacks Bcl-2 family proteins (17). Therefore, in this case the reduction of MOMP by Bcl-xL is not due to the neutralization of other proapoptotic proteins known to bind to Bcl-xL. This result cannot eliminate the possibility that Bcl-xL may interact with other components in the isolated mitochondria and interfere with MOMP. However, Bcl-xL is able to disassemble ceramide channels in pure phospholipid/cholesterol membranes (17). This indicates that Bcl-xL regulates the ceramide channels in the MOM directly. Moreover, the Hill coefficient of Bcl-xL preventing the MOMP is 1 (17). This suggests that Bcl-xL regulates the ceramide channel in an uncooperative manner and a ceramide channel is disassembled by a single monomeric Bcl-xL.

Both activated Bax and ceramide are each able to cause the permeabilization of the MOM or a phospholipid membrane. However, combinations of Bax and ceramide increase MOMP to a much higher level than the combined level of permeability caused by Bax alone and ceramide alone

(85). This suggests that activated Bax stabilizes the structure of ceramide channels or somehow these act synergistically.

1.1.3.6 Studies of the molecular mechanism by which Bcl-2 family proteins regulate ceramide channels

So far ceramide and its analogs are unique in their ability to form large stable lipid channels. Thus it is not surprising to learn that the regulation of lipid channels by proteins is a new field. Ceramide analogs were used to probe the how the ability of Bcl-xL to inhibit ceramide channels is influenced by the molecular structure of ceramide. The analogs studies indicate that Bcl-xL interacts with the acyl chain of ceramide (81). Bcl-xL optimally inhibits channels formed by intermediated chain-length ceramide, such as C16- and C18- ceramide. The ability of Bcl-xL to inhibit channel formation declines obviously when the length of the acyl chain is longer or shorter than that of C16 or C18 ceramide. In addition, small chemicals (ABT-737, ABT-263, and 2-methoxyantimycin A3), known to bind to the hydrophobic groove of Bcl-xL, interfere with the ability of Bcl-xL to inhibit ceramide-induced MOMP. These results suggest that Bcl-xL regulates the ceramide channels through binding of the hydrophobic tails of ceramide by its hydrophobic groove. Furthermore Bcl-xL needs to be bound to a membrane, because truncated Bcl-xL, lacking its transmembrane domain, is unable to reduce the ceramide-induced MOMP (17). Using this information, the structural model of the channel and a 1:1 interaction between Bcl-xL and the channel, Perera and Colombini proposed a molecular mechanism to explain how Bcl-xL disassembles the ceramide channels in the

MOM (81). Bcl-xL displaces the phospholipids covering the acyl chains of ceramide at the end of one of the columns. This displacement removes the influence of the phospholipids on that ceramide column causing it to relax into a form with less curvature. This column will be mismatched relative to the acyl chains of the adjacent columns resulting in a conformational stress that propagates throughout the structure through the hydrogen-bonded network. This is equivalent to the conformational propagation in an allosteric interaction. This stress destabilizes the channel structure and results in channel disassembly because the channel is in dynamic equilibrium with ceramide monomers and non-channel-forming aggregates.

1.2 Voltage-gated channels

Voltage-gated channels are transmembrane proteins whose permeability is dependent on the membrane electrical potential. While the channel is opened, water-soluble molecules or ions can passively cross the membrane down their electrochemical potential gradient. A change in the membrane potential results in a change in the probability of a typically charged voltage sensor domain (VSD) within the channel to move through the electric field resulting in a conformational change. This conformational change is the opening or closure of the channel. These channels have evolved to both control and respond to changes in the membrane potential. Most voltage-gated channels are found in the plasma membrane of excitable cells, such as neurons and muscles (86, 87). Voltage-gated sodium/potassium/calcium channels are typically found in the plasma membrane and are important in the formation and

propagation of action potentials and the secretion of hormones and neurotransmitters. Voltage-gated channels are also found in other types of membranes and cells, such as bacteria (88) and viruses (89), and intracellular organelles (90). For example, voltage-gated calcium channels allow Paramecium to regulate swimming direction and circumvent obstacles (91). VDAC channels, abundant proteins in the MOM, regulate the flux of metabolites across the MOM. However, the role of voltage-gated channels in bacteria is largely unclear (92).

Chapter 2: Materials and Methods

2.1 Purification of recombinant proteins

2.1.1 Construct Bcl-xL mutants

A full-length construct of human Bcl-xL in the pGEX2T vector (Amersham Pharmacia Biotech), which includes ampicillin-resistance, was a gift from Dr. Marie Hardwick. All single mutations of Bcl-xL were introduced using the QuickChange Site-Directed Mutagenesis procedure (Stratagene) outlined below unless noted. PCR was performed with 0.5 μM primers, 0.2 mM dNTPs, 1 ng/μl Bcl-xL/pGEX2T, and 50 mU/μl U PfuUltra (Agilent Technologies). Each PCR product was treated with 0.4 U/μl DpnI (New England BioLabs) at 37^{o}C for 1 hour. 5 μl of aliquot was transformed into Z-competent cells (Zymo Research) and then the cells were plated on LB with 100 μg/ml ampicillin, incubated at 37 ^{o}C overnight. A single colony was inoculated into 10 ml LB medium with 100 μg/ml ampicillin and incubated at 37 ^{o}C overnight. Each construct was isolated with GeneJet Plasmid Mimprep Kit (Thermo Fisher Scientific) and verified by DNA sequencing.

2.1.2 Purification of human full-length Bcl-xL and its mutants

The expression and purification of full-length Bcl-xL were previously described (93) and modified (81). In brief, a glutathione S-transferase (GST) tag was fused to the N-terminal of human full-length Bcl-xL with a thrombin cleavage site between the tag and Bcl-xL. The fusion protein was expressed in

Table 1 Primers used to produce Bcl-xL mutants (codon and base mutated are underlined and bold, respectively)

Mutant		Primer sequence 5' to 3'
E96L	Forward	GGGAGGCAGGCGAC**CT**GTTTGAACTGCGGT
E96L	Reverse	ACCGCAGTTCAAA**CAG**GTCGCCTGCCTCCC
F97Q	Forward	GAGGCAGGCGACGAG**CAG**GAACTGCGGTACCGG
F97Q	Reverse	CCGGTACCGCAGTTC**CTG**CTCGTCGCCTGCCTC
F100L	Forward	CGAGTTTGAACTG**CT**GTACCGGCGGGCAT
F100L	Reverse	ATGCCCGCCGGTA**CA**GCAGTTCAAACTCG
F105Q	Forward	GCGGTACCGGCGGGCA**CAG**AGTGACCTGACATC
F105Q	Reverse	GATGTCAGGTCACT**CTG**TGCCCGCCGGTACCGC
V126Q	Forward	GCATATCAGAGCTTTGAACAG**CAG**GTGAATGAACTCTTCCGGGAT
V126Q	Reverse	ATCCCGGAAGAGTTCATTCAC**CTG**CTGTTCAAAGCTCTGATATGC
V126W	Forward	AGCATATCAGAGCTTTGAACAG**TGG**GTGAATGAACTCTTCCGGGATG
V126W	Reverse	CATCCCGGAAGAGTTCATTCAC**CCA**CTGTTCAAAGCTCTGATATGCT
F146A	Forward	GTGGCCTTTTTCTCC**GC**CGGCGGGGCACTGTGC
F146A	Reverse	GCACAGTGCCCCGCC**GC**GGAGAAAAAGGCCAC
Y195A	Forward	GGGATACTTTTGTGGAACTC**GCG**GGGAACAATGCAGCAGCCGA
Y195A	Reverse	TCGGCTGCTGCATTGTTCCC**CGC**GAGTTCCACAAAAGTATCCC

a bacterial system and then isolated by using glutathione-agarose beads, which bind the GST tag. Adding biotinylated thrombin to the GST column results in the release of full-length Bcl-xL, while the GST tag remained in the GST column. The biotinylated thrombin was removed by using streptavidin beads.

The construct of Bcl-xL and its mutants was transformed into BL21 (DE3) pLysS competent cells and plated on LB/agar plates with 100 μg/ml ampicillin, following the *E. coli* Competent Cells: Multiple-Use protocol from Promega. One colony was inoculated into 50 ml seed culture and shaken at 37 ^{o}C overnight. The seed culture was inoculated into 1L LB with 100 μg/ml ampicillin and shaken at 37 ^{o}C until OD reached around 0.6. Then 10 μM Isopropyl β-$_{D}$-1-thiogalactopyranoside (IPTG) was added and shaking

continued for two hours. Cells from 4 L of culture were harvested by spinning at 5,000 g at 4 ^{o}C for 20 minutes (JS-4.2 rotor) and then were resuspended into 30 ml phosphate buffered saline (PBS) with 1% Triton-X100 and 36 μM phenylmethylsulfonyl fluoride (PMSF). The resuspended cells were stored at -20 ^{o}C.

To isolate the Bcl-xL and its mutants, the cells were thawed and shaking with 167 U/ml lysozyme resumed at 4 ^{o}C for 20 minutes. Cells were lysed by three passages through a French Press using 1,000 Psi. The following steps were performed at 4 ^{o}C. The lysate was spun at 100,000 g for 30 minutes by 50Ti rotor to remove cell fragments and debris. The supernatant was filtered through a 0.2 μm filter to remove particles that may clog the column. Then the supernatant was gently shaken with 5 ml glutathione agarose beads (Thermo Fisher Scientific), which were pre-equilibrated with PBS buffer, for two hours. The beads were packed into a column, washed with at least 10 column volumes (50 mL) of PBS buffer with 36 μM PMSF and then at least 10 column volumes (50 mL) of 20 mM Tris-HCl, pH8. After the washing process, the beads were gently shaken with 10 ml of 20 mM Tris-HCl, pH 8.0 containing 5 U of biotinylated thrombin overnight. The beads were packed into a column, the flow through was collected, and 1.5 ml of 20 mM Tris-HCl, pH 8.0 was added to replace the void volume of the column. The biotinylated thrombin in the aliquot was removed by gently shaking with 80 μl streptavidin beads (Thermo Fisher Scientific), pre-equilibrated with 20 mM Tris-HCl, pH 8.0, for 30 min. The streptavidin beads were removed by spinning at 500 g for 5 min. The protein

with 10 %, v/v glycerol was passed through 0.2 μm filter. Then 100 μl aliquots of the final product were rapidly shell-frozen in an ethanol-dry ice bath and were stored in -80 ^{o}C. BCA assay was used to determine the concentration of Bcl-xL and its mutants.

2.1.3 Purification of human Bax

The purification of human Bax was previous described (34) and modified (85, 94). In brief, the construct of human Bax/pTYB1, a gift from Dr. Richard Youle, expressed human Bax with a C-terminal intein tag. The intein tag allows the fusion protein to bind to chitin beads and the tag can be removed by addition of DTT (dithiothreitol). This results in a one column purification of human Bax.

The construct was transferred into BL21 (DE3) pLysS competent cells and plated on LB/agar plates with 100 μg/ml of ampicillin. A few colonies were inoculated into 40 ml of Terrific Broth medium and shaken at 37 ^{o}C until the OD reached 0.6 – 0.8. The culture was inoculated into 2 L of Terrific Broth medium (1 L medium in 2 L flask). When the OD reached 0.6, the cell culture was shaking with 1 mM IPTG for 3 hours. Then the cells were sedimented by spinning at 5,000 g (JS-4.2 rotor) at 4 ^{o}C for 20 min and resuspended in resuspension buffer (20 mM Tris-HCl, pH 8.0, 5 mM EDTA, and 500 mM NaCl). The resuspended cells were stored in -20 ^{o}C.

The procedure for cell lysis was the same as that described for the purification of human Bcl-xL except that no detergent, protease inhibitors, and lysozyme were added. In brief, the cells were lysed with a French Press and the

soluble proteins were obtained by centrifugation. The soluble proteins were then applied to a 3 ml chitin column ((New England BioLabs), at 4 ^{o}C, which was pre-equilibrated with TEN buffer (20 mM Tris-HCL, pH 8.0, 1 mM EDTA, and 500 mM NaCl). The chitin column was washed with 20 column volumes to remove unbound proteins. The column was flushed with 3 column volumes of TEN buffer with 30 mM DTT and was incubated at 4 ^{o}C for 48 hours to release the Bax. Bax was eluted by addition of 3 column volumes of TEN buffer. To remove the NaCl, EDTA, and DTT, Bax was dialyzed with 6,000 – 8,000 MW cut-off dialysis membrane against 3 L of 10 mM Tris-HCl, pH 8.0, 1 mM EDTA overnight followed by 5 L of 10 mM Tris-HCl, pH 8.0 overnight. After addition of glycerol (final concentration, 10 %, v/v), 100 μl aliquots of final product were shell-frozen in ethanol-dry ice bath and were stored in -80 ^{o}C. The protein concentration was determined by the BCA assay.

2.1.4 Purification of t-Bid

Full length Bid was engineered into pGEX4T1 vector. A GST tag was added to the N-terminal of Bid with a thrombin cleavage site between the tag and Bid. However, when cells undergo apoptosis, Bid is cleaved by caspase-8 to yield the C-terminal active fragment. This is known as truncated Bid (t-Bid). Therefore, a thrombin cleavage site was introduced to mimic the caspase-8 cleavage site. In this way, one is able to obtain both fragments of Bid with one enzyme (thrombin) reaction. This construct was a gift of Dr. Donald D. Newmeyer.

The purification was previously described (15, 95) and modified (85). In brief, the construct of full length of Bid was transformed into BL21 (DE3) pLysS and inoculated into 100 ml LB medium with ampicillin. When the OD reached 0.6, 0.4 mM IPTG was added and shaking resumed for 3 hours at 37 ^{o}C. The cells were spun and resuspended in PBS buffer with 1 mM EDTA, and 500 mM NaCl. Then 5 μl lysozyme was added and shaking at 4 ^{o}C for 30 minutes. After 3 passages through the French Press to lyse the cells, Triton-X100 was added (final concentration was 0.1 %) and shaking resumed at 4 ^{o}C for 15 more minutes. After spinning, the supernatant was filtered and shaking with 1 ml GST agarose beads at 4 ^{o}C overnight. The beads were spun at 500 g for 5 minutes at 4 ^{o}C, washed with 50 ml PBS buffer, and spun again. The beads were transferred to a column and washed with 10 ml PBS. The beads were resuspended in 0.5 ml PBS and were shaken with 10 U biotinylated thrombin at 4 ^{o}C overnight. The next morning, 3.5 ml of protein was collected and the thrombin was removed by using 70 μl of streptavidin beads. The supernatant was transferred to an 8,000 D MW cut-off dialysis bag and dialyzed against 5 L 50 mM Tris-HCl, pH 8.0 at 4 ^{o}C overnight. The concentration of the final product was determined by the BCA assay, and aliquots were shell-frozen in ethanol and dry ice bath, and stored at -80 ^{o}C.

2.2 Binding of ceramide to Bcl-xL

Because ceramide is insoluble in water, in an aqueous environment once bound it is unlikely to dissociate. Therefore an equilibrium binding experiment is not possible. We developed a fluorescence competition assay to look for

specific binding. In brief, fluorescently-labeled ceramide was dispersed into a solution containing Bcl-xL. Since ceramide is insoluble, ceramide not bound to Bcl-xL forms micelles. The density of the micelles is less than that of the aqueous solution and this difference was increased by using sucrose. Therefore, the fluorescent ceramide micelles were removed by centrifugation. The fluorescence of the subphase was recorded. The details of the assay are described below.

The excitation and emission wavelength of fluorescently-labeled ceramide (C11 TopFluor ceramide; Avanti Polar Lipids) in isopropanol is 490 nm and 504 nm, respectively. The fluorescently-labeled ceramide was stored at -20 ^{o}C. Before the binding assay, the concentration of fluorescently-labeled ceramide was determined by the standard curve (Em_{504} = 2.63 x 10^6 C+ 3.07 x 10^4) and the concentration of wild type Bcl-xL and its mutants was adjusted to 1.8 µM with 20 mM Tris-HCl, pH 8.0 (650 µl per sample). Nine microliters of 42 µg/ml fluorescently-labeled ceramide were dispersed to 590 µl containing 1.8 µM Bcl-xL wild-type or its mutants in 20 mM Tris, pH 7.4, 10% sucrose. The dispersal was performed by slow delivery of the ceramide solution into the protein solution while it was being vortexed (around 25 seconds). Entrainment of air was carefully avoided. In order to remove ceramide micelles, 50 µl of 20 mM Tris, pH 7.4, 5% sucrose was applied to the top of the mixture to produce a density gradient. Then the gradient was spun in MLA-130 at 55,000 rpm (around 140,000 g) at 25^{o}C for 30 min. 50 µl of the upper layer containing ceramide micelles was removed. 200 µl of the subphase was taken out by using

a gel loading tip to avoid contamination of ceramide micelles. The subphase was excited by 490 nm incident light and the emission spectrum from 495 to 520 nm was recorded in a FluoroMax-4. The fluorescence was not detected in the non-protein controls, so all fluorescence was due to ceramide associated with protein. The fluorescent quantum yield of the bound ceramide was varied depending on the protein used. Thus, in order to assess the amount of ceramide bound, a portion of the fluorescent solution was mixed with the same volume of isopropanol (to denature the protein and extract the ceramide) and spun at 18,000 g at 4℃ for 40 min. The emission spectrum of the supernatant was recorded.

2.3 Detection of mitochondrial outer membrane permeability

2.3.1 Isolation of rat liver mitochondria

Mitochondria were isolated from the liver of male Sprague Dawley rats as described originally (96) and as modified (81). A rat was fasted with water *ad labitum* overnight. All buffers needed were promptly thawed and keep on the ice. It is important that all the containers were pre-rinsed with buffer used and kept at ice cold to ensure the quality and integrity of purified mitochondria. 1.5 g fatty-acid depleted BSA was gently scattered on the top of 300 ml H buffer (5 mM HEPES, pH 7.5, 0.1 mM EGTA, 210 mM Mannitol, and 70 mM Sucrose) and waited until the BSA dissolved without stirring. Once BSA has dissolved, the solution was swirled to avoid making bubbles.

The rat was anesthetized with carbon dioxide and sacrificed by decapitation using a guillotine. The liver was excised and soaked in 100 ml H buffer with 0.5 % BSA (HB buffer). To remove the blood in the liver, the liver was chopped with scissors into small pieces and washed with H buffer with 0.5 % BSA. The liver was homogenized with H buffer with 0.5 % BSA by two passes of a motorized Potter-Thomas Teflon-glass homogenizer. The mitochondria were then isolated by differential centrifugation and all the following steps were performed at 4 ^{o}C. The homogenate was split into four centrifuge tubes and filled up with HB buffer. The tubes were spun at low speed (2,250 rpm in an SS-34 rotor; 605 g) for 10 minutes. The supernatant was transfer to a new tube and spun at high speed (8,750 rpm in an SS-34 rotor; 9,150 g) for 10 minutes. The supernatant was discarded. The fat and other contaminants attached on the walls of the tubes were wiped out by a Kimwipe. A Pasteur pipette without the capillary tip was used to gently resuspend the pellet with a small amount of HB buffer. Red blood cells and lysosomes might be left in the center of the pellet. The pellet was gently and carefully resuspended without disturbing any blood cells and lysosomes. The suspensions were combined to two centrifuge tubes. Then these two tubes were spun at low speed and the supernatant was transferred to new tubes. The supernatant was spun at high speed and the pellet was gently resuspended into small amount of H buffer using a blunted Pasture pipette. The isolated mitochondria were kept on ice. The animal use protocols were approved by the Institutional Animal Care and Use Committee. The animals were euthanized by a procedure

consistent with the Panel on Euthanasia of the AVMA (American Veterinary Medical Association). The animal facility used to house the animals is accredited by AAALAC (Association for Assessment and Accreditation of Laboratory Animal Care).

The concentration of mitochondrial protein was measured as previously describe (97). 500 ml of 1/20 dilution of the isolated mitochondria was mixed with 500 ml of P buffer (100 mM Tris-H_2SO_4, 0.4 % SDS, pH 8.0) and the absorbance read at 280 nm and 310 nm. The concentration was given by $40 \times \frac{(A_{280}-A_{310})}{1.05}$. Typically the concentration was 5 - 12 mg/ml.

2.3.2 Cytochrome c accessibility assay

The cytochrome *c* oxidation assay is used to monitor the permeability of isolated mitochondria to proteins. Reduced cytochrome *c* is added to isolated mitochondria. If it could cross the outer membrane, it would be oxidized by the cytochrome *c* oxidase on the inner membrane. If the mitochondria are intact, the oxidation rate is minimal. If the outer membrane is damaged, the oxidation rate is the maximum. After ceramide channel formation, the oxidation rate is somewhere between the maximum and background (17, 81). This indicates the rate of the cytochrome *c* crossing the MOM is the rate-limiting step. The initial rate of oxidation is a measure of the permeability of the MOM. It is also an indication of the size and the number of ceramide channels that formed.

Before performing the assay, reduced cytochrome *c* needs to be prepared. 5 mM horse-heart cytochrome *c* (Sigma) was dissolved into 700 μl of

0.2 M Tris-HCl, pH7.5 (J buffer) and then excess of ascorbate was added (final concentration, 97 mM). The reduced cytochrome *c* and ascorbate was separated by Sephadex G-10 gel-filtration column, which was pre-equilibrated with J buffer. After the mixture was loaded into the column, the column was wash with J buffer and the flow rate was 0.5 mL per minute. Because reduced cytochrome *c* is red, the red fraction was collected. The concentration of reduced cytochrome *c* was determined by spectrophotometry (ε_{550} = 18.5 $mM^{-1}cm^{-1}$) (98). Then the concentration was adjusted to 1.5 mM with J buffer and aliquotted. To prevent oxidation, the aliquots were flushed with argon, wrapped with Parafilm, and store at -20 ^{o}C.

The cytochrome *c* accessibility assay is performed as described (99) and modified (11, 17, 81). Mitochondria were isolated and used on the same day. They were kept on ice at high concentration and diluted prior to use. For each run (around 18 reactions), dilutions were freshly prepared. They were 1.0 ml of 0.25 mg/ml mitochondria in FH buffer (280 mM mannitol, 0.1 mM EGTA, 5 mM HEPES, pH 7.4). They were kept on ice. Typically, 50 µl of 0.25 mg/ml mitochondria was resuspended 650 ml of room temperature H* buffer (160 mM mannitol, 60 mM KCl, 0.1 mM EGTA, 5 mM HEPES, pH 7.25, 1.3 µM antimycin A, and 500 mM dinitrophenol). Then 50 µl of Bcl-xL was mixed into the suspension. After 5 minutes incubation at room temperate, 10 µl of 1 mg/ml ceramide (dissolved in isopropanol) was dispersed. The dispersal was performed by slow delivery of the ceramide solution into the protein solution, while it was being vortexed (around 25 seconds). Entrainment of air was

carefully avoided. 15 μl of reduced cytochrome *c* was added to the mixture. The sample was immediately inverted three times to mix and the absorbance at 550 nm was recorded. Because the sensitivity of the mitochondria to ceramide might be variable, the concentration of mitochondria (0.25 – 0.5 mg/ml), the amount of ceramide (5 μl – 20 μl of 1.0 mg/ml), and the concentration of Bcl-xL (10 nM – 100 mM) used needed to be adjusted in the beginning of the assay.

2.3.3 Release of adenylate kinase

The adenylate kinase assay measures the release adenylate kinase, 24 kDa protein, from the intermembrane space of mitochondria and determines the percentage of permeable mitochondria. The assay is a coupled-enzyme assay. In brief, ADP is converted to ATP by adenylate kinase. Then hexokinase converts ATP and glucose to ADP and glucose-6-phosphate, which is eliminated by glucose-6-phosphate dehydrogenase and produces NADPH. All reaction components are in excess, except adenylate kinase. Therefore, this allows one to determine the amount of adenylate kinase released.

The adenylate kinase assay was performed as previously described (100) and modified (11). Typically 24 adenylate kinase assays of Bax working solution (5 ml) were prepared. The Bax working solution was 15 nM Bax and 36 nM t-Bid in high salt FH buffer (5 mM HEPES, pH 7.4, 0.1 mM EGTA and 150 mM KCl). The Bax working solution was incubated at room temperature for 10 minutes to active Bax. Then 5 μl of Bcl-xL at the desired concentration was added to 200 μl of Bax working solution. At the same time, freshly prepare

a mitochondria working stock of mitochondria (10 ml of 160 μg/ml mitochondria with FH buffer (280 mM mannitol, 0.1 mM EGTA, 5 mM HEPES, pH 7.4). To form Bax channels, 300 μl of the mitochondria working stock was mixed with the protein mixture and incubated at 37 ^{o}C water bath for 30 minutes (60 mM KCl final). The mitochondria were sedimented at 14,000 g for 5 minutes at 4 ^{o}C and kept on ice. The supernatant containing the released adenylate kinase was kept on ice.

Because the ADP containing a little bit of ATP, 6 μl of 5 units of hexokinase and 5 units of glucose-6-phosphate dehydrogenase were incubated with 350 μl AK buffer (5 mM $MgSO_4$, 10 mM glucose, 5 mM ADP, 0.2 mM NADP, 50 mM Tris-HCl, pH 7.5) for 3 minutes prior to the assay to cover the remaining ATP to ADP. After the incubation, 150 μl of supernatant containing the release of adenylate kinase was added and absorbance of 340 nm was immediately recorded for 5 minutes. The initial slope of increase in absorbance was used as a measure of the amount of released adenylate kinase.

2.3.4 Statistics for all studies except the whole-cell experiments

The results are reported as the mean ± S.E. (standard error) of at least 3 independent experiments. Significance was determined by using the Student's *t*-test. Single, double, triple and quadruple symbols, indicate significance with P-values < 0.05, < 0.01, <0.001 and <0.0001 respectively.

2.4 Molecular dynamic simulations

The structure of full-length Bcl-xL-ceramide assembly was based on the published model from molecular dynamic (MD) studies (81) that were performed using the crystallographic structure of the Bcl-xL/Bim fragment complex (PDB ID: 1PQ1). In the experimental setting, the N-terminal part of Bcl-xL is preceded by a few extra amino acids (GSPRRS) inherited after thrombin cleavage. To better match with the experiments, we attached this fragment to N-terminus of Bcl-xL (however being so remote from the ceramide binding site, this modification should not have any significant effect). Fragments of Bcl-xL, unresolved in the crystal structure (residues 29 to 77) as well as the added N-terminal fragment were modeled using Robetta (101). N- and C-termini of the final Bcl-xL structure were modeled in the dissociated state.

The complete system (96080 atoms) contained 3686 protein atoms (239 residues), 106 atoms of C16-ceramide (one residue), and 2392 atoms of $_{D}$-mannitol (92 residues – matching 160 mM mannitol in the experimental medium). To maintain the electroneutrality of the system K^+ and Cl^- ions were added up to an equivalent of 60 mM salt concentration, 43 K^+ and 34 Cl^-. Assembly of the simulation system, introduction of the single mutations into the Bcl-xL structure (see chapter 3), analysis of the results and visualization were performed in VMD v1.9 (102) using custom-written Tcl scripts.

MD stimulations were done using the NAMD package (103). All the simulations were performed as an NPT ensemble using the CHARMM36 force

field (104) and TIP3P water model (105). Parameters for ceramide were taken from the previously published simulations (80). The acidic and basic residues of Bcl-xL were set in their default protonation state at pH 7.0 (estimated using PROPKA for neutral pH (106)). Langevin Dynamics (107, 108) was used to maintain constant pressure (1 atm) and constant temperature (295.15 ^{o}K). Periodic boundary conditions were maintained and the particle mesh used the Ewald method (109) with a real space cutoff distance of 1.2 nm and a grid width of 0.1 nm. Energy Minimization steps were performed using the steepest descent in the first 2000 steps and then a conjugate gradient in the subsequent 2000 steps. To attain the equilibrium, the system was subjected to gradual heating until it reached to 295.15 ^{o}K (22 ^{o}C), first with the protein backbone harmonically restrained (100 kcal/mol/nm^2 per backbone atom) to the initial coordinates for 1 ns, then simulated unrestrained for 30 ns.

2.5 Apoptosis induction in intact cells

2.5.1 Cell culture

Mouse embryonic fibroblast (MEF) Bcl-x-KO cell line was kindly provided by Dr. Chi Li (University of Louisville, Louisville, KY) (110). Cells were maintained in DMEM (Thermo Scientific, SH30243.01) containing 10% FBS (fetal bovine serum) (Thermo Scientific, SH30070.03) supplemented with 1X pen-strep (Gibco 15140-122). Cells were routinely tested to verify that they were free of mycoplasma infection.

2.5.2 Generation of cell lines

Full length human Bcl-xL cDNA and single point mutation Bcl-xL mutants (generated by using QuickChange II XL Site-Directed Mutagenesis kit from Agilent Technologies, # 200521-5 and verified by DNA sequencing) were cloned into the GFP (green fluorescent protein) expressing mammalian expression retroviral vector MIGRX EcoRI/XhoI to generate MIG-Bcl-xL or MIG-Bcl-mutant plasmids. MEF Bcl-xL-KO cells were infected with viruses expressing these mutants and infected cell populations were selected by sorting of GFP expressing cells by flow cytometry to generate stable cell lines. Presence of Bcl-xL WT and mutants in MEF-Bcl-xL-KO stable cell lines was confirmed by western blot as described below.

2.5.3 Western blot

Cell pellets were collected and lysed in NP-40 lysis buffer (Boston BioProducts, BP-119). Protein concentrations were determined using BCA protein assay reagent (Pierce #23223 and #23224). Twenty micrograms of protein samples were loaded on a 4-12 % Bolt Bis-Tris Plus gel (Life Technologies, BG04120BOX) and transferred to PVDF membrane (Bio-Rad, #162-0177). Membranes were blocked in TBS-T with 5 % milk for 1 hour at room temperature. Membranes were incubated overnight at 4°C with primary antibodies; anti-Bcl-xL (54H6) (Cell signaling, # 2764), anti-GFP (Abcam, ab6673) and anti-tubulin (Sigma Aldrich, #T5168) at 1: 20,000 dilutions. Anti-mouse and anti-rabbit peroxidases labeled secondary antibodies were added at a dilution of 1:40,000 for 1 hour at room temperature. Chemiluminescent

detection was performed using Pierce ECL Western Blot Substrate (Thermo Scientific, #32106).

2.5.4 Cell Viability Assay

MEF cells were cultured in 96- well plates (2,500 cells per well) overnight and then treated with different apoptotic stimuli at indicated drug concentrations for 24 hours. Cells were then incubated with 10% Alamar Blue reagent (Invitrogen, DAL1100) for 4 hours and the fluorescence of Alamar Blue reduction was determined using BioTek HT Synergy plate reader (540 nm excitation, 594 nm emission). Relative viability of treated cells was calculated by normalizing to vehicle treated cells. For bar graphs, relative cell viability was presented as normalized with respect to WT at that dose of a drug. Cisplatin (# 4394), Thapsigargin (# T9033), Etoposide (#, E1383) and Gemcitabine (#, G6423) were purchased from Sigma. Hydrogen peroxide was purchased from Fisher scientific (# H325-100). Doxorubicin (#,15007) was purchased from Cayman chemical company. Bortezomib was purchased from ChemieTek (#, CT-BZ001). All treatments were done in triplicate and each graph shown is a representative experiment of at least three biological replicates. Statistical analysis was performed using one-way ANOVA with Tukey's test. $p < 0.05$ was considered significant.

2.6 Permeabilization of planar phospholipid membranes

2.6.1 Preparation of E. coli extracts

The desired *E. coli* strain was inoculated in 40 ml Terrific Broth medium without antibiotics and shaken at 37 ^{o}C overnight. The overnight culture was transferred to 1 L Terrific Broth without antibiotics and shaken until an OD of 1.4 was reached. After sedimentation of the cells by centrifugation (5,000 g, JS-4.2 rotor), the cells and the culture medium were collected. Cells were resuspended in 30 ml of 100 mM NaCl, 50 mM Tris, pH 7.3. The resuspended cells were aliquotted and stored at -20 ^{o}C.

Five mL of resuspended cells were thawed. Protease inhibitors, including PMSF (36 μM in final concentration) and complete EDTA free protease inhibitor (Roche), were added. Cells were lysed by two passages through a French Press. To remove the unbroken cells, the lysate was spun at 8,500 g for 20 minutes. The cell-free solution was spun at 180,000 g (MLA-130) for one hour to separate the soluble fraction from particulates like membrane vesicles. The pellet fraction was shaken with 5 ml of 50 mM Tris, pH 7.3, 2 % n-laurylsarcosine (w/v), and protease inhibitors at room temperature for two hours to dissolve inner membrane proteins. The mixture was spun at 180,000 g (MLA-130) at 4 ^{o}C for four hours. The supernatant containing the proteins in the inner membrane was collected. The pellet was shaken with 1ml of 50 mM Tris, pH 7.3 and 33 mM octyl-glucoside at 4 ^{o}C overnight.

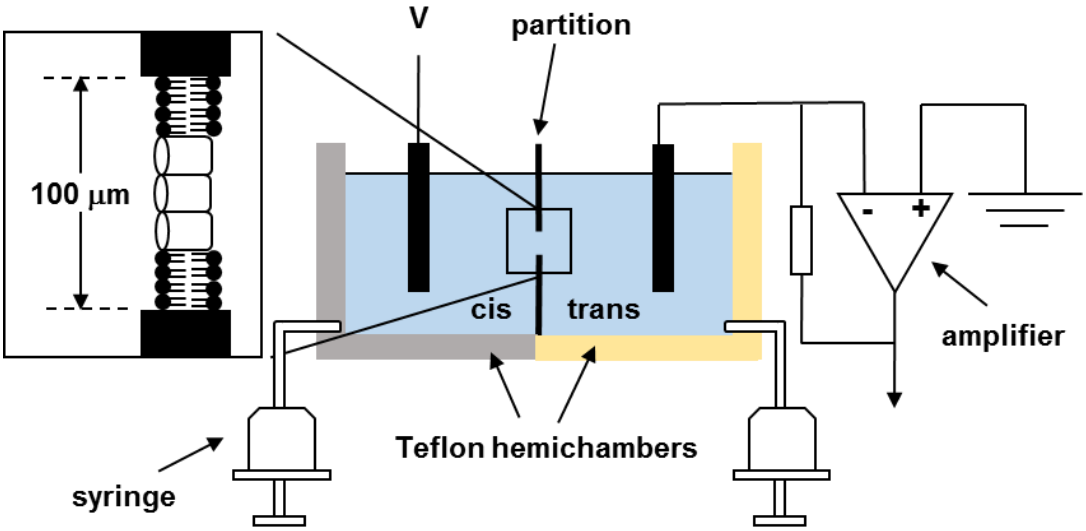

Figure 2.1. Schematic presentation of planar phospholipid membrane setup. Two Teflon hemi-chambers are separated by a PVDC partition. The *tans* side is maintained at virtual ground by the amplifier. The aqueous levels can be adjusted by the syringes.

The mixture was spun at 180,000 g at 4 ^{o}C for one hour. The supernatant containing the solubilized proteins from the outer membrane was collected for further analysis.

2.6.2 Planar phospholipid membranes

Solvent-free planar phospholipid membranes were formed by the monolayer method as previously described (111, 112). Two Teflon hemi-chambers were separated by a thin and non-conducting polyvinylidene chloride (PVDC) partition containing a 100-µm diameter hole across which the membrane was formed (Fig 2.1). The area around the hole was coated with a thin layer of petrolatum using a 5 % petrolatum (w/v) in petroleum ether. The aqueous solutions generally consisted of 1.0 M KCl, 1 mM $MgCl_2$, 5 mM PIPES, pH 6.9. Monolayers were formed by layering 30 – 60 µl of the lipid

solution (0.5 % diphytanoyl phosphatidylcholine, 0.5 % asolectin (polar extract of soybean phospholipids) and 0.05 % cholesterol in hexane) on the surface of each aqueous solution. Once the hexane had evaporated the levels of the solutions were raised above the hole thus forming a phospholipid bilayer membrane across the hole. Calomel electrodes with saturated KCl bridges were used to interface with the aqueous phase. The electrode in *trans* side was virtually ground by the amplifier. Therefore, the potential applied to the *cis* side was the transmembrane potential.

The *E. coli* extracts were pretreated with 1 % ß-octylglucoside (w/v) for 10 min on ice and then 15 µl of the extracts was successively dispersed in 5 ml aqueous solution in *cis* side while stirring until a channel inserted. The membrane voltage was clamped using a high quality operational amplifier wired in the inverted mode with an adjustable feedback resistor (typically 10^8 Ω resistance was selected) and the current was recorded using a Digidata 1322A digitizer and Clamplex 10.3 software (Axon Instruments). The constant voltage (above -70 mV) helped the insertion or formation of channels. Once a channel formed, voltage ramps (-70 mV to 70 mV) were applied to investigate the behavior of the channels. This allowed for quantitating the rectification of all 3 channels together. Then a positive voltage (above 70 mV) was applied in order to close the channel 1. The same triangular ramp was applied resulting in channel 2 gating. In this recording for part of it channel 2 and channel 3 are open, and for the rest only channel 3 is open. A constant high voltage (above

70 mV) was applied to close channel 3 resulting in only channel 2 being open. This allowed a quantification of the rectification of channel 2 alone.

2.6.3 Data Acquisition, correction and calculation

Before the addition of *E.* coli extracts, the offset of voltage and current were adjusted or recorded. After the experiments, the electrode asymmetry was measured and recorded. These were used to make small corrections of the recordings. The conductance was plotted as the function of voltage. The rectification was quantitated as the slope of the conductance-voltage curve. All average data are presented as mean ± S.E. (standard error).

Chapter 3: Ceramide Channels: Destabilization by Bcl-xL and Role in Apoptosis

3.1 Abstract

Ceramide is a bioactive sphingolipid involved in mitochondrial-mediated apoptosis. Our data suggest that ceramides directly regulate a key initiation step in apoptosis: mitochondrial outer membrane permeabilization (MOMP). MOMP allows release of intermembrane space proteins to the cytosol, inducing the execution of the cell. Ceramides form channels in planar phospholipid membranes and outer membranes of isolated mitochondria, channels large enough to facilitate passage of proteins released during MOMP. Bcl-xL inhibits MOMP in vivo and inhibits the formation of ceramide channels in vitro. However, the significance of Bcl-xL's regulation of ceramide channel formation within cells was untested. We engineered Bcl-xL point mutations that specifically affect the interaction between ceramide and Bcl-xL to probe the mechanism of ceramide channel regulation and the role of ceramide channels in apoptosis. Using these mutants and fluorescently-labeled ceramide, we identified the hydrophobic groove on Bcl-xL as the critical ceramide binding site and regulator of ceramide channel formation. Bcl-xL mutants with weakened interaction with ceramide also have reduced ability to interfere with ceramide channel formation. Some mutants have similar altered ability to inhibit both ceramide and Bax channel formation, whereas others act differentially, suggesting distinct but overlapping binding sites. To probe the

relative importance of these channels in apoptosis, Bcl-xL mutant proteins were stably expressed in Bcl-xL deficient cells. Weakening the inhibition of either Bax or ceramide channels decreased the ability of Bcl-xL to protect cells from apoptosis in a stimulus-dependent manner. These studies provide the first in vivo evidence for the role of ceramide channels in MOMP.

3.2 Introduction

The release of mitochondrial intermembrane space (MIS) proteins into the cytosol is a key decision-making step in the apoptotic process. The released proteins initiate the execution phase of apoptosis via a series of steps that ultimately lead to the activation of caspases, specific proteases that lead to the transformation of the cell into apoptotic bodies that are engulfed by phagocytes. Various mechanisms exist by which proteins can be released from the MIS (77, 113–115). Some of these involve the formation of large channels in the mitochondrial outer membrane (MOM). Two such channels are formed by either the translocation to the MOM and oligomerization of a cytosolic protein called Bax or the self-assembly of a MOM lipid called ceramide (5, 11, 14, 116, 117). Bax is a member of the Bcl-2 family of proteins that regulate apoptosis (118–120). Both Bax and Bak are pore-forming proapoptotic members of this family. Ceramide is a pore-forming member of the sphingolipid family of cell lipids, some of which are involved in the apoptotic process (121). The functions of Bax, Bak and ceramide are interdependent in a number of ways. In some systems, the induction of apoptosis by ceramide requires the presence of Bax

(122, 123). The Bak protein is required for ceramide synthase-dependent long-chain ceramide synthesis during apoptosis (124). There is evidence for synergy between Bax and ceramide in MOM permeabilization (MOMP) in isolated mitochondria (85, 125).

The role of Bax in MOMP is well established (120), although the structure of the Bax channels is only poorly understood (126). Ceramide's role in inducing apoptosis is also widely acknowledged (127, 128), although its ability to directly form channels in the MOM is still viewed with skepticism. Published work strongly supports the ability of ceramide to form channels in the MOM at physiologically relevant concentrations (77). Ceramide forms large channels (typically 10 nm in diameter) in phospholipid membranes lacking proteins and these have been visualized by electron microscopy (78). It has also been shown to release a variety of MIS proteins from isolated mitochondria while not releasing matrix proteins (11). Functional studies (79) and molecular dynamic (MD) simulations (80) support a model of the ceramide channels that consists of barrel-like structure whose staves are membrane-spanning strings of ceramide molecules organized in an anti-parallel manner (Fig. 1.6). These thin-walled pores behave like elastic discs that can be deformed but will regain their natural structure after relaxation (129). Yet all evidence indicates (11) that they are in dynamic equilibrium with ceramide monomers or non-conducting ceramide assemblies. Thus, there is a great deal of dynamic motion and structural changes associated with these channels.

The formation of both Bax and ceramide channels is inhibited by the anti-apoptotic protein, Bcl-xL (17, 33). Whereas, it is generally agreed that Bcl-xL inhibits Bax channel formation by forming heterodimers with activated Bax monomers (33, 130), the mechanism by which Bcl-xL inhibits ceramide channels is not well understood. Since ceramide channels are large assemblies of ceramide monomers, there is no precedent to indicate possible mechanisms by which such a structure could be prevented from forming or be destabilized by a protein although a mechanism has been proposed (81). Experiments with ceramide analogs demonstrated that the hydrophobic tails of ceramide are important for the inhibition by Bcl-xL (81). In addition, small molecule inhibitors (2-methoxyantimycin A3, ABT-737 and ABT-263), known as BH3 peptide mimetics because they bind to a hydrophobic grove on Bcl-xL and thus block its ability to bind to Bax, were also found to inhibit the ability of Bcl-xL to inhibit the formation of ceramide channels in the MOM (81). These inhibitors interfere with the anti-apoptotic activity of Bcl-xL (44, 131, 132) suggesting that the ability of Bcl-xL to interfere with ceramide channel formation may somehow be linked to its anti-apoptotic function. Here we provide insight into the molecular basis by which Bcl-xL acts to inhibit ceramide channels by providing evidence for direct binding and using point mutations to identify the region on Bcl-xL responsible for the inhibition. These same Bcl-xL mutants were expressed in cells lacking Bcl-xL to assess the importance of ceramide channels in the in vivo apoptotic process.

3.3 Results

Previous studies demonstrated that Bcl-xL inhibits ceramide channel formation in isolated mammalian mitochondria (17, 81). In addition, the use of ceramide analogs indicated that the hydrophobic regions of ceramide are important for this action of Bcl-xL (81). To distinguish between direct and indirect action, it would be desirable to determine whether Bcl-xL binds a ceramide channel. However, direct binding studies are not possible because ceramide channels are in dynamic equilibrium with ceramide monomers (11) and thus cannot be isolated and purified. The possibility of examining the binding of Bcl-xL to ceramide channels formed in liposomes is also not feasible because Bcl-xL binds to membranes regardless of the presence of ceramide channels and current methods of generating ceramide channels in liposomes cause only partial release of contents indicating that only one channel is formed per liposome (73, 133). Thus any binding studies would be plagued by very low signal to noise ratios. An alternative method is to determine whether a ceramide molecule is capable of binding to Bcl-xL. The binding of a ceramide molecule to Bcl-xL may mimic the binding between Bcl-xL and ceramide channels.

3.3.1 Binding of ceramide to Bcl-xL

Binding studies between Bcl-xL and ceramide are complicated by the physical properties of ceramide. Ceramide is inherently insoluble in water and Bcl-xL cannot be expected to function normally in an organic solvent. Therefore, an equilibrium binding experiment is not possible. However, when ceramide dissolved in isopropanol is dispersed in an aqueous environment,

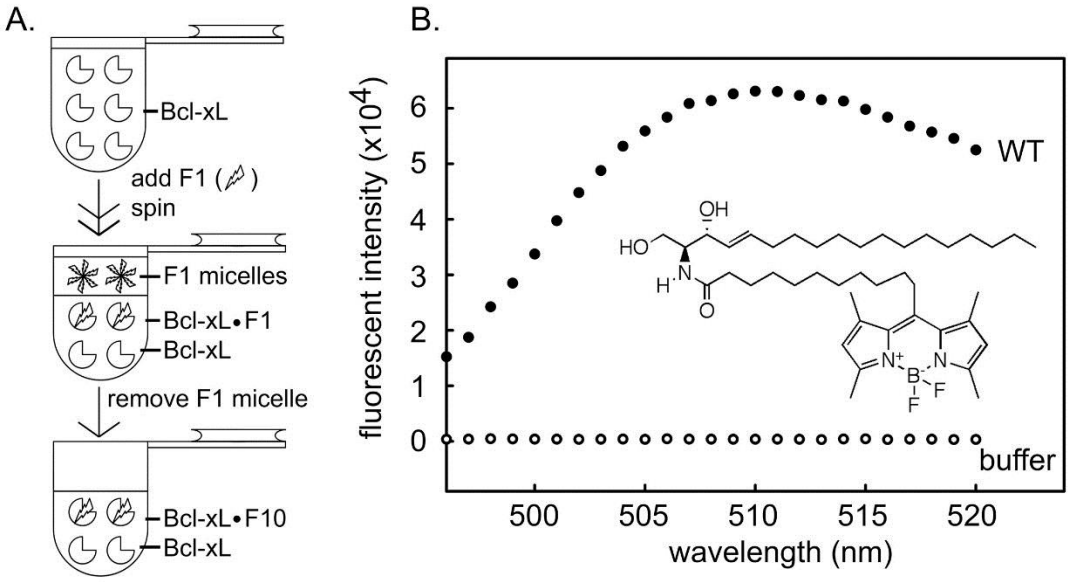

Figure 3.1. Fluorescently-labeled ceramide binds to Bcl-xL. A. Separation of fluorescently-labeled ceramide bound Bcl-xL from ceramide micelles. F1 is fluorescently-labeled ceramide: C11 TopFluor ceramide. B. Fluorescence spectrum of final sample from the separation shown in "A" (see methods for details). "WT" indicates the medium contained wild-type Bcl-xL and fluorescence was due to bound fluorescently-labeled ceramide. "buffer" indicates that there was no Bcl-xL in that separation procedure. The lack of fluorescence indicates that the procedure was effective at eliminating ceramide micelles. The inset is the structure of fluorescently-labeled ceramide.

ceramide molecules exist transiently in aqueous solution and these can either bind to Bcl-xL or combine with each other to form micelles. If the Bcl-xL/ceramide complex is formed it is unlikely to dissociate because of ceramide's insolubility in water. Thus the complex should be stable and can be detected. However, a binding constant cannot be determined. Thus fluorescently-labeled ceramide (C11 TopFluor ceramide) was dispersed into a solution containing Bcl-xL (Fig. 3.1A). Any fluorescent ceramide that does not bind must form micelles. The fluorescent ceramide micelles were removed by centrifugation taking advantage of the fact that the density of the micelles is

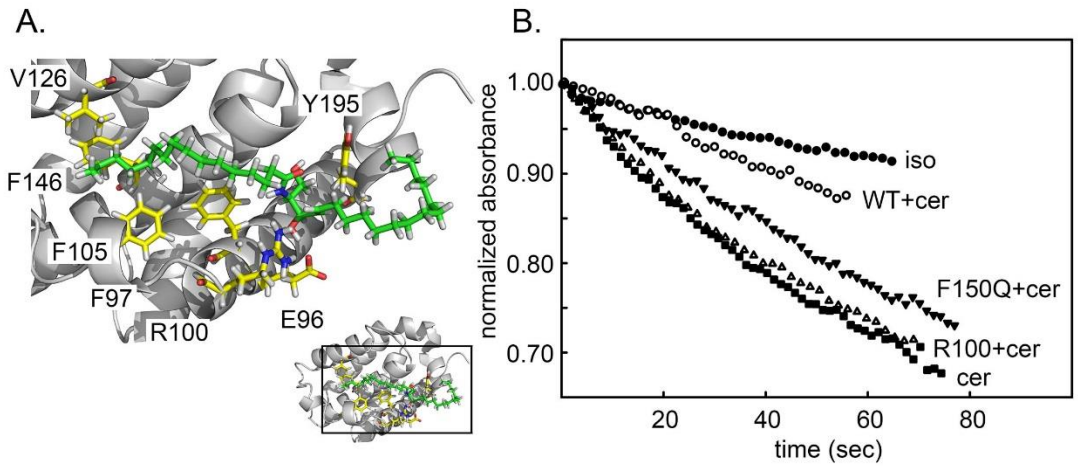

Figure 3.2. A. One docking pose of ceramide on the crystal structure of Bcl-xL. The amino acids to be mutated are illustrated (yellow). Ceramide is in green with the two chains specified. The ceramide amide linkage is in the middle with the amide nitrogen in blue and the carbonyl oxygen in red. The pose was obtained from the publication of Perera et al., 2012 (81). B. Permeabilization of the MOM to cytochrome *c* estimated by measuring the initial rate of oxidation of added cytochrome *c* (24.7 µM final). To 730 µL of 0.25 mg/mL rat liver mitochondrial suspension was added 15 µL of either isopropanol (iso) or C_{16} ceramide (cer). The results were normalized by the absorbance of cytochrome *c* at zero time. WT, F105Q, R100L indicated that mitochondria had been preincubated for 5 min with 47 nM wild-type Bcl-xL or the respective mutants.

less than that of the aqueous solution and this difference was increased by using 10 % sucrose. The fluorescence of the subphase was recorded. In the absence of Bcl-xL, the centrifugation cleared the solution of ceramide micelles resulting in no detectable fluorescence. However, in the presence of Bcl-xL substantial fluorescence was recorded (Fig. 3.1B). The results indicate that the ceramide molecule binds to Bcl-xL directly.

3.3.2 Determination of the location of the binding region on Bcl-xL

Previous studies showed that drug molecules that bind to hydrophobic groove on Bcl-xL (ABT-263 and ABT-737) interfered with the protein's ability

to inhibit ceramide channel formation (81). Thus this region of Bcl-xL is a good candidate for the putative binding site by which Bcl-xL inhibits ceramide channels. To identify residues in the hydrophobic groove that may be important in regulation of ceramide channels, molecular docking of a ceramide molecule to Bcl-xL was conducted and two low-energy modes were used (pose1 and 2) (81) (Fig 3.2A). Single amino acid substitutions were made so as to change the strength of the interaction at the putative docking sites. Changes in charge (E96L and R100L), polarity (F97Q, F105Q, V126Q), and physical volume (V126W, F146A, Y195A) were engineered into full-length Bcl-xL (Fig. 3.2A). These were tested in isolated mitochondria for their ability to interfere with ceramide channel formation.

As illustrated in Fig. 3.2B, the amount of reduced cytochrome *c* in the medium decreased as the added mitochondria oxidized the protein. The cytochrome *c* could only be oxidized if it could cross the outer membrane and bind to cytochrome *c* oxidase on the outer surface of the inner membrane. Thus the rate of oxidation of the cytochrome *c* is related to the degree of MOMP by ceramide channels. The baseline rate of oxidation occurred when the vehicle (isopropanol) was added to the mitochondria. When ceramide dissolved in isopropanol was dispersed into the mitochondrial suspension, the rate of oxidation increased. This rate was diminished by the presence of Bcl-xL in the medium. Many of the altered proteins had lost some of their ability to inhibit ceramide-induced MOMP, but one mutant was actually a more potent inhibitor than the wild-type. In order to achieve a greater dynamic range, experiments

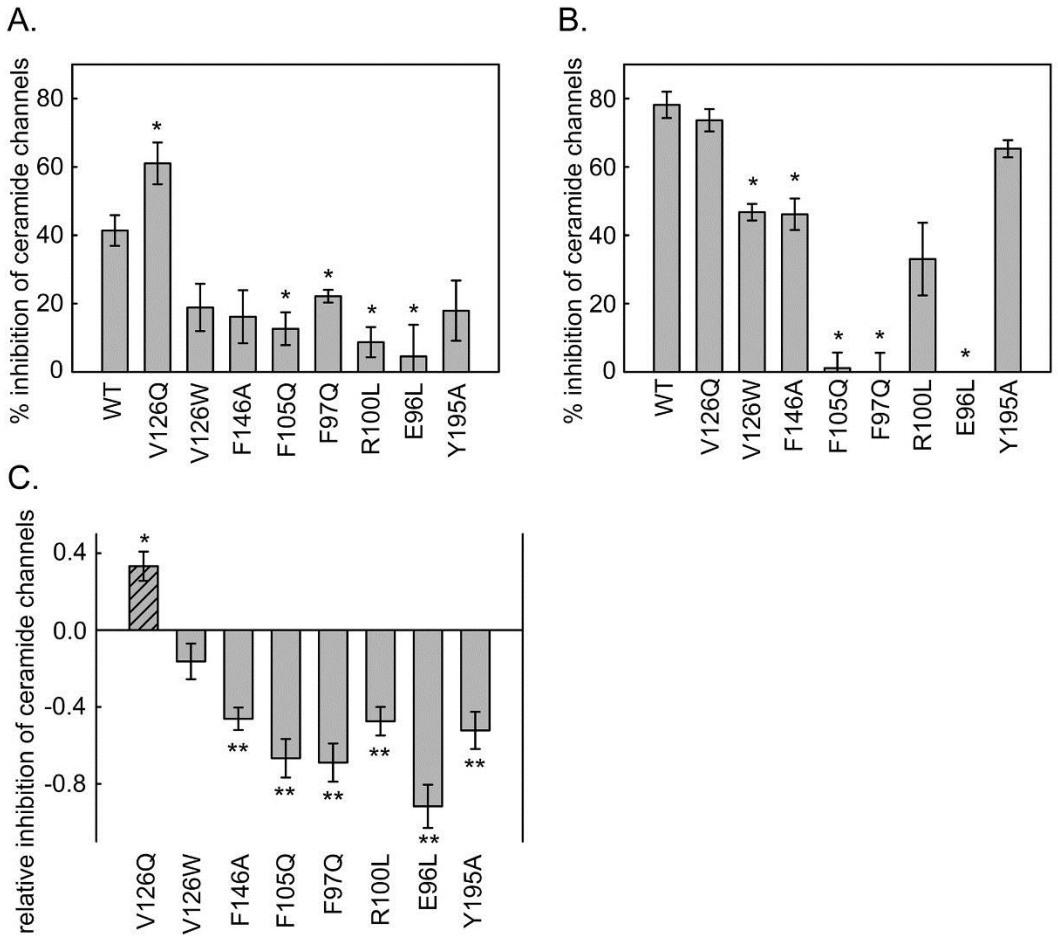

Figure 3.3. The inhibitory potency of Bcl-xL mutants on ceramide channels formed in isolated mitochondria. The final concentration of added Bcl-xL or mutant proteins was 0.72 μM (A) and 2.1 μM (B). C. Relative inhibition of ceramide induced MOMP by Bcl-xL mutants. The inhibitory ability is expressed relative to that of the wild-type so that if it is the same as the wild type the result would be 1. The statistically significant differences from the potency of the wild-type are indicated by the asterisk.

were performed at two levels of added Bcl-xL protein: a low level resulting in a weaker inhibition (i.e. a greater ceramide-induced MOMP) to detect mutant proteins that had a stronger inhibition than the wild type, and a high level to detect mutants with a weaker inhibitory affect. Figs. 3.3A and 3.3B show the measured % inhibition for one set of experiments using 0.72 and 2.1μM Bcl-xL protein, respectively. Note that the stronger inhibitory effect of V126Q was only

detected at the lower concentration and the weaker inhibitors were apparent at the higher protein concentration. Since experiments with wild-type and mutant Bcl-xL were performed in parallel, the level of inhibition of the ceramide channels was normalized to that of the wild-type protein (Fig. 3.3C) and then data from independent experiments were pooled and averaged. This normalization was necessary because the potency of the Bcl-xL varied from one batch of isolated mitochondria to another. The data for the enhanced inhibition came from the low Bcl-xL concentration experiments whereas the data for the reduced inhibition came from the high concentration experiments. The mutants are organized in a pattern reflecting their location on the docking site (Fig. 3.2A). The results follow a distinct pattern.

All but one of the mutants (E96L) were able to inhibit the formation of ceramide channels, the difference being the amount of protein needed to achieve the same level of inhibition. Thus perhaps E96 is such a critical site that removal of the carboxyl group results in failure to bind ceramide. V126W was nearly as effective as the wild-type, as expected from the mild change in the structure of the side chain. The inhibition capability of F97Q, R100L, F105Q, F146A and Y195A was weaker than that of the wild type whereas the capability of V126Q was stronger. From the docking pose, R100 hydrogen bonds with the C3 hydroxyl of ceramide. The same was seen in the MD simulations (Fig. 3.4). The hydroxyl group of tyrosine 195 interacts with the carbonyl of ceramide in the docking experiment whereas the MD simulations show intimate dipole-dipole interactions between this hydroxyl and the C1 hydroxyl of ceramide (Fig.

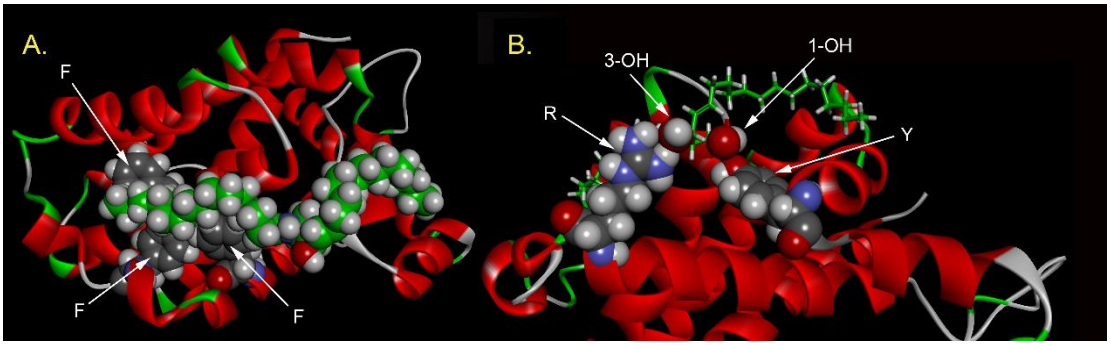

Figure 3.4 Structure of C_{16}-ceramide (green) bound to wild type Bcl-xL (ribbon mode) after 30 nsec of molecular dynamics simulation. a. Interactions between F97, F105 and F146 (in CPK labeled as "F") and the acyl chain of ceramide (also in CPK). Note the intimate contact between these side chains and the hydrophobic tail of ceramide. b. Interactions between ceramide hydroxyls (shown in CPK and labeled with arrows) and R100 and Y195 (side chains in CPK). R100 has 2 hydrogen bonds with the oxygen of the hydroxyl on carbon 3 of ceramide (labeled as 3-OH). The hydroxyl of Y195 (labeled as "Y") is aligned next to the C1 hydroxyl (labeled as 1-OH) of ceramide in such a way that their dipoles are antiparallel.

1.6A). Thus the weaker interaction of these mutations correlates with the structural information provided by the MD simulations. F97Q, F105Q and F146A disrupted hydrophobic interactions suggesting that these residues interact with the hydrophobic tails of ceramide. These results agree with one of the Bcl-xL/ceramide binding poses identified in the docking studies. In the MD simulations, these three residues form the major portion of the hydrophobic surface that interacts with the ceramide acyl chain again confirming the importance of retaining these apolar surfaces (Fig. 1.6B).

3.3.3 Correlation between the quantum yield of fluorescent ceramide bound to Bcl-xL mutants and their ability to inhibit MOMP

The Bcl-xL mutants were tested for their ability to bind fluorescently-labeled ceramide as was performed in Fig. 3.1. Direct binding measurements did not yield satisfactory results for 2 reasons: 1) The variability in the ceramide

dispersion process resulted in variable amounts of binding. 2) The unidirectional nature of the binding process in aqueous solution means that changes in the rates of dissociation could not affect the amount of binding. However, in attempting these experiments it was noted that fluorescently-labeled ceramide bound to mutated Bcl-xL produced much less fluorescence than the same ceramide bound to wild-type Bcl-xL. Fig. 3.5A shows the reduction of ceramide fluorescence upon binding to Bcl-xL. The solid circles show the spectrum of the ceramide bound to the Bcl-xL, whereas the open circles show the spectrum after extraction with isopropanol. These relative values were adjusted for the volume of the solution. The reduction in fluorescence is probably the result of exposing the fluorophore to a polar environment that quenches the fluorescence. Fig. 3.5B shows the fluorescent intensity of the same amount of ceramide bound to either wild-type Bcl-xL or Bcl-xL mutants. This difference is most likely due to greater interaction of the fluorophore with water. In a tight-binding situation water will have less contact with the fluorophore and thus result in less quenching. There is a good correlation between the intensity of the measured fluorescence and the potency of the mutant (Fig. 3.5C) to destabilize ceramide channels. These results indicate that binding of Bcl-xL to the ceramide channel was the basis for the inhibitory effect and thus the ceramide channel was being directly controlled by this anti-apoptotic protein.

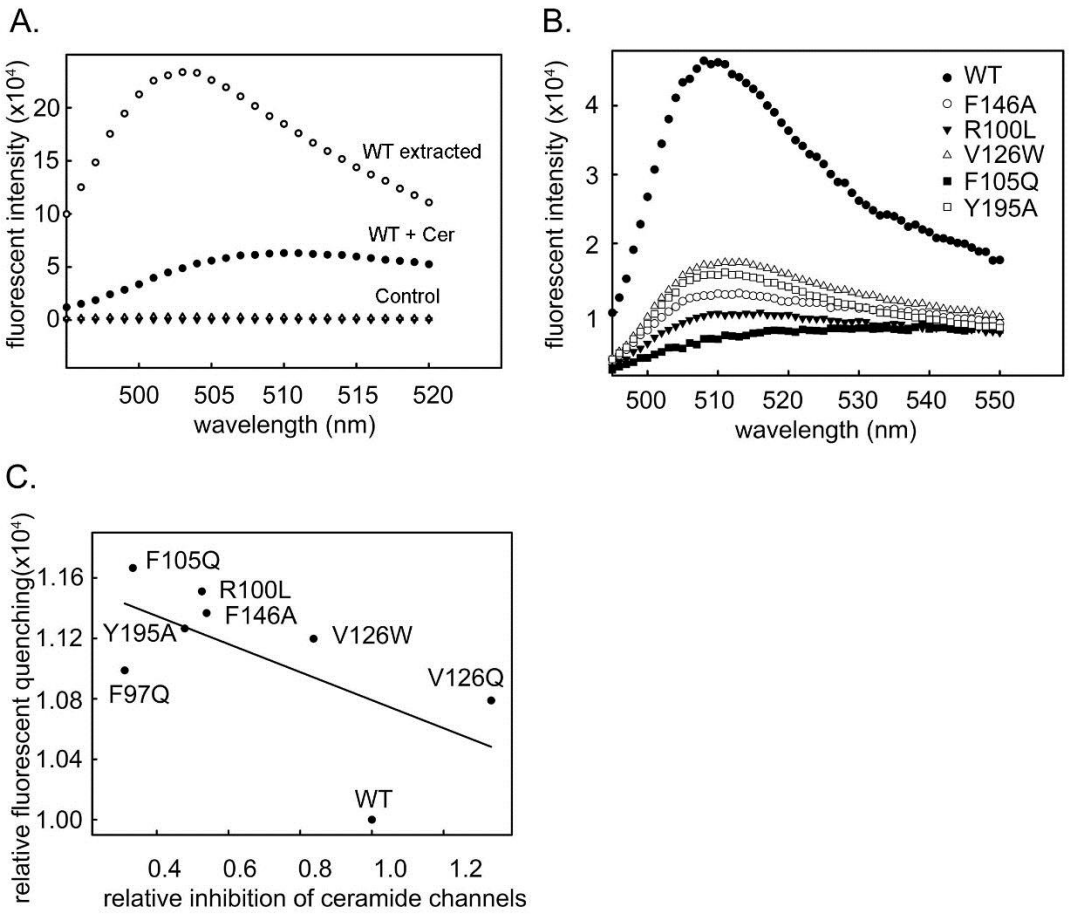

Figure 3.5. A. Fluorescence spectrum of C11 TopFlour bound to Bcl-xL (WT + Cer), C11 TopFlour extracted with isopropanol (WT extracted), and controls lacking Bcl-xL. B. Fluorescence spectrum of C11 TopFlour bound to wild-type Bcl-xL (WT) and to various Bcl-xL mutants. The curves were normalized by the fluorescence of the extracted fluorescent ceramide. Thus changes in fluorescence intensity were due to reductions in the quantum yield due to some quenching process. C. Correlation between the quenching of fluorescent ceramide bound to Bcl-xL mutant protein and the ability of the same protein to inhibit ceramide permeabilization of the MOM.

3.3.4 Molecular dynamic simulations of ceramide binding to Bcl-xL

Wild type Bcl-xL and 5 mutants (E96L, R100L, F105Q, V126Q and Y195A) that span the range of abilities to inhibit ceramide permeabilization of the MOM, were examined using MD simulations to explore their interaction with a C16-ceramide molecule. In the first few nanoseconds of simulation the

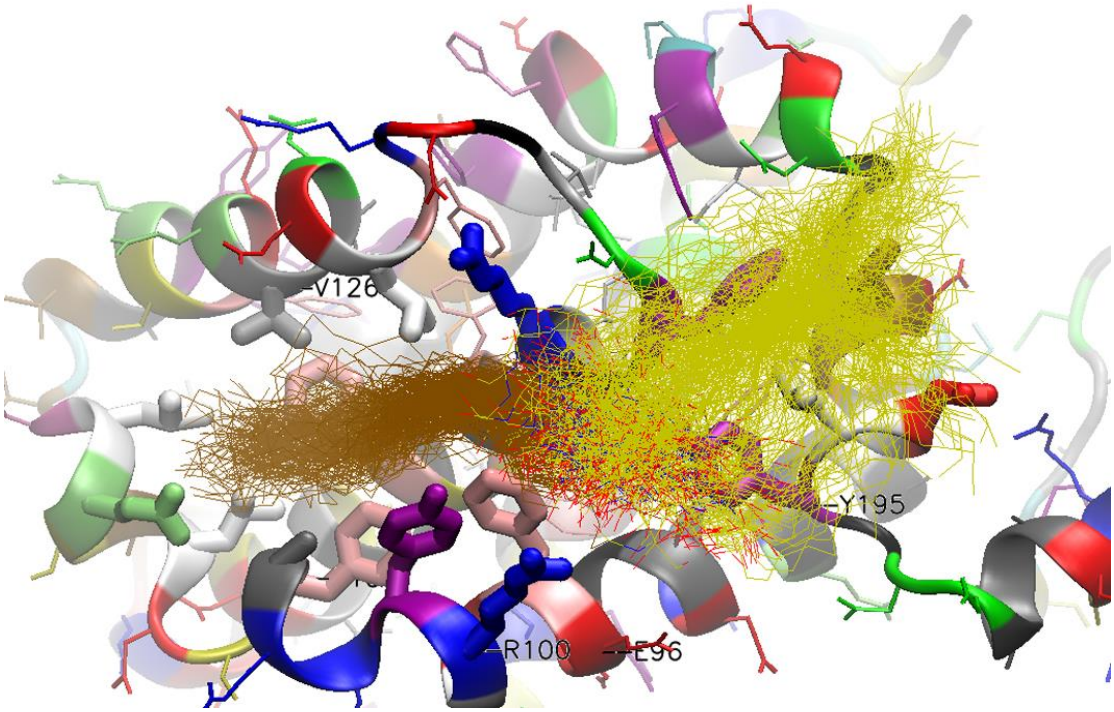

Figure 3.6. An example of the dynamic motion of the ceramide molecule in the hydrophobic groove of Bcl-xL. Illustrated is wild-type Bcl-xL and 30 locations (1 nsec apart) of the C_{16}-ceramide molecule (thin lines). The acyl and sphingosyl portions of the ceramide are distinguished by color: the former is brown and the latter, yellow.

ceramide found its optimal position in the Bcl-xL hydrophobic pocket and from then on the positions varied according to local interactions with the Bcl-xL protein and the water environment. All the introduced mutations are among the residues that are likely to interact with ceramide; they do not participate in any significant inter-helical interactions that maintain protein fold. Therefore, the mutants are not likely to affect the protein structure itself. Indeed, in simulations the structure of the ceramide-binding region of Bcl-xL changed very little in the mutants compared to the wild-type (0.15 ± 0.04 nm all-mutant mean deviation of the backbone from the WT position) indicating that the mutations acted locally, on the protein-ceramide interactions rather than globally, through a

change in the protein structure. However the results showed considerable changes in the location and dynamics of the bound ceramide –1.0 ± 0.3 nm all-mutant mean deviation of ceramide from its average position in WT Bcl-xL The dynamic motion of the ceramide molecule (Fig. 3.6) correlates very well with the loss of ability to inhibit ceramide permeabilization (Fig 3.7, Table 3.1), i.e. ceramide channel formation. The highest correlation was observed when the distal half of the sphingosine acyl chain was excluded. The fluorophore label experiencing more quenching with reduced inhibitory ability of the Bcl-xL mutant agrees with the simulation findings of greater mobility. Greater mobility should result in more access to water dipoles and thus more water-induced quenching. Note that the fluorophore is on the fatty acyl chain whose mobility correlates well with loss of Bcl-xL inhibitory ability.

The relative location of the ceramide on Bcl-xL compared to the wild-type also correlates, although more weakly, with the loss of inhibitory ability. This is reasonable as a change in location could influence the ability of the bound Bcl-xL to destabilize the channel.

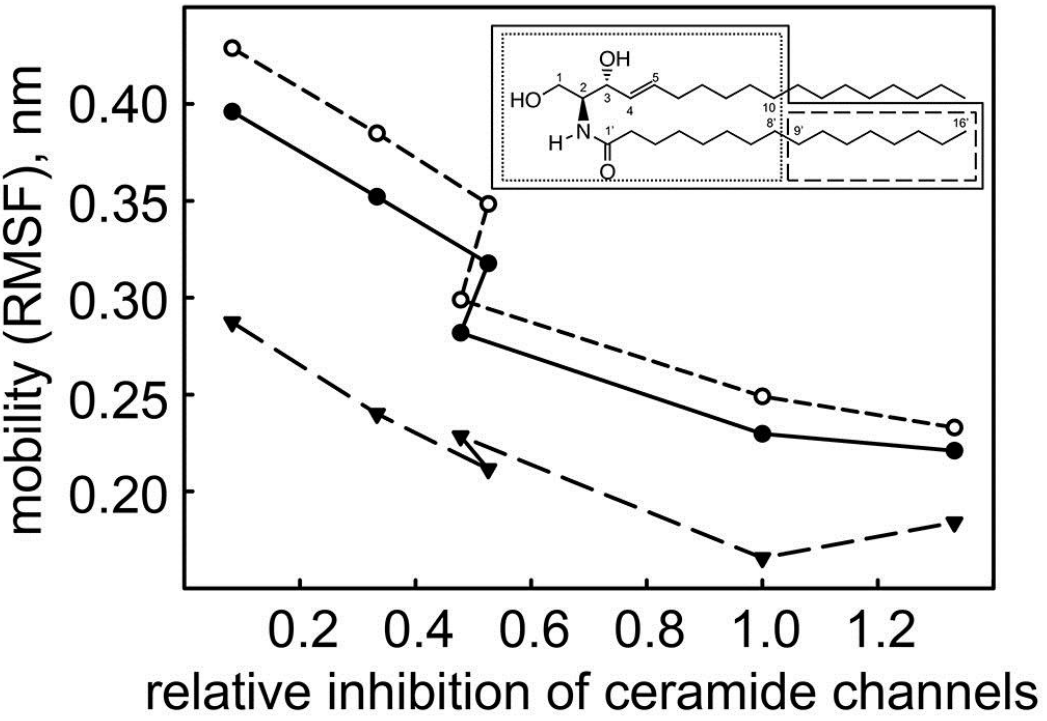

Figure 3.7 Correlation between the dynamic motion of the ceramide molecule and the ability of a Bcl-xL mutant to inhibit ceramide permeabilization of the MOM. The mobility (RMSF) of regions of the ceramide molecule (inset) were measured. Those regions surrounded by a solid line are plotted as a solid line in the main figure. Similarly for the dotted and dashed line. The inhibitory ability (horizontal axis) is expressed relative to that of the wild-type so that if it is the same as the wild type the result would be 1.

Table 3.1. Correlation between the dynamic motion (RMSF) of different regions of the ceramide molecule and the ability of Bcl-xL to inhibit ceramide permeabilization of the MOM

Mobility		Deviation from wild type	
Location	Correlation	Location	Correlation
Ceramide without sphingosine tail after C10	-0.96	Ceramide amide oxygen	-0.63
Ceramide up to C10 and C8’	-0.96	Ceramide polar atoms	-0.60
Ceramide amide tail C9’-C16’	-0.91	Ceramide headgroup	-0.59
Ceramide whole	-0.78	Ceramide fatty acid residue	-0.57
Ceramide tail C10-C8’	-0.57	Ceramide amide tail	-0.54
Bcl-xL	-0.09	Ceramide whole	-0.24
Bcl-xL in contact with Ceramide	-0.07		

3.3.5 Comparison of the binding footprint on Bcl-xL of Bax and the ceramide channel

Bcl-xL is known to inhibit the formation of Bax channels in the mitochondrial outer membrane. The hydrophobic pocket of Bcl-xL binds the BH3 domain of pro-apoptotic proteins such as Bax and Bid (27, 28, 51) and thus inhibits their pro-apoptotic activity, including channel formation. The Bcl-xL mutants were tested for their effects on Bax channel formation in the MOM to determine if their relative potency is similar to that observed for ceramide channels. A complicating factor is that truncated Bid (t-Bid) is necessary to activate Bax resulting in MOMP and thus one cannot distinguish between an inhibitory effect on Bax or on t-Bid. Regardless of which protein binds to Bcl-xL, the mutants will probe whether the same region of Bcl-xL is used in both cases. Once again, in order to achieve a greater dynamic range, the amount of wild type protein added was adjusted to obtain a weaker (Fig 3.8A) or a stronger (Fig. 3.8B) inhibition. The results show that V126Q and Y195A have a stronger inhibitory effect than the wild-type. F146A, R100L, V126W, F105Q, F97Q and E96L have a weaker inhibitory effect. As in the case of the ceramide channel, E96L has no effect. A comparison of the inhibitory effects of mutated Bcl-xL on Bax (Fig. 3.8C) and ceramide channels (Fig. 3.3C) reveals that two mutations have distinctly different effects on the two channels. A plot of one set of data vs the other (Fig. 3.9) shows that Y195A has stronger inhibition of Bax channels as compared to the wild-type protein but a weaker inhibitory

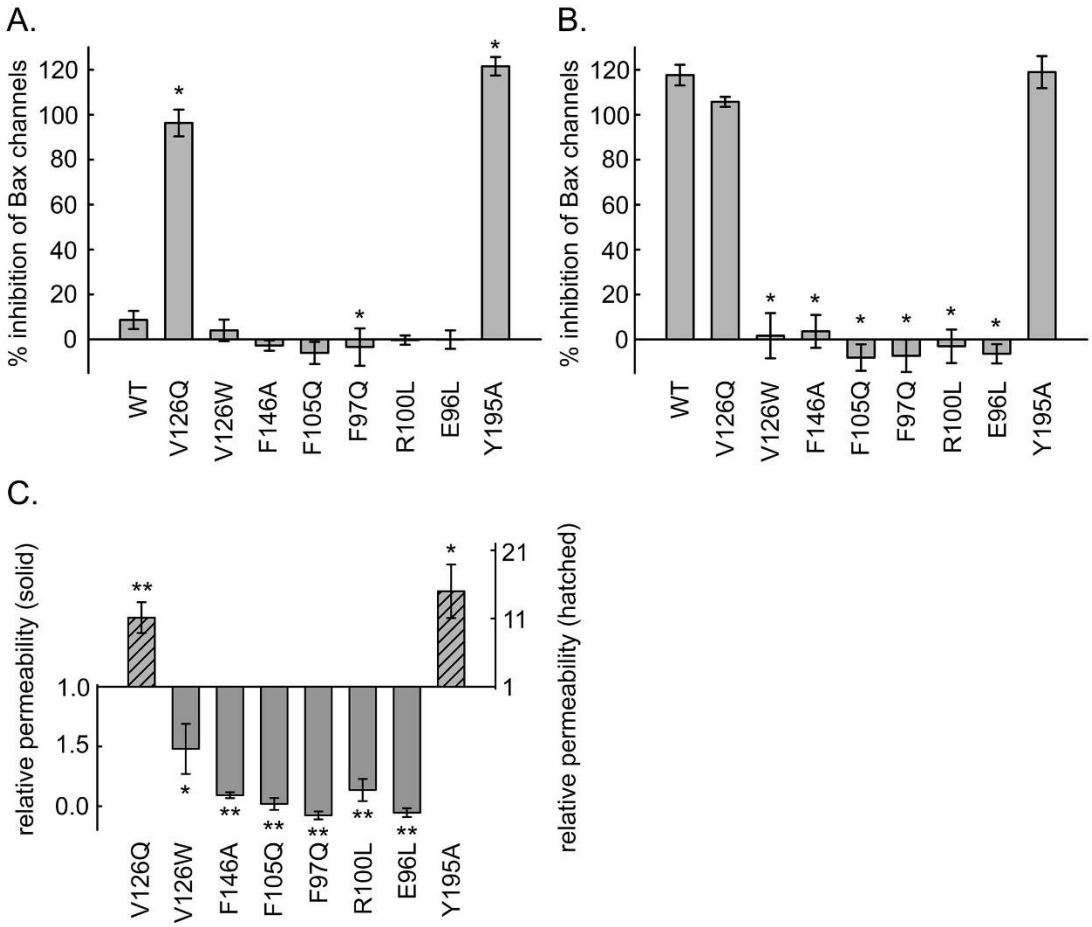

Figure 3.8. The inhibitory potency of Bcl-xL mutants on Bax permeabilization of the MOM. The final concentration of added Bcl-xL or mutants was 0.72 µM (A) and 0.86 µM (B). C. Relative inhibition of Bax permeabilization of MOM by Bcl-xL mutants. The inhibitory ability is expressed relative to that of the wild-type so that if it is the same as the wild type the result would be 1. The statistically significant difference from the potency of the wild-type is indicated by the asterisks.

effect on ceramide channels. V126W was not able to inhibit Bax channels as well as the wild type, but had the same ability to inhibit ceramide channels as the wild type. This information could be used to distinguish between apoptosis resulting from MOMP due to activated Bax or ceramide.

3.3.6 Probing the relative importance of ceramide and Bax channels in apoptosis in intact cells

Both ceramide and Bax form channels that release proteins from the MIS. These two agents also act synergistically to induce MOMP (85). However it is unclear which channel-former is used in vivo. The Bcl-xL mutant proteins were expressed in cells lacking Bcl-xL in order to obtain some insight into this question. Cells expressing either wild type or one of three mutants (Y195A, V126Q, and V126W) were stimulated to undergo apoptosis using 7 different chemical stimuli (cisplatin, gemcitabine, hydrogen peroxide, thapsigargin, doxorubicin, etoposide, or bortezomib) that activate different apoptotic pathways. A comparable level of expression of mutant proteins was achieved and a dose response curve was performed for all of the above stimuli. Fig. 3.10 shows an example of the dose-response curves. Two doses were selected for detailed statistical analysis, one in the transition region between no drug effect and the full effect and another immediately after a maximal effect of the chemical agent was achieved.

V126W inhibits ceramide channels as well as wild-type Bcl-xL (Fig. 3.11) but has only half the potency on Bax channels. In most cases, this mutant was less effective than the wild-type in protecting cells from apoptosis, consistent with the important role of Bax channels in the apoptotic process. V126Q is more effective at inhibiting both Bax and ceramide channels (Figs. 3.3 and 3.8); cells expressing V126Q were often more resistant to death stimuli than the wild type (gemcitabine low dose, bortezomib low dose, hydrogen

peroxide, and thapsigargin high dose). Y195A is also more potent at inhibiting Bax channels but only half as potent on ceramide channels (Figs. 3.3 and 3.8). Cells expressing Y195A were more sensitive to gemcitabine (low dose), doxorubicin (high dose), and bortezomib (low dose) than cells expressing V126Q even though Y195A is a more potent inhibitor of Bax channels (Fig. 3.11 and 3.11). In the case of the high dose of bortezomib, cells expressing Y195A are more sensitive than cells expressing the wild-type Bcl-xL (Fig. 3.11B). The results with Y195A provide evidence for the role of ceramide channels in cells treated with these compounds. In other cases, such as thapsigargin treatment, the weaker ability of Y195A to inhibit ceramide channels had no effect as the cell viability observed with cells expressing V126Q and Y195A were not different. Thus ceramide channels may play a role in apoptosis induced by specific stimuli.

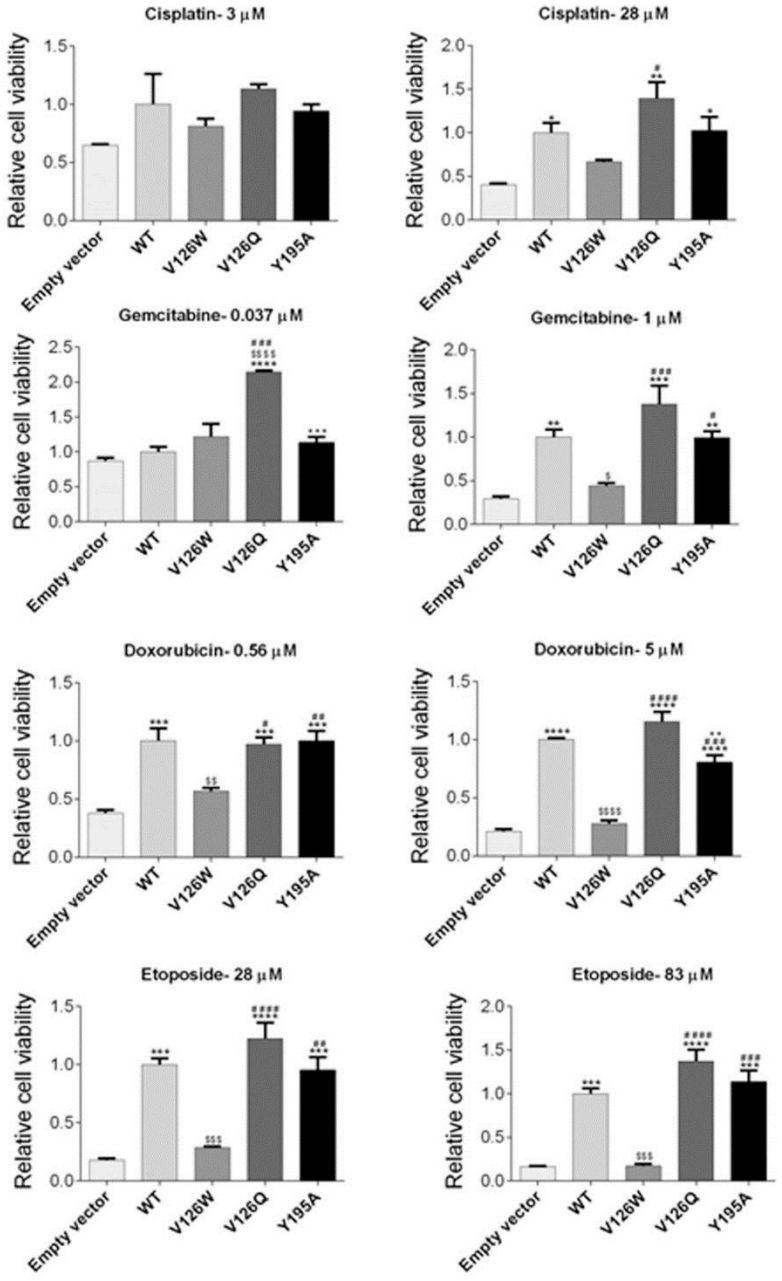

Figure 3.11. A. Relative viability of cell expressing the indicated Bcl-xL and induced to undergo apoptosis with the indicated amount chemical agent. The significant differences are indicated as follows: *, compared to empty vector; #, compared to V126W; $, compared to wild type (WT), +, compared to V126Q.

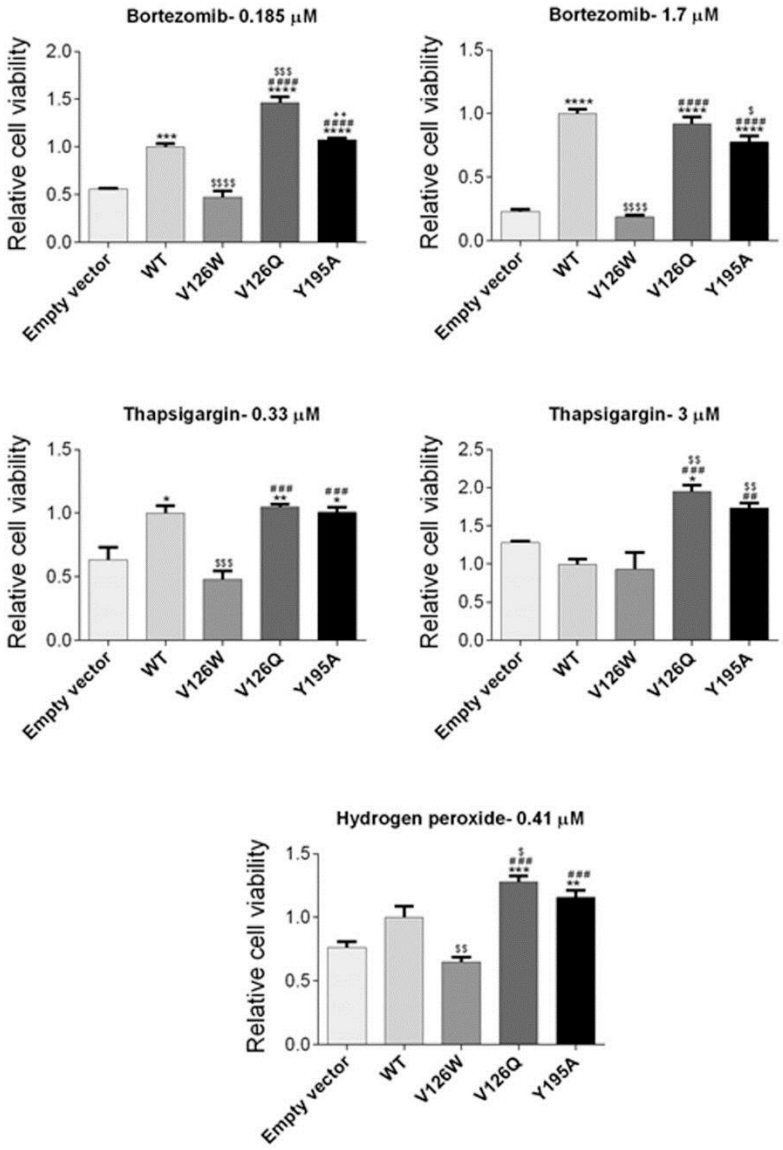

Figure 3.11. B. Relative cell viability after treatment with several apoptosis

3.4 Discussion

The surprising ability of a lipid, ceramide, to form large, and stable channels in phospholipid membranes was initially met with skepticism. Now the evidence supporting the existence of ceramide channels is overwhelming. This includes recording their properties in defined planar phospholipid membrane systems (10, 79), visualization by electron microscopy (78), demonstration of the stability of the ceramide channel model by molecular dynamic simulations (80), and examination of the elastic properties of these channels by microfluidic methods (129). The role of these channels in apoptosis was indicated by the ability of ceramide to permeabilize the MOM to proteins even when the source of the mitochondria was the yeast, S. cerevisiae, an organism lacking the Bcl-2 family of proteins (17). The evidence for this role was substantially increased by the findings that Bcl-2, Bcl-xL and CED-9 all inhibit ceramide channel formation in isolated mitochondria (17) whereas Bax acts synergistically with ceramide to permeabilize the MOM (85). Further support of a specific regulatory role of ceramide channels by Bcl-2 family proteins was the finding that Bcl-xL acts by interacting with the hydrophobic region of ceramide whereas Bax preferentially interacts with the polar regions (81). Here we actually identify the region of Bcl-xL that binds ceramide and it turns out to be a similar region to the one that binds Bax.

The direct binding experiments used fluorescently-labeled ceramide as a surrogate for ceramide channels. The ability of Bcl-xL to bind ceramide monomers raises the question of whether Bcl-xL might be acting by depleting

the free ceramide concentration, rather than binding to the ceramide channel. However, the amount of ceramide added to the mitochondrial suspension was 25 to 70 fold higher on a molar basis that Bcl-xL, making this possibility unlikely. Given that fact, one might wonder why the excess ceramide does not simply occupy all the sites on Bcl-xL and act as a competitive inhibitor, interfering with Bcl-xL binding to the ceramide channel. The answer might reside in the observation that Bcl-xL binds to the acyl chains of ceramide and typically these are buried either in the membrane bilayer or in the core of ceramide micelles and are thus unavailable for binding to Bcl-xL. However, according to the working model of the ceramide channel (Fig. 3.8), the ceramide molecules that form the channel are oriented parallel to the plane of the membrane and organized in columns that span the membrane. The ceramides at the ends of these columns would have their hydrophobic tails exposed to the water phase were it not for these being covered by the surrounding phospholipids to minimize the unfavorable interactions with water. However, these phospholipids are in a distorted, high-energy conformation. If Bcl-xL were to displace these lipids it would bind the hydrophobic tails of this ceramide and by doing so could change the structure of the channel. According to the current hypothesis that describes how Bcl-xL binding destabilizes ceramide channels (81), the binding changes the curvature of the ceramide columns. MD simulations show that the columns have a positive curvature resulting in the channel having a somewhat hourglass shape. This is due to the way the channel interfaces with the surrounding phospholipids in the bilayer. The neighboring

phospholipids that curve towards the channel to cover the hydrophobic ends of the ceramide columns are under stress and thus pull on the ceramide columns, bending them. Bcl-xL binding removes this bending force by displacing the phospholipids. This results in mismatch with adjacent columns still interacting with phospholipids and thus strain develops that propagates to the rest of the structure through the hydrogen-bonded network, thus destabilizing the entire structure. Mutations that weaken the binding of Bcl-xL to ceramide (fluorescence and MD simulations) should reduce the ability of Bcl-xL to destabilize ceramide channels and that was demonstrated in their reduced ability to inhibit ceramide permeabilization of the MOM. Altering the position of the ceramide-Bcl-xL interface, as indicated in the MD simulation, may alter the above hypothesized curvature change and thus the amount of strain and the degree of destabilization of the channel structure. This explains the correlation between a shift in the location of ceramide binding to mutant Bcl-xL and a reduction in the Bcl-xL's ability to inhibit the ceramide-induced MOMP.

The pro-apoptotic role of ceramide is well established (127, 128), whereas the in-vivo pro-apoptotic role of ceramide channels is not. Not only do these channels have the right properties, but mitochondrial ceramide levels have been shown to increase early in apoptosis to levels sufficient to form ceramide channels. However, these finding do not demonstrate that cells actually use ceramide channels during apoptosis. Indeed, ceramide metabolites were reported (135) to activate Bax and Bak and induce MOMP. In view of this one might question the role of ceramide in vivo especially considering the

fact that cells lacking both Bax and Bak are very resistant to apoptosis. But here again the simple conclusion is misleading, because cells lacking Bax and Bak also fail to increase mitochondrial ceramide levels (124), unlike the parental cells. It turns out that Bak is required for ceramide synthase-mediated long-chain ceramide generation during apoptosis. Thus the situation is far more complex and a more direct approach is needed. Here we report experiments with mutants of Bcl-xL that have an altered ability to inhibit MOMP induced by either ceramide or Bax. The results show that the ability of Bcl-xL to inhibit Bax channels is indeed, as expected, important for Bcl-xL to promote cell survival. However, when the ability of Bcl-xL to inhibit ceramide channels is reduced, the ability of Bcl-xL to protect cells from particular death stimuli was also reduced. This lack of protection from cell death in the mutant Bcl-xL occurred despite it being 15-fold more potent at inhibiting Bax channels. Thus it seems that inhibiting Bax channels alone is insufficient for Bcl-xL to protect from apoptosis and that under certain conditions ceramide channels take over the role of releasing proteins from mitochondria. Of course there are alternative explanations that seem less likely. For instance if Bcl-xL were to facilitate the transfer of ceramide between membranes and this transfer were important to the progress of apoptosis then mutations that weaken the binding of Bcl-xL to ceramide would also weaken the propensity to undergo apoptosis. This hypothetical function would not explain the results with isolated mitochondria but cannot be excluded as a possibility in the in vivo experiments. Regardless

role of ceramide channels needs to be considered when interpreting experimental results.

3.5 Acknowledgements

We thank Shang H. Lin for purification of Bax. We also thank Justin M. Wang for purification of mutated Bcl-xL. We thank Timothy Troppoli for helping with the cytochrome *c* accessibility assay. We thank Timothy Walsh for helping with the adenylate kinase assay. We also thank Chris Worth for assistance with cell sorting and Douglas Saforo and Cameron Conway for their technical assistance. This work was supported by a grant from the National Science Foundation MCB-1023008 (to M.C.), the National Institute of Diabetes and Digestive and Kidney Diseases of the National Institute of Health (R01DK093462 to L.J.S.), and the Kosair Pediatric Cancer Research Program Award (to L.J.B.).

This research was originally published in Biochimica et Biophysica Acta (BBA)- Biomembranes. Kai-Ti Changa, Andriy Anishkina, Gauri A. Patwardhanb, Levi J. Beverlyb, c, d, Leah J. Siskindb, c, Marco Colombinia,, Ceramide channels: destabilization by Bcl-xL and role in apoptosis. Biochim. Biophys. Acta. 2015; 1848, 2374–84.

Chapter 4: Insight into the structure and dynamics of channels by measuring rectification

4.1 Introduction

4.1.1 A novel channel discovered in E. coli extract

Shang H Lin et al. found a steeply voltage-gated cation channel in Escherichia coli extracts (136). The steepness is remarkably high, rivaling that of channels in excitable membranes. In addition, the channel seems to exist as an assembly of three channels that are highly cooperative. The physiological function of such a channel is completely unclear, but the remarkable properties indicate an important regulatory role. Figure 4.1 shows the current model of how this channel functions. One channel unit consists of three cylindrical channels arranged in a row. The shading indicates the structural orientation. The middle channel (channel 2) is proposed to have an opposite orientation with respect to its neighbors (channel 1 and 3). The arrows indicate the dipole moment of the voltage sensor in each channel. An open circle on the top of each cylinder indicates an open channel and a filled circle indicates a closed channel. The positive and negative signs above the unit are the signs of the applied voltages. Note that the closure of one channel results in the realignment of the voltage sensor dipole with the electrical field but does not change the structural orientation. The channels have strong positive cooperativity. This means that channels prefer to be in the same conformation with the adjacent channels, i.e. all open or all closed. If channel 1 closes, it allows channel 2 to respond to voltage and close as well. Likewise, channel 3 gating only takes place after the

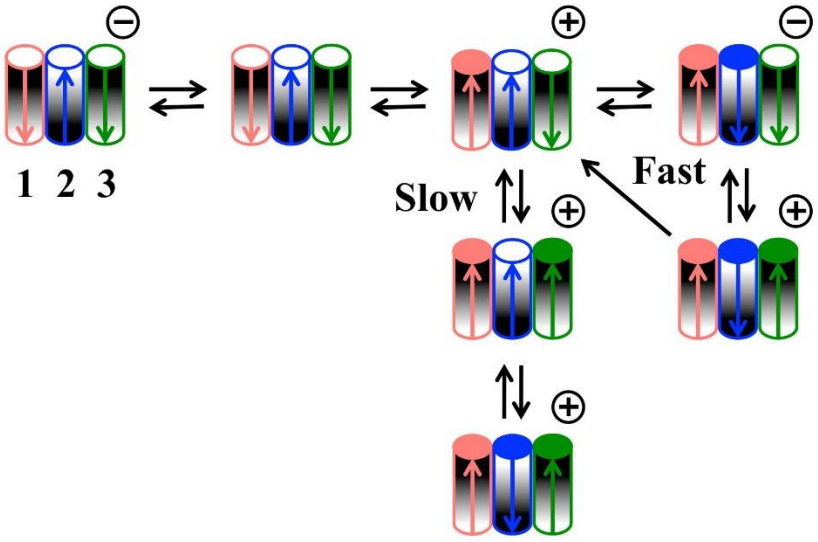

Figure 4.1. Model of the highly cooperative and voltage-gated *E. coli* channels. Three cylindrical channels constitute a 4.5 nS conducting unit. The channels designated as channel 1, 2, and 3. The shading indicates the orientation of the channel. The orientation of channel 2 is opposite to its neighbors. The arrows show the dipole moment of each channels, originally from the distribution of gating charge. Open and solid circles on the top of cylinders show open and closed channels, respectively. Closure of channel results in the rearrangement of electric distribution of the channel, and changes the dipole moment. However, the orientation of each channel is still the same. Channel interacts with its adjacent channel cooperatively and prefers to have the same conformation as its neighbor, ie. both open or close. The sign at the upper right corner of each conducting unit indicates the applied voltage. The fast path indicates, using triangular ramps, the closure of channel 1 favors the close of channel 2, which occurs at negative voltages. Applying fast triangular voltage ramps and the kinetic delay of channel 2 reopening result in channel 2 remaining closed and allowing channel 3 to close. As the voltage declines, either channel 3 reopens followed by channel 2 or channel 2 and 3 reopen simultaneously. The slow path indicates the slow rate of closure. However, applying a high positive potential closes both channel 1 and 3, and then forces channel 2 to close through cooperativity with its neighbors. Reproduced with permission, from Lin SH, Cherian N, Wu B, et al., 2014, Bax channel triplet: co-operativity and voltage gating, Biochem. J., 459(2), 397–404. © the Biochemical Society. (136).

closure of channel 2. The model explains this by illustrating the changes that occur following different experimental treatments. Channels remain open with a negative voltage applied and at low potentials (upper left in Figure 4.1). The closure of channel 1 is induced with a high positive voltage applied (typically

70 mV or above). The “slow” indicates a slow rate of closure when a constant positive voltage was applied. This is due to conflicting forces on the channel’s gating propensity. A high positive voltage induced the closure of channel 1 and 3 in spite of inhibitory effects from the open channel 2. In addition, although channel 2 should not close at positive voltages, the cooperativity with the adjacent channels forces the closure of channel 2, despite the applied field favoring the open state. The “fast” pathway indicates what happens following the application of triangular voltage ramps. Channel 2 closes at low negative potentials because, in addition to the applied electric field, the closure of channel 1 results in an unfavorable dipole-dipole interaction. Channel 3 closes at low positive potentials only after the closure of channel 2 for the same reason.

The model is based on several assumptions including (a) the triplet is composed of three identical proteins, having the same structure, each forming one channel, (b) the orientation of channel 2 is opposite to that of the adjacent channels, and (c) the dipole-dipole interactions between adjacent channels of the voltage sensors result in the cooperativity. Although it is possible that a different protein froms each one of the channels, several observations support assumption (a). The conductance of each channel is indistinguishable, the selectivity of each channel is the same, and the voltage dependence of channels 2 and 3 seems the same.

Assumption (b) seems problematic. It is almost unprecedented that the same protein should insert in two directions in the same membrane. Without structural information it is difficult to investigate the orientation of the channels.

However, we took a functional approach to address this question. To test whether the orientation of channels 2 is opposite to that of the adjacent channels, the rectification of the channels was measured.

4.1.2 Rectification

Rectification is a condition where a conductor does not obey Ohm's law. Current flow in one direction is greater than that in the opposite direction despite the same voltage magnitude. In other words, the current-voltage relationship is non-linear or the conductance depends on voltage. A famous example of rectification in membrane channels is the inwardly rectifying potassium channel (Kir). Inwardly rectifying means that the flow of potassium ions in the inward direction (into the cell) is easier than flow in the outward direction (out of the cell). It plays an important role in regulating neuronal activity and in stabilizing the resting potential. In the cell, when the membrane potential is negative relative to the reversal potential of the channel, potassium ions flow into the cell and restore the resting potential. However, when the membrane potential would cause potassium ions to move out of the cell, endogenous polyamines, such as spermine, block the Kir channel, facilitating membrane depolarization.

Rectification can be caused by either an external asymmetry, i.e. due to differences in the medium on the two sides of the membrane, or an internal asymmetry, one intrinsic to the channel's structure. The latter provides information on the orientation of the channel.

4.2 Results and discussion

The proposed anti-parallel orientation of the three channels in the triplet was tested by measuring the direction of the rectification of the current flowing through each channel. This rectification in the presence of symmetrical salt solutions across the membrane must be caused by an inherent asymmetry in the channels. In order to record the current rectification of individual channels, it is necessary to insert a single triplet into the planar membrane. A single triplet is composed of three highly cooperative and voltage gated channels (designated channel 1, 2, and 3) (Fig 4.1). All three channels have the same conductance, 1.5 nS. Thus they cannot be distinguished using conductance measurements. They are distinguished by their voltage-gating behavior and this behavior allowed us to tease apart the current flowing through each. The gating model generated from previous studies (2) was used to apply a voltage protocol to close channels sequentially and identify the channel(s) whose current was being recorded. The application of voltage ramps to the membrane resulted in current records (e.g. Fig 4.2) from which the conductance was calculated. The rectification was quantified as the slope of the conductance-voltage curve.

Typically a 10 to 30μL aliquot of the active fraction was dispersed into the aqueous phase on the *cis* side of the planar phospholipid membrane. After a variable lag time, the conductance increased. A conductance of 4.5 nS indicated the insertion or formation of a single triplet in the membrane, as expected as from previous studies (94, 136). Typically the application of

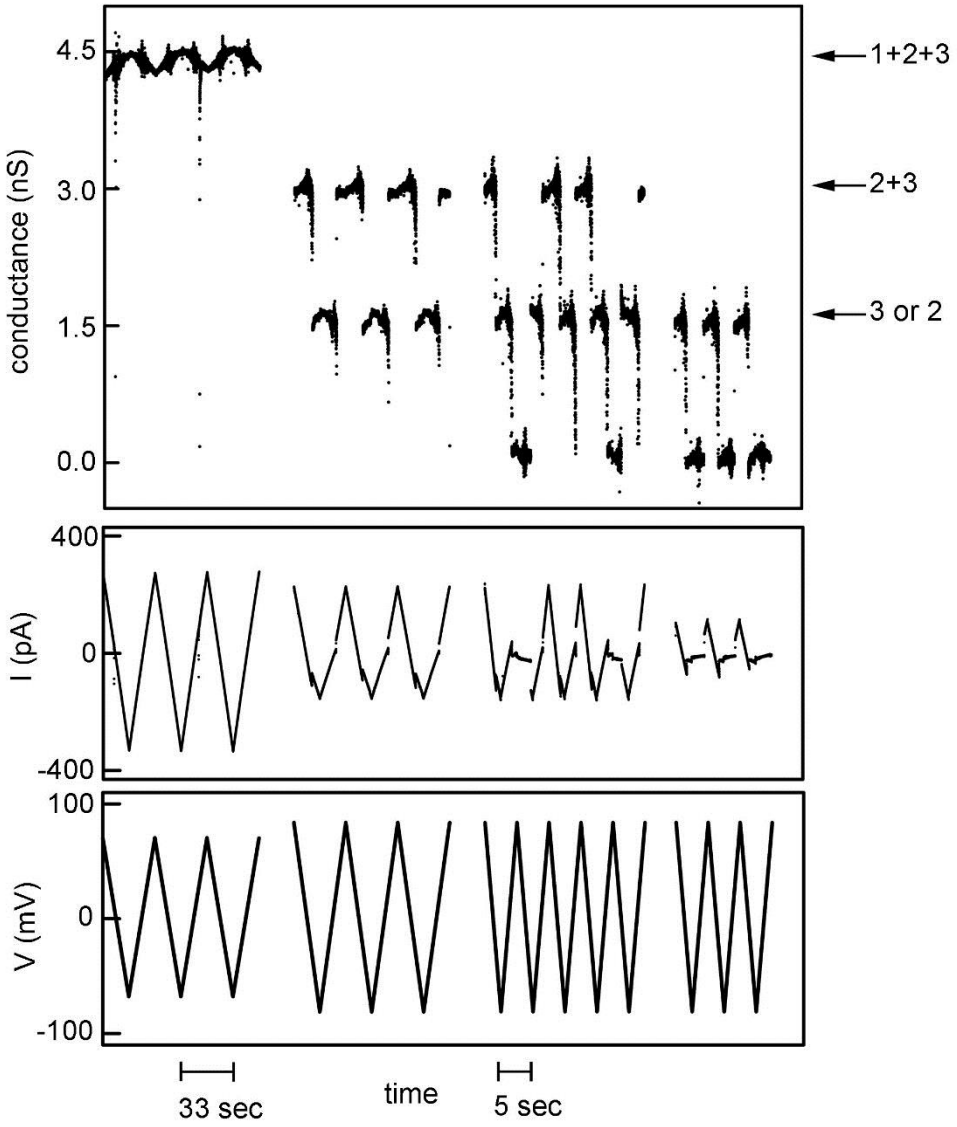

Figure 4.2. Voltage gating of a single triplet. Triangular voltage ramps (bottom panel) were applied to the membrane and the resulting current record (middle panel) and calculated conductance (upper panel) are shown. The segments from left to right are all channels open, only channel 2 gating (channel 3 was open), channel 2 and channel 3 gating, and channel 2 gating while others are closed, respectively. The frequency of the left two segments was 30 mHz (8.3 mV/sec) and that of the right segments was 200 mHz (65.6 mV/sec).

voltage ramps (e.g. 8.3 mV/sec, from 70 to -67 mV) showed no voltage gating (first segment of Fig 4.2 and Fig 4.3A). Under this condition one is probably recording the current flowing through all three channels simultaneously. This

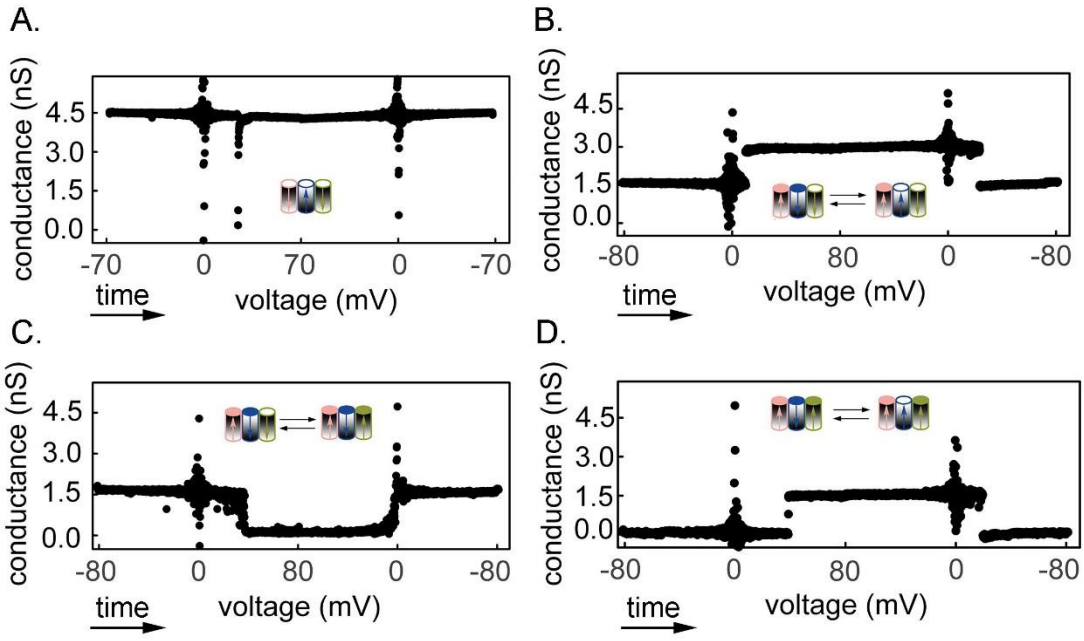

Figure 4.3. Pattern of a single triplet. A single triplet was probed by triangular voltage ramps. Cartoons show the status of channels described in Fig 4.1. A. When all three channels are opened, no voltage gating was observed. B. After the closure of channel 1, channel 2 gated at negative potential and reopened at nearly zero. C. Channel 3 closed at positive potential and reopened at nearly zero potential. D. After the closure of channel 1 and 3, channel 2 closed at a negative potential and reopened at a positive potential.

was usually the case but only became certain after gating was induced and normal behavior was observed. The rectification of current flowing through all three channels was measured as a slope in the conductance/voltage relation. An example of the results of this measurement is shown in Fig. 4.3A. When the current is divided by the applied voltage there is an artifact close to zero that should be ignored. To begin the gating process a constant high positive voltage (typically +70 to +90mV) was applied until a 1.5 nS drop of conductance was observed. This was the closure of channel 1. If the channel reopened, then the application of the high potential was repeated. Typically channel 1 adapted

quickly to the closed state and did not reopen. Once channel 1 was closed, this allowed another channel to gate at low negative potentials. This was channel 2. It was the only one that reproducibly gated at negative potentials. Under these conditions channel 3 often remained open. This is illustrated in the second segment of Fig 4.2 and the sample result in Fig 4.3B. This gating of channel 2 caused the conductance to alternate between 3.0 and 1.5 nS. Channel 2 closure occurred at around -27 mV with reopening taking place at a more positive potential due to kinetic delays. In the illustrated experiment the voltage was changed at a rate of 9.8 mV/sec, from +83 to -80 mV.

As noted the closure and reopening of channel 2 took place at different potentials. This is due to the fact that the closing process is faster than the reopening process. This is also true of channel 3. Therefore, the voltage at which channels 2 and 3 reopen is highly dependent on the rate of voltage change. The kinetic delay of channel 2 reopening allowed us to set conditions that favored the closure of channel 3, because almost invariably channel 3 closure did not occur until channel 2 was closed. The problem is that channel 3 closure takes place at positive potentials, conditions favoring channel 2 opening. By raising the frequency of the voltage ramp from 9.8 mV/sec to 65.6 mV/sec, channel 2 often remained closed long enough for channel 3 to close (third segment of Fig 4.2 and the sample result in Fig 4.3C). Channel 3 gating took place around +28 mV with reopening occurring as the positive potential declined. Once channel 3 closes, the reopening of channel 2 is inhibited, interpreted as being due to favorable dipole-dipole interactions (Fig 4.1).

To study whether the orientation of channel 2 is opposite to that of the other channels, the rectification of channel 2 itself is required. Although channel 3 is inhibited from closing when channel 2 is open, a high positive potential similar to that used to close channel 1 was used to close channel 3, leaving only channel 2 to conduct. This outcome was verified by noting that the remaining channel gated at negative potentials (fourth segment of Fig. 4.2 and the sample result in Fig. 4.3D). The closure of channel 2 occurred at around -27 mV with reopening at positive potentials.

4.2.1 Rectification of channels

Data was collected by measuring the current as a function of voltage using a variety of rates of change of voltage. This raises the question as to whether the rectification measured depends on the rate of voltage change. Membrane channel rectification generally arises from an asymmetric distribution of mobile charges within the channel. It does not involve changes in the structural state of the channel. The redistribution of free ions occurs at the nsec time scale and thus much faster than the rates of voltage change used in these experiments. Only the much slower conformational changes of the channel-former should be affected by the rates of voltage change used. However, it is possible that these channels are unusually compliant and their structure may be distorted by the applied electric field, up to 200,000 Volts per cm. This possibility was tested (Fig. 4.4B) and no significant change was detected (Ch 2 + 3, $P = 0.45$; Ch 3, $P = 0.82$).

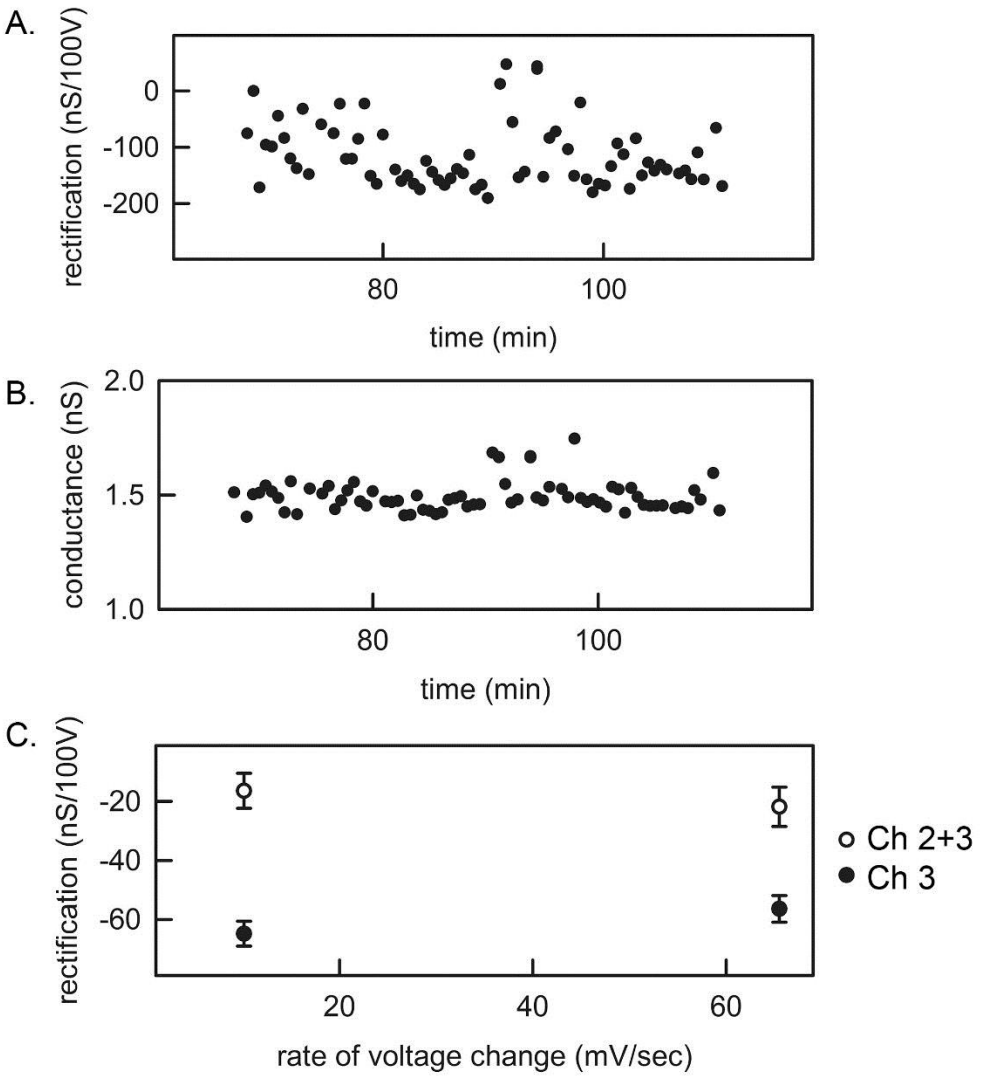

Figure 4.4. Independence of channel rectification on time or the rate of voltage change. The rectification (A) and conductance (B) of channel 3 were independent of time following a series of recordings. (C) The rectification of channel 2 +3 (empty circle), and 3 (solid circle) were independent on the rate of voltage change.

Some channels adapt to the applied electric field and it is possible that the application of a long set of voltage ramps might result in changes in the structure of the channels and thus changes in the value of the rectification. The possibility of such time-dependent effects was tested. The results indicate that the rectification and the conductance did not dependent on time after initiating

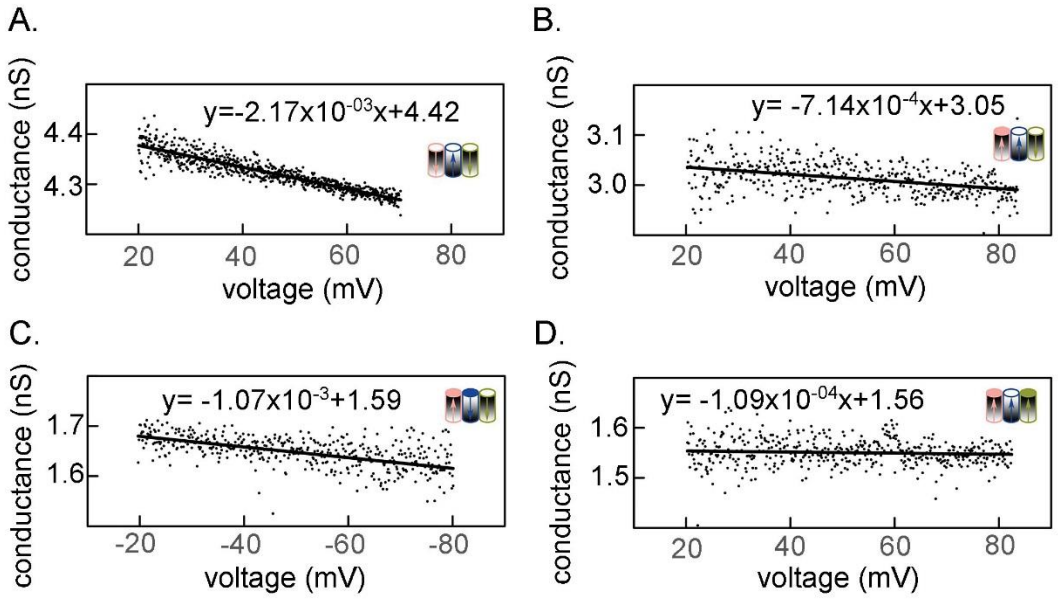

Figure 4.5. Rectification of a single triplet. A single triplet was probed by applying triangular voltage ramps. Cartoons show the state of channels as described in Fig 4.1. Rectification of channel 1+2+3 (A), 2+3 (B), 3 (C), and 2 (D).

a sequence of voltage ramps (Fig. 4.4A and B). Thus it was possible to combine the rectification values calculated from each ramp to obtain an average value.

The measurements of rectification are expressed as changes in the conductance in nanoSiemens per 100 Volt change in applied potential. This was done so that the values would be in a convenient numeric range. The results are shown in Table 4.1 and Fig. 4.6. The rectification of channel 1 + 2 +3 was -162 ± 8 nS/100V (mean ± S.E.), 11 measurements in 6 separate experiments (Fig 4.5A). The quantification of the rectification of the combined channels 2 and 3 yielded -82 ± 12 nS/100V, 10 measurements in 5 separate experiments (Fig 4 .5B), and that of channel 3 was -89 ± 7 nS/100V, 10 measurements in 5 separate experiments (Fig 4.5C). The rectification of channel 2 was 2 ± 21 nS/100V, 4

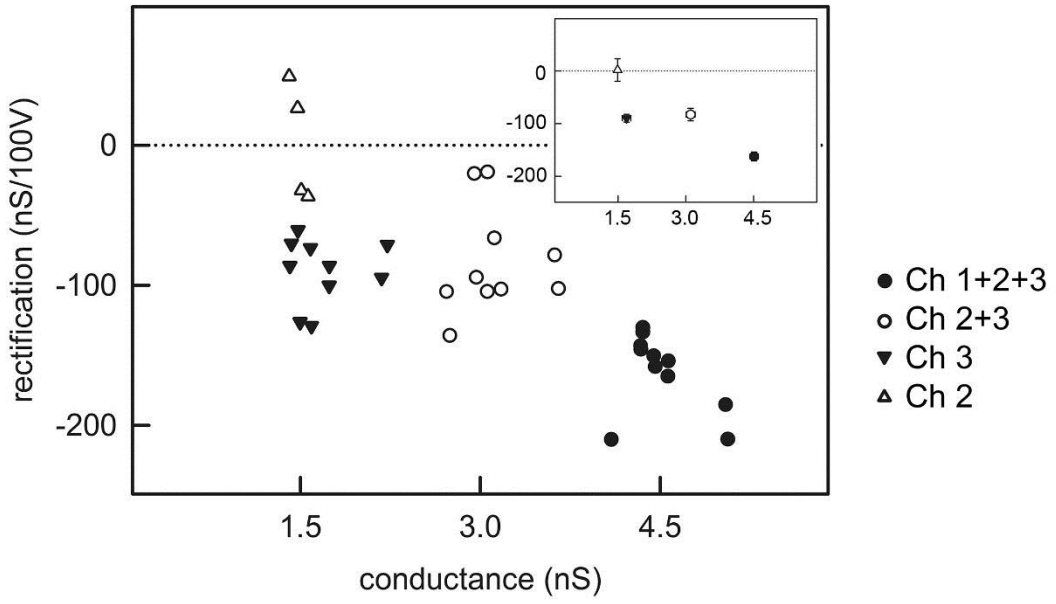

Figure 4.6. Rectification of channels from a variety of experiments. The main figure shows the rectification as a function of the conductance measured at low voltages. Each point is the average result from one experiment. The inset shows the average and the standard error for all data of one kind. Channel 1 + 2 + 3, 2 + 3, 3, and 2 are shown in solid circle, empty circle, solid triangle, and empty triangle, respectively.

Table 4.1 Measured and calculated rectification of each channel. Columns 2 and 3 show the measured conductance and rectification averaged over all experiments (average ± standard error). The columns on the right show calculated values from the adjacent measured values as a test of self-consistency. The calculated rectification was compared to the measured one using the Student's T-test and the P values are listed.

	Measured Conductance (nS)	Measured Rectification (nS/100V)	Calculated Rectification (nS/100V)				
Channels open			1	2	23	123	123
1, 2, 3	4.51 ± 0.09	-162± 8	-86 ± 12 (P=0.60)				
2, 3	3.11 ± 0.10	-83± 12		7 ± 11 (P=0.58)			-173 ± 17 (P=0.70)
3	1.69 ± 0.09	-89± 7			-96 ± 28 (P=0.65)	-193 ± 41 (P=0.74)	
2	1.49 ± 0.03	2 ± 21					

measurements in 2 separate experiments (Fig. 4.5D). All values shown collected are in Fig. 4.6 and the calculated means and standard errors are shown in the inset and table 4.1. Only the rectification values for channels 2 and 3 were

determined directly but even those measurements should be compared with care because they were determined in different regions of the voltage scale.

4.2.2 Channel 2 has an orientation opposite to that of other channels

If the orientation of channel 2 is opposite to that of its adjacent channels and the structure of each channel is the same, the rectification of channel 2 should be opposite to that of the others. Thus, the rectification when all channels are open should be the same as that when only either channel 1 or channel 3 is open. The rectification of channel 2 + 3 should be zero. The results, as summarized in Fig. 4.6 and Table 4.1, are not that straightforward but are largely self-consistent. For instance, the difference between channel 2 + 3 and channel 3 is +7 ± 11 nS/100V, which is close to measured channel 2 (2 ± 21 nS/100V) (P = 0.58). In addition, combing the rectification of channel 2 and 3 yields -96 ± 28 nS/100V, which is not far away from the measured value, -83 ± 12 nS/100V (p = 0.65). The rectification of channel 1 (-86 ± 12 nS/100V), which is the difference between channel 1 + 2 + 3 and channel 2 + 3, is similar to measured value of channel 3 (-89 ± 7 nS/100V) (P = 0.60). This result is consistent with the proposal that the orientation of channel 1 is the same as that of channel 3. We can add the rectification of channel 2 to twice that of channel 3. This yields -193 ± 41 nS/100V, which is close to the measured value, -162 ± 8 nS/100V (P = 0.74). We can also combine the measure value of channel 3 with that of channel 2 + 3, and get a result of -173 ± 17 nS/100V which is essentially the same as the measured value, -162 ± 8 nS/100V (P = 0.70). The results are consistent with channel 2 being fundamentally different from

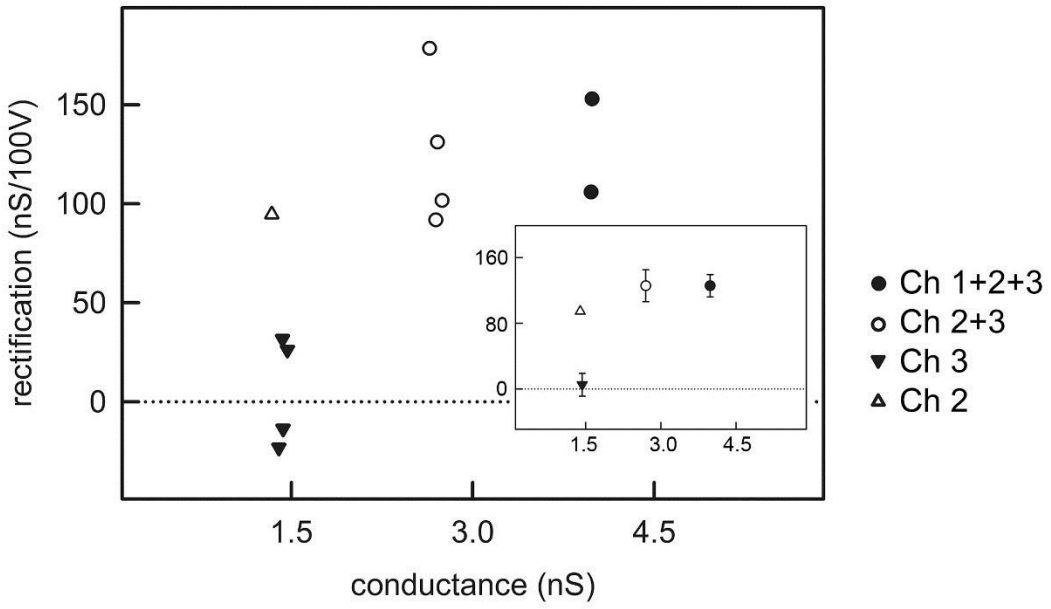

Figure 4.7. Rectification of channels in an anomalous condition. Illustrate the variation of rectification of each channel status in an anomalous condition. The inset shows the average and the standard error. Channel 1 + 2 + 3, 2 + 3, 3, and 2 are shown in solid circle, empty circle, solid triangle, and empty triangle, respectively.

Table 4.2 Measured and calculated rectification in the anomalous experiment. Columns 2 shows the measured rectification (average ± standard error). The columns on the right show calculated values from the adjacent measured values as a test of self-consistency.

	Measured Rectification (nS/100V)	Calculated Rectification (nS/100V)				
Channels open		1	2	23	123	123
1, 2, 3	130 ± 14	4 ± 24				
2, 3	126 ± 20		121 ± 24			131 ± 24
3	5 ± 14			100 ± 14	105 ± 14	
2	95					

channel 1 and 3. Indeed, this would be consistent with channel 2 being in an opposite orientation from channels 1 and 3 if there were some asymmetry in the system. An anomalous experiment supports this hypothesis.

4.2.3 An asymmetrical surface potential changes the rectification of channels

In one experiment, the rectification values were quite different but the results are still self-consistent as in the typical cases, arguing for some unusual asymmetry in this experiment. In this experiment, as in the others, many measurements of the rectification of the channels were performed, thus the values reported are well substantiated. In this anomalous case, although the rectification values for the channels are different from the ones measured in the typical cases, the gating behaviors of channels are unchanged. That is to say that channels 2 and 3 gated at the typical potentials both in sign and magnitude. Channel 2 still closed around -27 mV and channel 3 closed around +28 mV. Therefore, the orientation of this anomalous triplet was the same as that in the other experiments. The rectification values for channels 1 + 2 + 3, 2 + 3, 3 and 2 were 130 ± 14, 126 ± 20, 5 ± 14, and 95 nS/100V, respectively (Table 4.2 and Fig 4.7). The calculated rectification values of each channel state are close to those measured directly. The measured rectification of channel 3 is similar to the calculated one of channel 1 and different from that of channel 2. This result indicates that channel 3 has a similar structure as that of 1 but is fundamentally different from that of channel 2. This suggests that the orientation of channel 2 is opposite to that of channel 1 or 3. Therefore, the orientation of each channel in the anomalous case is the same as that in the typical cases. The difference can be understood as a fundamental asymmetry in the experimental system that shifted all the rectification values.

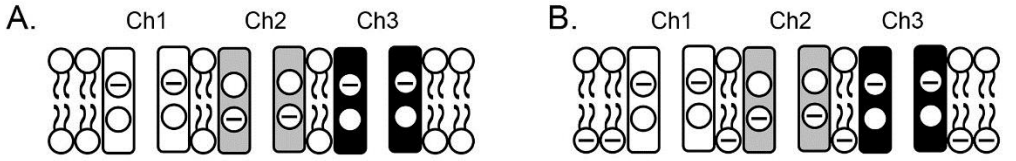

Figure 4.8. Surface potential changes the rectification of channels. Three cylindrical channels in a membrane are arranged in a row. The negative charges in each channel show the asymmetric distribution of charge in the channel. The middle channel (channel 2) has the opposite orientation with its adjacent channels. The cartoon shows the channels without the surface potential (A) or with the surface potential (B).

If the observed rectification is due to an asymmetric charge distribution in the channels, resulting in an asymmetric distribution of mobile ions, the asymmetric charge distribution in channels 2 and 3 in the anomalous case became more and less asymmetric than that in the typical cases, respectively. This shift of the rectification properties may be the consequence of an asymmetric surface potential. The model illustrated in Fig. 4.8 incorporates the finding that each channel is cation selective, so the wall of the channels is shown as containing fixed negative charges (2). For simplicity all the charge distributions within the channels are the same except that channel 2 has an orientation opposite to that if channels 1 and 3. If the surface potential results in more negative surface charges on the bottom side of the membrane affecting each channel, this eliminates the electrical asymmetry of channel 1, and 3, and increases the electric asymmetry of channel 2. Therefore, the surface potential

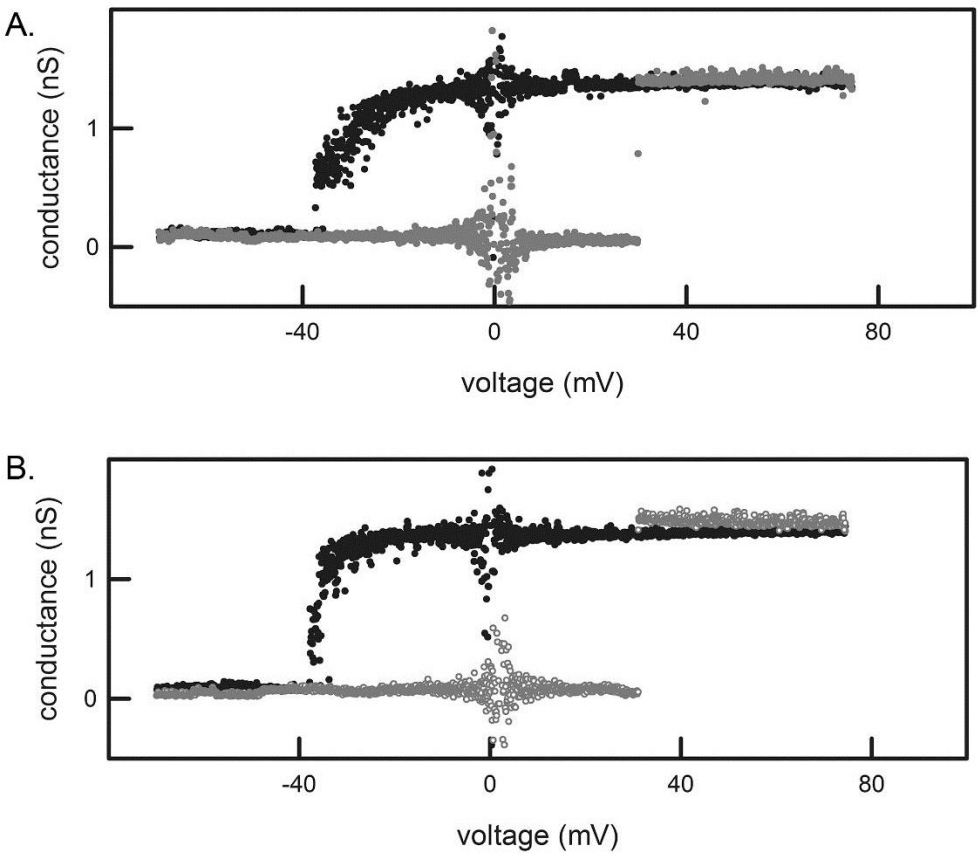

Figure 4.9. Adaptation of channel 2 reopening. The conductance-voltage curve of channel 2 reopening (gray) was overlapped to that of channel 2 closing (black), which occurred later. A. Illustrates a case where channel 2 reopened to a state and stayed in that state until channel closure. B. Illustrates channel 2 reopening to a slightly more conductive state and transitioning to the more typical conducting state at high positive potentials.

would make the rectification of channel 2 much greater in the anomalous case (i.e. with the asymmetric surface potential) as compared to the typical cases.

Another possibility that would result in an overall asymmetry and thus shift the measured rectification would be the presence of some modulating factor in the sample added to the chamber. This factor could bind to the triplet resulting in the observed shift in rectification.

4.2.4 Adaptation of channel 2

The experiments have shown signs of more complex behavior. Indeed, some of the variability in the data could be attributed to channels entering somewhat different conformation when they transition between the open and closed state. Some clear observations show that a channel may transition from a closed state to an open state that may not be the most stable state and then switch to the more typical conductance state by way of a small conductance change. Two examples are illustrated in Fig. 4.7. In panel A, the channel reopened and stayed in the same state, as far as can be discerned from the record, until it closed at negative potentials. In panel B, channel 2 reopened to a slightly more conductive state with negative rectification and then underwent a change at high positive potentials to a state with slightly positive rectification, resembling that illustrated in panel A. It is likely that in the reopening process illustrated in panel B, channel 2 entered a higher energy state and then adapted to the lower energy state with time (Fig 4.7B). Such transitions were observed from time to time.

4.3 Conclusion and Discussion

4.3.1 Orientation of channel 2 is opposite to other channels

Rectification probes the structure and dynamics of channels in their native state. It is different from other methods, such as mutations or chemical modifications, which may alter the structure or dynamics of the channel. Although the surface potential resulting from the asymmetric arrangement of

negatively charged lipids or the inherent surface charges of the channel may influence to the rectification, it is clear that the rectification of channel 3 is different from that of channel 2 and is the same as that of channel 1. In addition, channel 2 closes at the same magnitude but different sign of voltage as compared to channel 3. This indicates the orientation of channel 1 and 3 are the same, but the orientation of channel 2 is antiparallel to other channels. Antiparallel orientation is rare in protein channels. A recently discovered fluoride ion channel, which is composed of an antiparallel homodimer, is an example of the same polypeptide inserting into a membrane in two opposite directions (137, 138). Typically, channel inserts into membranes in only one direction. However, the mitochondrial channel, VDAC, has been shown to insert into a planar membranes in both direction (139, 140). In addition, it is possible that the triple channel may insert into the membrane as a complex, instead of inserting into the membrane as an individual channel and forming a triplet channel later. Although it is possible the channel 2 is formed by a different protein from other channels, channel 2 and 3 have the same properties, including their conductance, cation selectivity and steepness of voltage dependence. Once the channel former is identified, we may be able to distinguish between these possibilities.

4.3.2 Identification of the channel former

The proteins responsible for forming the triplet channel were first present as a contamination of the isolation of the Bax protein. Originally, the triplet channel was believed to be a Bax channel, because Bax was purified

using an affinity column and Bax is able to translocate to the MOM and formed channels to release IMS proteins. However, the triplet channel was still observed when the product was isolated from an *E*. coli strain without the Bax construct. The triplet channel is probably formed by a protein, instead of small molecules, such as peptides, because the sample (less than 20 mL) was dialyzed with an 8,000 MW cut-off dialysis membrane against 3 L and then 5 L of buffer. In any case, the channel former is minor, a minor constituent of the purified Bax fraction. Only a single band for Bax was observed on the silver-stained SDS-PAGE (~ 450 ng of protein was loaded). The isolated sample was sent to the Proteomics Core Facility at University of Maryland at College Park for analysis by mass-spectrometry-based proteomics to search for possible candidates of the channel former. The workflow was performed with trypsin digestion, reversed-phase liquid chromatography, linear ion trap-Orbitrap instrument, and MS/MS ions searching on the Mascot search engine. No suitable candidate was identified.

4.3.2.1 Identify the cellular compartment in which the triplet resides

Although the triplet channel was discovered in the soluble fraction (the cytosol fraction) of the cell lysate, it is still possible that the channel former arose from a membrane, either the inner or outer membrane. The channel former could also be secreted into the culture medium as an exotoxin. The culture medium was collected after the intact cells and cell debris are removed by centrifugation. Proteins were extracted from the inner and outer membranes using the published method of selective detergent extraction (141). Two percent

Table 4.3 Properties of some porins and the triplet channel.

	Open channel conductance (nS) (in 1M KCl,)	Selectivity (Po/Pa) (0.01M/0.1 M KCl gradient)	Pore size (nm)	Number of channels
Triplet channel (136)	1.5	3.6	0.9	3
OmpC (156)	1.5	26	1.0	3
OmpF (156)	2.1	3.6	0.7 or 1.2	3
PhoE (156)	1.8	0.3	1.1	3

n-laurylsarcosine (w/v) is used to extract the proteins from the inner membrane and then octyl-glucoside was used to extract those from the outer membrane (141). Each fraction was tested using the planar membrane technique to determine is the presence of the triplet channel. Our preliminary data indicated that the channel former is in the outer membrane.

4.3.2.2 Testing whether the triplet channel is a porin

The triplet channel is a three-channel unit. It has a large conductance, 1.5 nS in 1 M KCl. That translates into a pore that is ~ 0.9 nm in diameter (94, 136). These properties are similar to those of bacterial porins, located on the outer membrane. Table 4.3 shows the properties of each channel of the triplet and those of some porins. Although the properties of porins are well established, perhaps, however unlikely, experimental conditions may affect the results (142–144). Therefore, the major porins with similar properties were tested with our planar membrane setup. Neither OmpC nor OmpF showed the characteristic properties of the triplet channel, such as highly cooperativity and high voltage dependence. Instead the characteristic behavior of OmpC and OmpF were

observed. Thus neither OmpC nor OmpF is responsible for the channel forming activity.

4.3.2.3 Single- and multi- Porin knock outs

Another way to search for the triplet channel former is by utilizing *E*. coli strains with single- or multi-porin knock-outs. In this way, if the gene of channel former was removed, the characteristic cooperative behaviors should not be observed and these behaviors should be observed if a construct with the gene is restored and expressed. *E*. coli BL21 (DE3) omp9 *ΔlamB ompF::Tn5 ΔompA ΔompC ompN::Ω*, in which several genes of porin were either removed or interrupted, was used (141). Moreover, several candidates of the channel former obtained from a computational analysis were also tested. To conduct the computational analysis, protein BLAST was performed with known porins as query sequences, such as OmpF, OmpN, and ScrY, to find candidates. In addition, the candidates need to show channel structures by using the SWISS-MODEL from ExPASY. The *E*. coli strains with corresponding single knock-outs (*ΔrhsD, ΔrhsE, ΔhtrE, or ΔflgE*) were purchased from the Coli Genetic Stock Center. We found the triplet channel in all the knock-outs tested. The results demonstrate that LamB, OmpF, OmpA, OmpC, OmpN, RhsD, RhsE, HtrE, and FlgE are not the channel formers.

4.3.3 Possible physiological role of the triplet channel

The triple channel has not only a large single channel conductance and triplet behavior, but also possesses idiosyncratic features: steep voltage

dependence and high cooperativity. These properties indicates that the triplet channel is (a) permeable to small molecules, such as metabolites, nutrients, and antibiotics, (b) very sensitive to changes in transmembrane potential and (c) highly regulated. These unprecedented properties most likely point to a highly regulated structure with critical physiological functions for *E*. coli.

Because nonspecific porins reside in the outer membrane, typically it is impossible to establish transmembrane potential across the outer membrane based on maintenance of ion gradients or the use of ion pumps. However, a Donnan potential does exist. The polyanionic oligosaccharides in the periplasmic space result in a Donnan potential, which is less than 30 mV (with 100 mM of cation concentration in the bulk solution) (145, 146). This can close channels 2 or 3 depending on the sign and orientation. Higher potentials would be present at lower ionic strengths.

The similarity to the porins indicates that the physiological role of the triplet channel may be similar to that of the porins. Porins are involved in the facilitating the translocation of small molecules including antibiotics across the outer membrane (147, 148). Bacteria have developed several strategies to survive in the presence of antibiotics. For example, bacteria reduce the expression level of certain porins (149, 150), express mutated porins with lower permeability to antibiotics (151, 152), and raise the expression level of some efflux pumps (153, 154). Perhaps the triplet channel is involved in the process of controlling the entry of molecules into the cells.

4.4 Acknowledgements

We thank Shang H. Lin, Benjamin Wu and Jennifer Kunselman for helping with the experiments on planar membranes.

References

1. Kerr, J. F., Wyllie, A. H., and Currie, A. R. (1972) Apoptosis: a basic biological phenomenon with wide-ranging implications in tissue kinetics. *Br. J. Cancer*. **26**, 239–57

2. Searle, J., Kerr, J. F., and Bishop, C. J. (1982) Necrosis and apoptosis: distinct modes of cell death with fundamentally different significance. *Pathol. Annu.* **17 Pt 2**, 229–59

3. Saelens, X., Festjens, N., Vande Walle, L., van Gurp, M., van Loo, G., and Vandenabeele, P. (2004) Toxic proteins released from mitochondria in cell death. *Oncogene*. **23**, 2861–74

4. Crompton, M. (1999) The mitochondrial permeability transition pore and its role in cell death. *Biochem. J.* **341 (Pt 2**, 233–49

5. Antonsson, B., Montessuit, S., Lauper, S., Eskes, R., and Martinou, J. C. (2000) Bax oligomerization is required for channel-forming activity in liposomes and to trigger cytochrome c release from mitochondria. *Biochem. J.* **345 Pt 2**, 271–8

6. Saito, M., Korsmeyer, S. J., and Schlesinger, P. H. (2000) BAX-dependent transport of cytochrome c reconstituted in pure liposomes. *Nat. Cell Biol.* **2**, 553–5

7. Pavlov, E. V., Priault, M., Pietkiewicz, D., Cheng, E. H., Antonsson, B., Manon, S., Korsmeyer, S. J., Mannella, C. A., and Kinnally, K. W. (2001) A novel, high conductance channel of mitochondria linked to apoptosis in mammalian cells and Bax expression in yeast. *J. Cell Biol.* **155**, 725–31

8. Belaud-Rotureau, M. A., Leducq, N., Macouillard Poulletier de Gannes, F., Diolez, P., Lacoste, L., Lacombe, F., Bernard, P., and Belloc, F. (2000) Early transitory rise in intracellular pH leads to Bax conformation change during ceramide-induced apoptosis. *Apoptosis*. **5**, 551–60

9. Pastorino, J. G., Tafani, M., Rothman, R. J., Marcinkeviciute, A., Hoek, J. B., Farber, J. L., and Marcineviciute, A. (1999) Functional consequences of the sustained or transient activation by Bax of the mitochondrial permeability

transition pore. *J. Biol. Chem.* **274**, 31734–9

10. Siskind, L. J., and Colombini, M. (2000) The lipids C2- and C16-ceramide form large stable channels. Implications for apoptosis. *J. Biol. Chem.* **275**, 38640–4

11. Siskind, L. J., Kolesnick, R. N., and Colombini, M. (2002) Ceramide channels increase the permeability of the mitochondrial outer membrane to small proteins. *J. Biol. Chem.* **277**, 26796–803

12. Yang, J., Liu, X., Bhalla, K., Kim, C. N., Ibrado, A. M., Cai, J., Peng, T. I., Jones, D. P., and Wang, X. (1997) Prevention of apoptosis by Bcl-2: release of cytochrome c from mitochondria blocked. *Science*. **275**, 1129–32

13. Kluck, R. M., Bossy-Wetzel, E., Green, D. R., and Newmeyer, D. D. (1997) The release of cytochrome c from mitochondria: a primary site for Bcl-2 regulation of apoptosis. *Science*. **275**, 1132–6

14. Lovell, J. F., Billen, L. P., Bindner, S., Shamas-Din, A., Fradin, C., Leber, B., and Andrews, D. W. (2008) Membrane binding by tBid initiates an ordered series of events culminating in membrane permeabilization by Bax. *Cell*. **135**, 1074–84

15. Kuwana, T., Mackey, M. R., Perkins, G., Ellisman, M. H., Latterich, M., Schneiter, R., Green, D. R., and Newmeyer, D. D. (2002) Bid, Bax, and lipids cooperate to form supramolecular openings in the outer mitochondrial membrane. *Cell*. **111**, 331–42

16. Bender, T., and Martinou, J.-C. (2013) Where killers meet--permeabilization of the outer mitochondrial membrane during apoptosis. *Cold Spring Harb. Perspect. Biol.* **5**, a011106

17. Siskind, L. J., Feinstein, L., Yu, T., Davis, J. S., Jones, D., Choi, J., Zuckerman, J. E., Tan, W., Hill, R. B., Hardwick, J. M., and Colombini, M. (2008) Anti-apoptotic Bcl-2 Family Proteins Disassemble Ceramide Channels. *J. Biol. Chem.* **283**, 6622–30

18. Andersen, J. L., and Kornbluth, S. (2012) Mcl-1 rescues a glitch in the matrix. *Nat. Cell Biol.* **14**, 563–5

19. Mikhailov, V., Mikhailova, M., Pulkrabek, D. J., Dong, Z., Venkatachalam, M. A., and Saikumar, P. (2001) Bcl-2 prevents Bax oligomerization in the mitochondrial outer membrane. *J. Biol. Chem.* **276**, 18361–74

20. Lazarou, M., Stojanovski, D., Frazier, A. E., Kotevski, A., Dewson, G., Craigen, W. J., Kluck, R. M., Vaux, D. L., and Ryan, M. T. (2010) Inhibition of Bak activation by VDAC2 is dependent on the Bak transmembrane anchor. *J. Biol. Chem.* **285**, 36876–83

21. Cheng, E. H. Y., Sheiko, T. V, Fisher, J. K., Craigen, W. J., and Korsmeyer, S. J. (2003) VDAC2 inhibits BAK activation and mitochondrial apoptosis. *Science*. **301**, 513–7

22. Boise, L. H., González-García, M., Postema, C. E., Ding, L., Lindsten, T., Turka, L. A., Mao, X., Nuñez, G., and Thompson, C. B. (1993) bcl-x, a bcl-2-related gene that functions as a dominant regulator of apoptotic cell death. *Cell*. **74**, 597–608

23. Yao, Y., Bobkov, A. A., Plesniak, L. A., and Marassi, F. M. (2009) Mapping the interaction of pro-apoptotic tBID with pro-survival BCL-XL. *Biochemistry*. **48**, 8704–11

24. Er, E., Oliver, L., Cartron, P.-F., Juin, P., Manon, S., and Vallette, F. M. (2006) Mitochondria as the target of the pro-apoptotic protein Bax. *Biochim. Biophys. Acta*. **1757**, 1301–11

25. Antonsson, B., Montessuit, S., Sanchez, B., and Martinou, J. C. (2001) Bax is present as a high molecular weight oligomer/complex in the mitochondrial membrane of apoptotic cells. *J. Biol. Chem.* **276**, 11615–23

26. Leber, B., Lin, J., and Andrews, D. W. (2010) Still embedded together binding to membranes regulates Bcl-2 protein interactions. *Oncogene*. **29**, 5221–30

27. Leber, B., Lin, J., and Andrews, D. W. (2007) Embedded together: the life and death consequences of interaction of the Bcl-2 family with membranes. *Apoptosis*. **12**, 897–911

28. Tan, C., Dlugosz, P. J., Peng, J., Zhang, Z., Lapolla, S. M., Plafker, S. M., Andrews, D. W., and Lin, J. (2006) Auto-activation of the apoptosis protein Bax increases mitochondrial membrane permeability and is inhibited by Bcl-2.

J. Biol. Chem. **281**, 14764–75

29. Llambi, F., Moldoveanu, T., Tait, S. W. G., Bouchier-Hayes, L., Temirov, J., McCormick, L. L., Dillon, C. P., and Green, D. R. (2011) A unified model of mammalian BCL-2 protein family interactions at the mitochondria. *Mol. Cell*. **44**, 517–31

30. Du, H., Wolf, J., Schafer, B., Moldoveanu, T., Chipuk, J. E., and Kuwana, T. (2011) BH3 domains other than Bim and Bid can directly activate Bax/Bak. *J. Biol. Chem.* **286**, 491–501

31. Czabotar, P. E., Lee, E. F., van Delft, M. F., Day, C. L., Smith, B. J., Huang, D. C. S., Fairlie, W. D., Hinds, M. G., and Colman, P. M. (2007) Structural insights into the degradation of Mcl-1 induced by BH3 domains. *Proc. Natl. Acad. Sci. U. S. A.* **104**, 6217–22

32. Chen, L., Willis, S. N., Wei, A., Smith, B. J., Fletcher, J. I., Hinds, M. G., Colman, P. M., Day, C. L., Adams, J. M., and Huang, D. C. S. (2005) Differential targeting of prosurvival Bcl-2 proteins by their BH3-only ligands allows complementary apoptotic function. *Mol. Cell*. **17**, 393–403

33. Billen, L. P., Kokoski, C. L., Lovell, J. F., Leber, B., and Andrews, D. W. (2008) Bcl-XL inhibits membrane permeabilization by competing with Bax. *PLoS Biol.* **6**, e147

34. Suzuki, M., Youle, R. J., and Tjandra, N. (2000) Structure of Bax: coregulation of dimer formation and intracellular localization. *Cell*. **103**, 645–54

35. Hinds, M. G., Lackmann, M., Skea, G. L., Harrison, P. J., Huang, D. C. S., and Day, C. L. (2003) The structure of Bcl-w reveals a role for the C-terminal residues in modulating biological activity. *EMBO J.* **22**, 1497–507

36. Liu, X., Dai, S., Zhu, Y., Marrack, P., and Kappler, J. W. (2003) The structure of a Bcl-xL/Bim fragment complex: implications for Bim function. *Immunity*. **19**, 341–52

37. Sattler, M., Liang, H., Nettesheim, D., Meadows, R. P., Harlan, J. E., Eberstadt, M., Yoon, H. S., Shuker, S. B., Chang, B. S., Minn, A. J., Thompson, C. B., and Fesik, S. W. (1997) Structure of Bcl-xL-Bak peptide complex: recognition between regulators of apoptosis. *Science*. **275**, 983–6

38. Lessene, G., Czabotar, P. E., and Colman, P. M. (2008) BCL-2 family antagonists for cancer therapy. *Nat. Rev. Drug Discov.* **7**, 989–1000

39. Hanahan, D., and Weinberg, R. A. (2011) Hallmarks of cancer: the next generation. *Cell*. **144**, 646–74

40. Kang, M. H., and Reynolds, C. P. (2009) Bcl-2 inhibitors: targeting mitochondrial apoptotic pathways in cancer therapy. *Clin. Cancer Res.* **15**, 1126–32

41. Billard, C. (2013) BH3 mimetics: status of the field and new developments. *Mol. Cancer Ther.* **12**, 1691–700

42. van Delft, M. F., Wei, A. H., Mason, K. D., Vandenberg, C. J., Chen, L., Czabotar, P. E., Willis, S. N., Scott, C. L., Day, C. L., Cory, S., Adams, J. M., Roberts, A. W., and Huang, D. C. S. (2006) The BH3 mimetic ABT-737 targets selective Bcl-2 proteins and efficiently induces apoptosis via Bak/Bax if Mcl-1 is neutralized. *Cancer Cell*. **10**, 389–99

43. Oltersdorf, T., Elmore, S. W., Shoemaker, A. R., Armstrong, R. C., Augeri, D. J., Belli, B. A., Bruncko, M., Deckwerth, T. L., Dinges, J., Hajduk, P. J., Joseph, M. K., Kitada, S., Korsmeyer, S. J., Kunzer, A. R., Letai, A., Li, C., Mitten, M. J., Nettesheim, D. G., Ng, S., Nimmer, P. M., O'Connor, J. M., Oleksijew, A., Petros, A. M., Reed, J. C., Shen, W., Tahir, S. K., Thompson, C. B., Tomaselli, K. J., Wang, B., Wendt, M. D., Zhang, H., Fesik, S. W., and Rosenberg, S. H. (2005) An inhibitor of Bcl-2 family proteins induces regression of solid tumours. *Nature*. **435**, 677–81

44. Tse, C., Shoemaker, A. R., Adickes, J., Anderson, M. G., Chen, J., Jin, S., Johnson, E. F., Marsh, K. C., Mitten, M. J., Nimmer, P., Roberts, L., Tahir, S. K., Xiao, Y., Yang, X., Zhang, H., Fesik, S., Rosenberg, S. H., and Elmore, S. W. (2008) ABT-263: a potent and orally bioavailable Bcl-2 family inhibitor. *Cancer Res.* **68**, 3421–8

45. Rudin, C. M., Hann, C. L., Garon, E. B., Ribeiro de Oliveira, M., Bonomi, P. D., Camidge, D. R., Chu, Q., Giaccone, G., Khaira, D., Ramalingam, S. S., Ranson, M. R., Dive, C., McKeegan, E. M., Chyla, B. J., Dowell, B. L., Chakravartty, A., Nolan, C. E., Rudersdorf, N., Busman, T. A., Mabry, M. H., Krivoshik, A. P., Humerickhouse, R. A., Shapiro, G. I., and Gandhi, L. (2012)

Phase II study of single-agent navitoclax (ABT-263) and biomarker correlates in patients with relapsed small cell lung cancer. *Clin. Cancer Res.* **18**, 3163–9

46. Wilson, W. H., O'Connor, O. A., Czuczman, M. S., LaCasce, A. S., Gerecitano, J. F., Leonard, J. P., Tulpule, A., Dunleavy, K., Xiong, H., Chiu, Y.-L., Cui, Y., Busman, T., Elmore, S. W., Rosenberg, S. H., Krivoshik, A. P., Enschede, S. H., and Humerickhouse, R. A. (2010) Navitoclax, a targeted high-affinity inhibitor of BCL-2, in lymphoid malignancies: a phase 1 dose-escalation study of safety, pharmacokinetics, pharmacodynamics, and antitumour activity. *Lancet. Oncol.* **11**, 1149–59

47. Todt, F., Cakir, Z., Reichenbach, F., Youle, R. J., and Edlich, F. (2013) The C-terminal helix of Bcl-x(L) mediates Bax retrotranslocation from the mitochondria. *Cell Death Differ.* **20**, 333–42

48. Griffiths, G. J., Dubrez, L., Morgan, C. P., Jones, N. A., Whitehouse, J., Corfe, B. M., Dive, C., and Hickman, J. A. (1999) Cell damage-induced conformational changes of the pro-apoptotic protein Bak in vivo precede the onset of apoptosis. *J. Cell Biol.* **144**, 903–14

49. Ferrer, P. E., Frederick, P., Gulbis, J. M., Dewson, G., and Kluck, R. M. (2012) Translocation of a Bak C-terminus mutant from cytosol to mitochondria to mediate cytochrome C release: implications for Bak and Bax apoptotic function. *PLoS One*. **7**, e31510

50. Nechushtan, A., Smith, C. L., Hsu, Y. T., and Youle, R. J. (1999) Conformation of the Bax C-terminus regulates subcellular location and cell death. *EMBO J.* **18**, 2330–41

51. Hsu, Y. Te, and Youle, R. J. (1997) Nonionic detergents induce dimerization among members of the Bcl-2 family. *J. Biol. Chem.* **272**, 13829–34

52. Annis, M. G., Soucie, E. L., Dlugosz, P. J., Cruz-Aguado, J. A., Penn, L. Z., Leber, B., and Andrews, D. W. (2005) Bax forms multispanning monomers that oligomerize to permeabilize membranes during apoptosis. *EMBO J.* **24**, 2096–103

53. Gavathiotis, E., Reyna, D. E., Davis, M. L., Bird, G. H., and Walensky, L. D. (2010) BH3-triggered structural reorganization drives the activation of proapoptotic BAX. *Mol. Cell*. **40**, 481–92

54. Dewson, G., Kratina, T., Sim, H. W., Puthalakath, H., Adams, J. M., Colman, P. M., and Kluck, R. M. (2008) To trigger apoptosis, Bak exposes its BH3 domain and homodimerizes via BH3:groove interactions. *Mol. Cell*. **30**, 369–80

55. Birbes, H., El Bawab, S., Obeid, L. M., and Hannun, Y. A. (2002) Mitochondria and ceramide: intertwined roles in regulation of apoptosis. *Adv. Enzyme Regul.* **42**, 113–29

56. Masamune, A., Igarashi, Y., and Hakomori, S. (1996) Regulatory role of ceramide in interleukin (IL)-1 beta-induced E-selectin expression in human umbilical vein endothelial cells. Ceramide enhances IL-1 beta action, but is not sufficient for E-selectin expression. *J. Biol. Chem.* **271**, 9368–75

57. Geilen, C. C., Bektas, M., Wieder, T., Kodelja, V., Goerdt, S., and Orfanos, C. E. (1997) 1alpha,25-dihydroxyvitamin D3 induces sphingomyelin hydrolysis in HaCaT cells via tumor necrosis factor alpha. *J. Biol. Chem.* **272**, 8997–9001

58. García-Ruiz, C., Colell, A., Marí, M., Morales, A., and Fernández-Checa, J. C. (1997) Direct effect of ceramide on the mitochondrial electron transport chain leads to generation of reactive oxygen species. Role of mitochondrial glutathione. *J. Biol. Chem.* **272**, 11369–77

59. Modur, V., Zimmerman, G. A., Prescott, S. M., and McIntyre, T. M. (1996) Endothelial cell inflammatory responses to tumor necrosis factor alpha. Ceramide-dependent and -independent mitogen-activated protein kinase cascades. *J. Biol. Chem.* **271**, 13094–102

60. Obeid, L. M., Linardic, C. M., Karolak, L. A., and Hannun, Y. A. (1993) Programmed cell death induced by ceramide. *Science*. **259**, 1769–71

61. Kolesnick, R. N., and Krönke, M. (1998) Regulation of ceramide production and apoptosis. *Annu. Rev. Physiol.* **60**, 643–65

62. Dbaibo, G. S., Perry, D. K., Gamard, C. J., Platt, R., Poirier, G. G., Obeid, L. M., and Hannun, Y. A. (1997) Cytokine response modifier A (CrmA) inhibits ceramide formation in response to tumor necrosis factor (TNF)-alpha: CrmA and Bcl-2 target distinct components in the apoptotic pathway. *J. Exp. Med.* **185**, 481–90

63. Hannun, Y. A. (1996) Functions of ceramide in coordinating cellular responses to stress. *Science*. **274**, 1855–9

64. Bielawska, A., Crane, H. M., Liotta, D., Obeid, L. M., and Hannun, Y. A. (1993) Selectivity of ceramide-mediated biology. Lack of activity of erythro-dihydroceramide. *J. Biol. Chem.* **268**, 26226–32

65. Jarvis, W. D., Kolesnick, R. N., Fornari, F. A., Traylor, R. S., Gewirtz, D. A., and Grant, S. (1994) Induction of apoptotic DNA damage and cell death by activation of the sphingomyelin pathway. *Proc. Natl. Acad. Sci. U. S. A.* **91**, 73–7

66. Cifone, M. G., De Maria, R., Roncaioli, P., Rippo, M. R., Azuma, M., Lanier, L. L., Santoni, A., and Testi, R. (1994) Apoptotic signaling through CD95 (Fas/Apo-1) activates an acidic sphingomyelinase. *J. Exp. Med.* **180**, 1547–52

67. Chmura, S. J., Mauceri, H. J., Advani, S., Heimann, R., Beckett, M. A., Nodzenski, E., Quintans, J., Kufe, D. W., and Weichselbaum, R. R. (1997) Decreasing the apoptotic threshold of tumor cells through protein kinase C inhibition and sphingomyelinase activation increases tumor killing by ionizing radiation. *Cancer Res.* **57**, 4340–7

68. Alphonse, G., Bionda, C., Aloy, M.-T., Ardail, D., Rousson, R., and Rodriguez-Lafrasse, C. (2004) Overcoming resistance to gamma-rays in squamous carcinoma cells by poly-drug elevation of ceramide levels. *Oncogene*. **23**, 2703–15

69. Selzner, M., Bielawska, A., Morse, M. A., Rüdiger, H. A., Sindram, D., Hannun, Y. A., and Clavien, P. A. (2001) Induction of apoptotic cell death and prevention of tumor growth by ceramide analogues in metastatic human colon cancer. *Cancer Res.* **61**, 1233–40

70. Ardail, D., Popa, I., Alcantara, K., Pons, A., Zanetta, J. P., Louisot, P., Thomas, L., and Portoukalian, J. (2001) Occurrence of ceramides and neutral glycolipids with unusual long-chain base composition in purified rat liver mitochondria. *FEBS Lett.* **488**, 160–4

71. Dai, Q., Liu, J., Chen, J., Durrant, D., McIntyre, T. M., and Lee, R. M. (2004) Mitochondrial ceramide increases in UV-irradiated HeLa cells and is mainly

derived from hydrolysis of sphingomyelin. *Oncogene*. **23**, 3650–8

72. Birbes, H., El Bawab, S., Hannun, Y. A., and Obeid, L. M. (2001) Selective hydrolysis of a mitochondrial pool of sphingomyelin induces apoptosis. *FASEB J.* **15**, 2669–79

73. Stiban, J., Fistere, D., and Colombini, M. (2006) Dihydroceramide hinders ceramide channel formation: Implications on apoptosis. *Apoptosis*. **11**, 773–80

74. Bionda, C., Portoukalian, J., Schmitt, D., Rodriguez-Lafrasse, C., and Ardail, D. (2004) Subcellular compartmentalization of ceramide metabolism: MAM (mitochondria-associated membrane) and/or mitochondria? *Biochem. J.* **382**, 527–33

75. El Bawab, S., Roddy, P., Qian, T., Bielawska, A., Lemasters, J. J., and Hannun, Y. A. (2000) Molecular cloning and characterization of a human mitochondrial ceramidase. *J. Biol. Chem.* **275**, 21508–13

76. Shimeno, H., Soeda, S., Sakamoto, M., Kouchi, T., Kowakame, T., and Kihara, T. (1998) Partial purification and characterization of sphingosine N-acyltransferase (ceramide synthase) from bovine liver mitochondrion-rich fraction. *Lipids*. **33**, 601–5

77. Siskind, L. J., Kolesnick, R. N., and Colombini, M. (2006) Ceramide forms channels in mitochondrial outer membranes at physiologically relevant concentrations. *Mitochondrion*. **6**, 118–25

78. Samanta, S., Stiban, J., Maugel, T. K., and Colombini, M. (2011) Visualization of ceramide channels by transmission electron microscopy. *Biochim. Biophys. Acta*. **1808**, 1196–201

79. Siskind, L. J., Davoody, A., Lewin, N., Marshall, S., and Colombini, M. (2003) Enlargement and contracture of C2-ceramide channels. *Biophys. J.* **85**, 1560–75

80. Anishkin, A., Sukharev, S., and Colombini, M. (2006) Searching for the molecular arrangement of transmembrane ceramide channels. *Biophys. J.* **90**, 2414–26

81. Perera, M. N., Lin, S. H., Peterson, Y. K., Bielawska, A., Szulc, Z. M., Bittman, R., and Colombini, M. (2012) Bax and Bcl-xL exert their regulation on different sites of the ceramide channel. *Biochem. J.* **445**, 81–91

82. Mullen, T. D., Hannun, Y. A., and Obeid, L. M. (2012) Ceramide synthases at the centre of sphingolipid metabolism and biology. *Biochem. J.* **441**, 789–802

83. Birbes, H., Luberto, C., Hsu, Y.-T., El Bawab, S., Hannun, Y. A., and Obeid, L. M. (2005) A mitochondrial pool of sphingomyelin is involved in TNFalpha-induced Bax translocation to mitochondria. *Biochem. J.* **386**, 445–51

84. Rodriguez-Lafrasse, C., Alphonse, G., Broquet, P., Aloy, M. T., Louisot, P., and Rousson, R. (2001) Temporal relationships between ceramide production, caspase activation and mitochondrial dysfunction in cell lines with varying sensitivity to anti-Fas-induced apoptosis. *Biochem. J.* **357**, 407–16

85. Ganesan, V., Perera, M. N., Colombini, D., Datskovskiy, D., Chadha, K., and Colombini, M. (2010) Ceramide and activated Bax act synergistically to permeabilize the mitochondrial outer membrane. *Apoptosis*. **15**, 553–62

86. Hille, B. (1978) Ionic channels in excitable membranes. Current problems and biophysical approaches. *Biophys. J.* **22**, 283–94

87. Hodgkin, A. L., and Huxley, A. F. (1990) A quantitative description of membrane current and its application to conduction and excitation in nerve. 1952. *Bull. Math. Biol.* **52**, 25–71; discussion 5–23

88. Bainbridge, G., Gokce, I., and Lakey, J. H. (1998) Voltage gating is a fundamental feature of porin and toxin beta-barrel membrane channels. *FEBS Lett.* **431**, 305–8

89. Plugge, B., Gazzarrini, S., Nelson, M., Cerana, R., Van Etten, J. L., Derst, C., DiFrancesco, D., Moroni, A., and Thiel, G. (2000) A potassium channel protein encoded by chlorella virus PBCV-1. *Science*. **287**, 1641–4

90. Colombini, M. (2012) Mitochondrial outer membrane channels. *Chem. Rev.* **112**, 6373–87

91. Kung, C., and Saimi, Y. (1982) The physiological basis of taxes in

Paramecium. *Annu. Rev. Physiol.* **44**, 519–34

92. Martinac, B., Saimi, Y., and Kung, C. (2008) Ion channels in microbes. *Physiol. Rev.* **88**, 1449–90

93. Basañez, G., Zhang, J., Chau, B. N., Maksaev, G. I., Frolov, V. A., Brandt, T. A., Burch, J., Hardwick, J. M., and Zimmerberg, J. (2001) Pro-apoptotic cleavage products of Bcl-xL form cytochrome c-conducting pores in pure lipid membranes. *J. Biol. Chem.* **276**, 31083–91

94. Lin, S. H., Perera, M. N., Nguyen, T., Datskovskiy, D., Miles, M., and Colombini, M. (2011) Bax forms two types of channels, one of which is voltage-gated. *Biophys. J.* **101**, 2163–9

95. von Ahsen, O., Renken, C., Perkins, G., Kluck, R. M., Bossy-Wetzel, E., and Newmeyer, D. D. (2000) Preservation of mitochondrial structure and function after Bid- or Bax-mediated cytochrome c release. *J. Cell Biol.* **150**, 1027–36

96. Parsons, D. F., Williams, G. R., and Chance, B. (1966) Characteristics of isolated and purified preparations of the outer and inner membranes of mitochondria. *Ann. N. Y. Acad. Sci.* **137**, 643–66

97. Clarke, S. (1976) A major polypeptide component of rat liver mitochondria: carbamyl phosphate synthetase. *J. Biol. Chem.* **251**, 950–61

98. MARGOLIASH, E., and FROHWIRT, N. (1959) Spectrum of horse-heart cytochrome c. *Biochem. J.* **71**, 570–2

99. Wojtczak, L., Zaluska, H., Wroniszewska, A., and Wojtczak, A. B. (1972) Assay for the intactness of the outer membrane in isolated mitochondria. *Acta Biochim. Pol.* **19**, 227–34

100. Schnaitman, C., and Greenawalt, J. W. (1968) Enzymatic properties of the inner and outer membranes of rat liver mitochondria. *J. Cell Biol.* **38**, 158–75

101. Kim, D. E., Chivian, D., and Baker, D. (2004) Protein structure prediction and analysis using the Robetta server. *Nucleic Acids Res.* **32**, W526–31

102. Humphrey, W., Dalke, A., and Schulten, K. (1996) VMD: visual molecular dynamics. *J. Mol. Graph.* **14**, 33–8, 27–8

103. Phillips, J. C., Braun, R., Wang, W., Gumbart, J., Tajkhorshid, E., Villa, E., Chipot, C., Skeel, R. D., Kalé, L., and Schulten, K. (2005) Scalable molecular dynamics with NAMD. *J. Comput. Chem.* **26**, 1781–802

104. MacKerell, A. D. J., Bashford, D., Bellott, M., Dunbrack, R. L., Evanseck, J. D., Field, M. J., Fischer, S., Gao, J., Guo, H., Ha, S., Joseph-McCarthy, D., Kuchnir, L., Kuczera, K., Lau, F. T., Mattos, C., Michnick, S., Ngo, T., Nguyen, D. T., Prodhom, B., Reiher, W. E., Roux, B., Schlenkrich, M., Smith, J. C., Stote, R., Straub, J., Watanabe, M., Wiórkiewicz-Kuczera, J., Yin, D., and Karplus, M. (1998) All-atom empirical potential for molecular modeling and dynamics studies of proteins. *J. Phys. Chem. B.* **102**, 3586–616

105. Jorgensen, W. L., Chandrasekhar, J., Madura, J. D., Impey, R. W., and Klein, M. L. (1983) Comparison of simple potential functions for simulating liquid water. *J. Chem. Phys.* **79**, 926–35

106. Rostkowski, M., Olsson, M. H. M., Søndergaard, C. R., and Jensen, J. H. (2011) Graphical analysis of pH-dependent properties of proteins predicted using PROPKA. *BMC Struct. Biol.* **11**, 6

107. Martyna, G. J., Tobias, D. J., and Klein, M. L. (1994) Constant pressure molecular dynamics algorithms. *J. Chem. Phys.* **101**, 4177–89

108. Feller, S. E., Zhang, Y., Pastor, R. W., and Brooks, B. R. (1995) Constant pressure molecular dynamics simulation: The Langevin piston method. *J. Chem. Phys.* **103**, 4613–21

109. Darden, T., York, D., and Pedersen, L. (1993) Particle mesh Ewald: An N⊕log(N) method for Ewald sums in large systems. *J. Chem. Phys.* **98**, 10089–92

110. Eno, C. O., Eckenrode, E. F., Olberding, K. E., Zhao, G., White, C., and Li, C. (2012) Distinct roles of mitochondria- and ER-localized Bcl-xL in apoptosis resistance and Ca2+ homeostasis. *Mol. Biol. Cell*. **23**, 2605–18

111. Montal, M., and Mueller, P. (1972) Formation of bimolecular membranes from lipid monolayers and a study of their electrical properties. *Proc. Natl. Acad.*

Sci. U. S. A. **69**, 3561–6

112. Colombini, M. (1987) Characterization of channels isolated from plant mitochondria. *Methods Enzymol.* **148**, 465–75

113. Chiara, F., Castellaro, D., Marin, O., Petronilli, V., Brusilow, W. S., Juhaszova, M., Sollott, S. J., Forte, M., Bernardi, P., and Rasola, A. (2008) Hexokinase II detachment from mitochondria triggers apoptosis through the permeability transition pore independent of voltage-dependent anion channels. *PLoS One*. **3**, e1852

114. Montessuit, S., Somasekharan, S. P., Terrones, O., Lucken-Ardjomande, S., Herzig, S., Schwarzenbacher, R., Manstein, D. J., Bossy-Wetzel, E., Basañez, G., Meda, P., and Martinou, J.-C. (2010) Membrane remodeling induced by the dynamin-related protein Drp1 stimulates Bax oligomerization. *Cell*. **142**, 889–901

115. Dejean, L. M., Martinez-Caballero, S., Guo, L., Hughes, C., Teijido, O., Ducret, T., Ichas, F., Korsmeyer, S. J., Antonsson, B., Jonas, E. A., and Kinnally, K. W. (2005) Oligomeric Bax is a component of the putative cytochrome c release channel MAC, mitochondrial apoptosis-induced channel. *Mol. Biol. Cell*. **16**, 2424–32

116. Terrones, O., Antonsson, B., Yamaguchi, H., Wang, H.-G., Liu, J., Lee, R. M., Herrmann, A., and Basañez, G. (2004) Lipidic pore formation by the concerted action of proapoptotic BAX and tBID. *J. Biol. Chem.* **279**, 30081–91

117. Colombini, M. (2013) Membrane channels formed by ceramide. *Handb. Exp. Pharmacol.* 10.1007/978-3-7091-1368-4_6

118. Gross, A., McDonnell, J. M., and Korsmeyer, S. J. (1999) BCL-2 family members and the mitochondria in apoptosis. *Genes Dev.* **13**, 1899–911

119. Reed, J. C., Jurgensmeier, J. M., and Matsuyama, S. (1998) Bcl-2 family proteins and mitochondria. *Biochim. Biophys. Acta*. **1366**, 127–37

120. Gillies, L. A., and Kuwana, T. (2014) Apoptosis regulation at the mitochondrial outer membrane. *J. Cell. Biochem.* **115**, 632–40

121. Bartke, N., and Hannun, Y. A. (2009) Bioactive sphingolipids: metabolism and function. *J. Lipid Res.* **50 Suppl**, S91–6

122. Kim, H. J., Mun, J. Y., Chun, Y. J., Choi, K. H., and Kim, M. Y. (2001) Bax-dependent apoptosis induced by ceramide in HL-60 cells. *FEBS Lett.* **505**, 264–8

123. von Haefen, C., Wieder, T., Gillissen, B., Stärck, L., Graupner, V., Dörken, B., and Daniel, P. T. (2002) Ceramide induces mitochondrial activation and apoptosis via a Bax-dependent pathway in human carcinoma cells. *Oncogene*. **21**, 4009–19

124. Siskind, L. J., Mullen, T. D., Romero Rosales, K., Clarke, C. J., Hernandez-Corbacho, M. J., Edinger, A. L., and Obeid, L. M. (2010) The BCL-2 protein BAK is required for long-chain ceramide generation during apoptosis. *J. Biol. Chem.* **285**, 11818–26

125. Lee, H., Rotolo, J. A., Mesicek, J., Penate-Medina, T., Rimner, A., Liao, W.-C., Yin, X., Ragupathi, G., Ehleiter, D., Gulbins, E., Zhai, D., Reed, J. C., Haimovitz-Friedman, A., Fuks, Z., and Kolesnick, R. (2011) Mitochondrial ceramide-rich macrodomains functionalize Bax upon irradiation. *PLoS One*. **6**, e19783

126. Bleicken, S., Classen, M., Padmavathi, P. V. L., Ishikawa, T., Zeth, K., Steinhoff, H.-J., and Bordignon, E. (2010) Molecular details of Bax activation, oligomerization, and membrane insertion. *J. Biol. Chem.* **285**, 6636–47

127. Woodcock, J. (2006) Sphingosine and ceramide signalling in apoptosis. *IUBMB Life*. **58**, 462–6

128. Siskind, L. J. (2005) Mitochondrial ceramide and the induction of apoptosis. *J. Bioenerg. Biomembr.* **37**, 143–53

129. Shao, C., Sun, B., DeVoe, D. L., and Colombini, M. (2012) Dynamics of ceramide channels detected using a microfluidic system. *PLoS One*. **7**, e43513

130. Ding, J., Mooers, B. H. M., Zhang, Z., Kale, J., Falcone, D., McNichol, J., Huang, B., Zhang, X. C., Xing, C., Andrews, D. W., and Lin, J. (2014) After embedding in membranes antiapoptotic Bcl-XL protein binds both Bcl-2 homology region 3 and helix 1 of proapoptotic Bax protein to inhibit apoptotic

mitochondrial permeabilization. *J. Biol. Chem.* **289**, 11873–96

131. Wendt, M. D., Shen, W., Kunzer, A., McClellan, W. J., Bruncko, M., Oost, T. K., Ding, H., Joseph, M. K., Zhang, H., Nimmer, P. M., Ng, S.-C., Shoemaker, A. R., Petros, A. M., Oleksijew, A., Marsh, K., Bauch, J., Oltersdorf, T., Belli, B. A., Martineau, D., Fesik, S. W., Rosenberg, S. H., and Elmore, S. W. (2006) Discovery and structure-activity relationship of antagonists of B-cell lymphoma 2 family proteins with chemopotentiation activity in vitro and in vivo. *J. Med. Chem.* **49**, 1165–81

132. Manion, M. K., O'Neill, J. W., Giedt, C. D., Kim, K. M., Zhang, K. Y. Z., and Hockenbery, D. M. (2004) Bcl-XL mutations suppress cellular sensitivity to antimycin A. *J. Biol. Chem.* **279**, 2159–65

133. Minn, A. J., Vélez, P., Schendel, S. L., Liang, H., Muchmore, S. W., Fesik, S. W., Fill, M., and Thompson, C. B. (1997) Bcl-x(L) forms an ion channel in synthetic lipid membranes. *Nature*. **385**, 353–7

134. Eskes, R., Desagher, S., Antonsson, B., and Martinou, J. C. (2000) Bid induces the oligomerization and insertion of Bax into the outer mitochondrial membrane. *Mol. Cell. Biol.* **20**, 929–35

135. Chipuk, J. E., McStay, G. P., Bharti, A., Kuwana, T., Clarke, C. J., Siskind, L. J., Obeid, L. M., and Green, D. R. (2012) Sphingolipid metabolism cooperates with BAK and BAX to promote the mitochondrial pathway of apoptosis. *Cell*. **148**, 988–1000

136. Lin, S. H., Cherian, N., Wu, B., Phee, H., Cho, C., and Colombini, M. (2014) Bax channel triplet: co-operativity and voltage gating. *Biochem. J.* **459**, 397–404

137. Stockbridge, R. B., Kolmakova-Partensky, L., Shane, T., Koide, A., Koide, S., Miller, C., and Newstead, S. (2015) Crystal structures of a double-barrelled fluoride ion channel. *Nature*. **525**, 548–51

138. Stockbridge, R. B., Robertson, J. L., Kolmakova-Partensky, L., and Miller, C. (2013) A family of fluoride-specific ion channels with dual-topology architecture. *Elife*. **2**, e01084

139. Zizi, M., Thomas, L., Blachly-Dyson, E., Forte, M., and Colombini, M. (1995)

Oriented channel insertion reveals the motion of a transmembrane beta strand during voltage gating of VDAC. *J. Membr. Biol.* **144**, 121–9

140. Xu, X., and Colombini, M. (1996) Self-catalyzed insertion of proteins into phospholipid membranes. *J. Biol. Chem.* **271**, 23675–82

141. Mohammad, M. M., Howard, K. R., and Movileanu, L. (2011) Redesign of a plugged beta-barrel membrane protein. *J. Biol. Chem.* **286**, 8000–13

142. Lakey, J. H., Lea, E. J., and Pattus, F. (1991) ompC mutants which allow growth on maltodextrins show increased channel size and greater voltage sensitivity. *FEBS Lett.* **278**, 31–34

143. Saint, N., Prilipov, A., Hardmeyer, A., Lou, K. L., Schirmer, T., and Rosenbusch, J. P. (1996) Replacement of the sole histidinyl residue in OmpF porin from E. coli by threonine (H21T) does not affect channel structure and function. *Biochem. Biophys. Res. Commun.* **223**, 118–22

144. Benz, R. (2004) *Bacterial and Eukaryotic Porins* (Benz, R. ed), Wiley-VCH Verlag GmbH & Co. KGaA, Weinheim, FRG, 10.1002/3527603875

145. Nikaido, H. (2003) Molecular basis of bacterial outer membrane permeability revisited. *Microbiol. Mol. Biol. Rev.* **67**, 593–656

146. Sen, K., Hellman, J., and Nikaido, H. (1988) Porin channels in intact cells of Escherichia coli are not affected by Donnan potentials across the outer membrane. *J. Biol. Chem.* **263**, 1182–7

147. Nikaido, H. (1994) Prevention of drug access to bacterial targets: permeability barriers and active efflux. *Science*. **264**, 382–8

148. Nikaido, H., and Normark, S. (1987) Sensitivity of Escherichia coli to various beta-lactams is determined by the interplay of outer membrane permeability and degradation by periplasmic beta-lactamases: a quantitative predictive treatment. *Mol. Microbiol.* **1**, 29–36

149. Hocquet, D., Bertrand, X., Köhler, T., Talon, D., and Plésiat, P. (2003) Genetic and phenotypic variations of a resistant Pseudomonas aeruginosa epidemic clone. *Antimicrob. Agents Chemother.* **47**, 1887–94

150. Medeiros, a a, O'Brien, T. F., Rosenberg, E. Y., and Nikaido, H. (1987) Loss of OmpC porin in a strain of Salmonella typhimurium causes increased resistance to cephalosporins during therapy. *J. Infect. Dis.* **156**, 751–7

151. Chevalier, J., Pagès, J. M., and Malléa, M. (1999) In vivo modification of porin activity conferring antibiotic resistance to Enterobacter aerogenes. *Biochem. Biophys. Res. Commun.* **266**, 248–51

152. Dé, E., Baslé, A., Jaquinod, M., Saint, N., Malléa, M., Molle, G., and Pagès, J. M. (2001) A new mechanism of antibiotic resistance in Enterobacteriaceae induced by a structural modification of the major porin. *Mol. Microbiol.* **41**, 189–98

153. Deng, X., Sun, F., Ji, Q., Liang, H., Missiakas, D., Lan, L., and He, C. (2012) Expression of multidrug resistance efflux pump gene norA is iron responsive in Staphylococcus aureus. *J. Bacteriol.* **194**, 1753–62

154. Hocquet, D., Llanes, C., Patry, I., El Garch, F., and Plésiat, P. (2004) Two efflux systems expressed simultaneously in clinical Pseudomonas aeruginosa. *Pathol. Biol. (Paris).* **52**, 455–61

155. Chang, K.-T., Anishkin, A., Patwardhan, G. A., Beverly, L. J., Siskind, L. J., and Colombini, M. (2015) Ceramide channels: destabilization by Bcl-xL and role in apoptosis. *Biochim. Biophys. Acta*. **1848**, 2374–84

156. Benz, R., Schmid, A., and Hancock, R. E. (1985) Ion selectivity of gram-negative bacterial porins. *J. Bacteriol.* **162**, 722–7